

**A nonlinear model of stationary planetary
waves in the Northern Hemisphere
stratosphere**

**Thomas Charles Box
C²GCR Report No. 94-10
December 1994**

A NONLINEAR MODEL OF STATIONARY PLANETARY WAVES
IN THE NORTHERN HEMISPHERE STRATOSPHERE

by

Thomas Charles Box

Department of Atmospheric and Oceanic Sciences

McGill University

Montreal, Canada

August 1994

A thesis submitted to the Faculty of Graduate Studies and Research in partial fulfillment
of the requirements for the degree of Doctor of Philosophy.

© Thomas Charles Box 1994

ABSTRACT

A steady-state primitive equations model is used to study the structure of stationary planetary waves in the Northern Hemisphere stratosphere. The zonal mean circulation is specified using observed January mean data, as is the wave structure at the lower boundary of 100 hPa. Experiments are performed using data from four years, 1982-84 and 1986. Numerical solutions are found for the structures of zonal wavenumbers 1 to 3 throughout the Northern Hemisphere stratosphere.

In one series of experiments, a linear model is employed, with forcing only by stationary waves at the lower boundary. This model reproduces the gross features of the stratospheric stationary waves, but the wave amplitudes are much less than those observed in nature.

In a second series of experiments, the January means of the transient vorticity and heat flux divergences are calculated using observed data, and applied as an additional forcing term in the model, along with the lower boundary forcing. The model yields significantly larger wave amplitudes, closer to those observed in nature, when forcing by transients is included.

In a third series of experiments, a model which includes the nonlinear interactions among the stationary waves is employed, with forcing only by the waves at the lower boundary. This yields somewhat better results than the linear model, but the change in the wave structure due to the inclusion of nonlinear interactions among the stationary waves is smaller than that due to the inclusion of forcing by transients.

The ability of the model to reproduce the observed features of the monthly mean stratospheric circulation varies greatly, depending on the year studied.

RÉSUMÉ

Un modèle aux équations générales est employé pour étudier la structure des ondes planétaires stationnaires dans la stratosphère de l'hémisphère nord. La circulation zonale moyenne est précisée en employant la moyenne mensuelle de janvier calculée à partir d'observations. La structure des ondes à la limite inférieure du modèle à 100 hPa est précisée de la même façon. Des solutions numériques sont calculées pour les structures des ondes zonales 1 à 3 dans toute la stratosphère de l'hémisphère nord.

Dans une série d'expériences, un modèle linéaire est employé, forcé uniquement par les ondes stationnaires à la limite inférieure. Ce modèle reproduit les caractéristiques générales des ondes stationnaires dans la stratosphère, mais les amplitudes des ondes sont beaucoup plus faibles que celles observées dans la nature.

Dans une deuxième série d'expériences, les moyennes mensuelles de janvier des divergences de transport du tourbillon et de la chaleur par l'écoulement transitoire sont calculées en employant des données observées. Ces divergences sont employées comme un terme de forçage qui s'ajoute au forçage à la limite inférieure. Les ondes calculées par le modèle ont des amplitudes nettement supérieures, et plus proche de celles observées dans la nature, lorsque le forçage par l'écoulement transitoire est inclus.

Dans une troisième série d'expériences, un modèle qui inclut les interactions nonlinéaires entre les ondes stationnaires est employé, forcé uniquement par les ondes à la limite inférieure. Ce modèle donne des résultats légèrement meilleurs que ceux du modèle linéaire, mais le changement dans la structure des ondes dû à l'inclusion des interactions nonlinéaires entre les ondes stationnaires est moindre que celui dû à l'inclusion du forçage par l'écoulement transitoire.

La habileté du modèle à reproduire les caractéristiques observées de la moyenne mensuelle de la circulation dans la stratosphère varie considérablement d'une année à l'autre.

ACKNOWLEDGEMENTS

I wish to thank my thesis supervisor, Prof. Jacques Derome, for his constant guidance, advice and criticism throughout the course of this work. I also wish to thank Dr. Charles McLandress for providing me with a preliminary version of the model used in this study. The data set used in this work was compiled by Dr. Kevin Hamilton, and conveyed to me by Dr. McLandress.

Financial support from the J.W. McConnell Foundation, the Atmospheric Environment Service of Canada, and le Fonds pour la Formation de Chercheurs et l'Aide à la Recherche is gratefully acknowledged.

TABLE OF CONTENTS

Abstract		i
Résumé		ii
Acknowledgements		iii
Table of Contents		iv
List of Figures		vi
List of Symbols		viii
Statement of Originality		x
Chapter 1	INTRODUCTION	1
Chapter 2	OBSERVATIONS	11
(2.1)	Introduction	11
(2.2)	Data set	12
(2.3)	Mean zonal wind	13
(2.4)	Refractive index	19
(2.5)	Stationary planetary waves	22
Chapter 3	DESCRIPTION OF MODEL	36
(3.1)	Introduction	36
(3.2)	Derivation of model equations	37
(3.3)	Model domain and boundary conditions	44
(3.4)	Zonal mean state	46

(3.5)	Test of model using Hough functions	49
(3.6)	Computation of transient forcing fields	51
(3.7)	Iterative solution technique for nonlinear model	52
(3.8)	Smoothing of model fields	56
Chapter 4	RESULTS OF MODEL SIMULATIONS	58
(4.1)	Introduction	58
(4.2)	Linear model without transients	59
(4.3)	Linear model with transients	71
(4.4)	Nonlinear model without transients	84
Chapter 5	DISCUSSION AND CONCLUSIONS	95
Appendix A	COEFFICIENTS OF MODEL EQUATIONS	101
Appendix B	NUMERICAL SOLUTION OF MODEL EQUATIONS	108
References		115

LIST OF FIGURES

Figure		Page
2.1	Zonal mean wind. Monthly mean for January (a) 1982, (b) 1983, (c) 1984, and (d) 1986.	15
2.2	Daily value of zonal mean wind speed at 65°N latitude and 32 km height.	18
2.3	Refractive index Q_1 computed from monthly mean of zonal mean wind for January (a) 1982, (b) 1983, (c) 1984, and (d) 1986.	20
2.4	January 1983 monthly mean stationary waves, from observations. Solid lines are amplitude, broken lines are phase. (a) zonal wavenumber $k=1$, (b) $k=2$, (c) $k=3$.	24
2.5	January monthly mean geopotential height field (sum of zonal waves 1-3), from observations, for log-pressure height 32 km. (a) 1982, (b) 1983, (c) 1984, (d) 1986.	26
2.6	January monthly mean stationary zonal wave $k=1$, from observations. Solid lines are amplitude, broken lines are phase. (a) 1982, (b) 1983, (c) 1984, (d) 1986.	28
2.7	As in Fig. 2.6, but for zonal wave $k=2$.	31
2.8	January monthly mean geopotential height field (sum of zonal waves 1-3), from observations, for 100 hPa surface. (a) 1982, (b) 1983, (c) 1984, (d) 1986.	33
4.1	Stationary waves from linear model without transients, for January 1983. Solid lines are amplitude, broken lines are phase. (a) zonal wavenumber $k=1$, (b) $k=2$, (c) $k=3$.	60
4.2	Geopotential height field (sum of zonal waves 1-3), from linear model without transients, for log-pressure height 32 km. (a) 1982, (b) 1983, (c) 1984, (d) 1986.	64

4.3	Stationary zonal wave $k=1$, from linear model without transients. Solid lines are amplitude, broken lines are phase. (a) 1982, (b) 1983, (c) 1984, (d) 1986.	67
4.4	As in Fig. 4.3, but for zonal wave $k=2$.	69
4.5	Geopotential height field (sum of zonal waves 1-3), from linear model with transients, for log-pressure height 32 km. (a) 1982, (b) 1983, (c) 1984, (d) 1986.	72
4.6	Stationary zonal wave $k=1$, from linear model with transients. Solid lines are amplitude, broken lines are phase. (a) 1982, (b) 1983, (c) 1984, (d) 1986.	76
4.7	Amplitude of forcing field G_1^T due to monthly mean of transient momentum and heat flux divergences, as computed from observations, for January (a) 1982, (b) 1983, (c) 1984, (d) 1986.	80
4.8	As in Fig. 4.6, but for zonal wave $k=2$.	82
4.9	Geopotential height field (sum of zonal waves 1-3), from nonlinear model without transients, for log-pressure height 32 km. (a) 1982, (b) 1983, (c) 1984, (d) 1986.	86
4.10	Stationary zonal wave $k=1$, from nonlinear model without transients. Solid lines are amplitude, broken lines are phase. (a) 1982, (b) 1983, (c) 1984, (d) 1986.	89
4.11	As in Fig. 4.10, but for zonal wave $k=2$.	93

LIST OF SYMBOLS

a	mean radius of earth (= 6.371×10^6 m)
c_p	specific heat of dry air at constant pressure
f	Coriolis parameter (= $2 \Omega \sin \theta$)
g	mean acceleration of gravity (= 9.807 m s ⁻²)
p	pressure
p_s	standard reference pressure (= 1000 hPa)
t	time
u	zonal component of velocity
v	meridional component of velocity
w	vertical component of velocity
z	vertical log-pressure coordinate (= $-H \ln (p/p_s)$)
H	mean scale height (= RT_s/g)
N	buoyancy frequency ($N^2 = \Phi_{zz} + \kappa\Phi_z/H$)
R	gas constant for dry air
T	temperature
T_s	constant reference temperature
κ	ratio of gas constant and heat capacity for dry air (= R/c_p)
θ	latitude
λ	longitude
ρ_0	basic state density ($\rho_0(z) = \rho_s e^{-z/H}$)

ρ_s constant reference density (= p_s/RT_s)

Φ geopotential

Ω angular rotation rate of earth ($7.292 \times 10^{-5} \text{ s}^{-1}$)

D/Dt material derivative ($\frac{D}{Dt} = \frac{\partial}{\partial t} + \frac{u}{a \cos \theta} \frac{\partial}{\partial \lambda} + \frac{v}{a} \frac{\partial}{\partial \theta} + w \frac{\partial}{\partial z}$)

\bar{A} time mean of A ($= \frac{1}{t_2 - t_1} \int_{t_1}^{t_2} A dt$)

A' departure from time mean of A (= $A - \bar{A}$)

$[A]$ zonal mean of A ($= \frac{1}{2\pi} \int_0^{2\pi} A d\lambda$)

\hat{A} departure from zonal mean of A (= $A - [A]$)

STATEMENT OF ORIGINALITY

The original work contained in this study includes:

- (1) the development of a numerical model of stationary waves in the winter stratosphere which is based on the primitive equations and which includes the effects of nonlinear interactions among these waves,
- (2) the use of data from several individual years to specify the zonal mean basic state and the lower boundary forcing in this model, allowing one to study the interannual variability in the behaviour of the stratospheric stationary waves,
- (3) the computation of the time-averaged transient momentum and heat flux divergences in the stratosphere from observed data, and their inclusion in the numerical model as an additional forcing term.

CHAPTER 1

INTRODUCTION

In the last quarter-century, there has been a considerable effort to understand the circulation of the stratosphere through studies using observations and numerical models. It is certain that the troposphere has an important effect on the stratosphere. Although the importance of the effect of the stratosphere on the troposphere is somewhat less clear, it seems certain that this effect is not negligible, and that a proper understanding of the dynamics of the stratosphere is necessary to understand fully the behaviour of the troposphere.

Interest in the stratosphere has been heightened in recent years by the concern that pollutants such as chlorofluorocarbons and oxides of nitrogen are contributing to a depletion of the stratospheric ozone and affecting the global climate. An understanding of the stratospheric circulation is vital in the study of this phenomenon, since it is this circulation which transports the radiatively and photochemically active substances. Furthermore, the temperature structure of the stratosphere, upon which the ozone-depleting chemical reactions are crucially dependent, is determined in part by dynamical processes.

The circulation of the stratosphere displays a strong seasonal dependence. The very direction of the mean polar vortex reverses from summer to winter. The present work deals with the circulation in the Northern Hemisphere in January. The zonal mean flow (*i.e.* averaged over longitude) is driven primarily by differential heating owing to

absorption of solar ultraviolet radiation by ozone and infrared emission by carbon dioxide and ozone. Because of the negative declination of the sun in January, there is maximum heating at the South Pole and maximum cooling at the North Pole. The resulting strong horizontal temperature gradient, combined with the Coriolis force owing to the earth's rotation, produces an easterly flow in the Southern (summer) Hemisphere, and a westerly flow in the Northern (winter) Hemisphere.

When averaged over a period of a month, the circulation in the summer hemisphere is almost completely zonal (*i.e.* east-west), while that in the winter hemisphere shows large deviations from a purely zonal flow. These deviations are known as (quasi-) stationary waves. They are produced principally by disturbances produced in the troposphere by the earth's topography and by land-water thermal contrasts, which propagate upward into the stratosphere. These disturbances are unable to propagate in the easterly flow of the summer stratosphere, so they remain trapped in the troposphere and the circulation of the summer stratosphere remains almost purely zonal. In contrast, the westerly flow of the winter stratosphere permits the propagation of these disturbances, resulting in the presence of stationary waves in the winter stratosphere. The present work is concerned primarily with the modelling of these waves.

It is convenient to retain the vertical and latitudinal dependence of these disturbances, but to transform the longitudinal dependence, expressing it as a sum of zonal harmonics. Because the disturbances are large in scale, the gravest harmonics,

principally zonal wavenumbers 1 and 2, are much more important than the higher harmonics, so the expansion can be truncated at a low wavenumber.

In principle, the circulation of the atmosphere is governed by the Navier-Stokes equations of fluid dynamics. In practice, however, the full Navier-Stokes equations are never used in studies of large-scale atmospheric dynamics. Various simplifications are always used. Following Holton (1975), these may be divided into three categories. The first, dynamical simplification, involves dropping from the governing equations terms which are shown by scale analysis to be of negligible importance in the problem being considered. Besides the obvious advantage of reducing the complexity of the equations to be dealt with, this simplification also has the advantage of filtering out phenomena such as sound waves which, though they are valid solutions of the Navier-Stokes equations, are of no meteorological importance. The most complete system of equations generally used in large-scale atmospheric dynamics is the system of so-called primitive equations, in which the vertical component of the equation of motion is replaced by the equation of hydrostatic balance between gravity and the vertical pressure gradient, and the Coriolis force due to vertical motion is neglected. Using the observed fact that the rotational part of large-scale atmospheric motions is much larger than the divergent part, one can derive a more highly simplified system of equations known as the quasi-geostrophic system. This system has been used in many previous studies. In the present work, the more complete primitive equations are used.

The second category is a geometrical simplification. Although the spherical shape of the earth is of great importance in atmospheric dynamics, the extreme thinness of the

atmosphere compared to the earth's radius allows one to replace the variable distance to the centre of the earth by a constant mean radius. A more extreme simplification is the so-called beta-plane approximation, where spherical coordinates are replaced by cartesian coordinates, and the sinusoidal dependence of the Coriolis force on latitude is replaced by a linear dependence. This may be a reasonable approximation when modelling phenomena over a restricted range of latitude, but in the present work, where the entire Northern Hemisphere is to be considered, spherical coordinates are used.

The third category of simplification is linearization. The nonlinear nature of the equations of motion for the atmosphere makes them very difficult to solve, either analytically or numerically. If one considers the flow field as the sum of a zonal mean and a perturbation, then assumes that the perturbations are sufficiently small that terms involving products of perturbations may be neglected, one obtains a system of equations that are linear in the perturbations, and therefore much easier to solve. This form of simplification has been used in many previous studies, and is found to give qualitatively good results. However, the assumption that the perturbations are small compared to the zonal mean flow is not valid for the winter stratosphere, so it is clearly of interest to use a nonlinear model in an effort to simulate better the observed atmospheric circulation. It is also of interest to investigate why linear models give reasonably good results when the assumption of small perturbations, on which they are based, is not valid.

Although there are transient phenomena in the stratosphere, occurring on a time scale of days, in this work we wish to focus on the quasi-stationary waves which persist over a period of a month or more. This allows us to use the steady-state equations

obtained by averaging the equations of motion over the time period of interest, thereby eliminating the time-dependence of the equations. In the previous works employing this technique, the effect of the time-averaged transient fluxes of heat and momentum has been neglected. It is of interest to determine the importance of these transients in the forcing of the stationary waves, by retaining these terms in the model, calculating their value from observed data, and including them as an additional forcing term.

In the present work, as in several previous studies, the mean zonal flow throughout the domain of the model is specified from observations, as are the stationary waves at the lower boundary, representing the forcing propagating upward from the troposphere. The model then finds the structure of the stationary waves throughout the domain. Since the mean zonal flow is specified, the model does not allow for the effect of the waves on the zonal flow. This is not entirely realistic, and must be regarded as a limiting case of strong forcing of the zonal flow, so that the effect of the waves on the mean flow is negligible. Ideally, one would like to model both the mean flow and the waves, allowing for wave-mean flow interaction. This would require inclusion in the model of the radiative forcing and mechanical damping of the mean flow. There are general circulation models of the stratosphere which attempt to simulate completely the dynamics of the atmosphere, given only the external conditions. These models are vastly more complex and demand much greater computing resources than the model used in the present study. The relatively simple model employed here allows one to isolate the effect of wave-wave interactions, to attempt to determine their importance.

The pioneering work in the study of stratospheric stationary waves was that of Charney and Drazin (1961). Using the quasi-geostrophic equations on a beta-plane and an idealized mean flow, they showed that disturbances could not propagate upward through an easterly mean flow, and only the largest scale disturbances could propagate upward through a westerly mean flow, thus explaining the observed restriction of planetary waves to the winter hemisphere. This result remains qualitatively valid when a spherical geometry and a more realistic mean flow are used, although the quantitative details are modified.

Matsuno (1970) developed a linear quasi-geostrophic steady-state model with spherical geometry. Linearizing about a realistic zonal basic state and using observed mean 500 hPa heights as a forcing at the lower boundary of the model, his model computed wave solutions very similar to the observed waves for zonal wavenumbers 1 and 2, though there were significant differences between the observed and computed waves. This ability to reproduce a wave structure essentially similar to that observed, using lower-boundary forcing, strongly suggests that the stratospheric stationary waves are driven by disturbances in the troposphere.

Matsuno also showed that the behaviour of the waves is dependent on the structure of the basic state. In particular, he showed that a refractive index governing the behaviour of the waves could be defined as a function of spatial derivatives of the basic-state wind field. The structure of the basic-state wind creates a sort of wave guide which tends to confine the waves to a restricted range in latitude and height.

Schoeberl and Geller (1977) used a slightly generalized version of Matsuno's model. By varying the basic-state wind field, they showed explicitly that the stationary wave structure is very sensitive to the structure of the basic state. This is as one would expect, given Matsuno's finding that the wave propagation is governed by a refractive index depending on spatial derivatives of the basic-state wind field. Schoeberl and Geller also found that the wave structure is highly dependent on the rate of radiative cooling, but relatively insensitive to the vertical profile of the basic-state temperature field.

Lin (1982) used a linear primitive-equations model with spherical geometry, including both the troposphere and the stratosphere, to study stationary waves. Forcing by topography and diabatic heating in the troposphere was included explicitly, unlike in previous models where the forcing was provided by the lower boundary condition. By experimenting with different mean zonal wind fields, Lin found that the stationary wave response is very sensitive to the structure of the mean zonal wind. He also found that the model could reproduce most of the features of the stationary wave pattern, with topography being a more important source of forcing than diabatic heating.

Jacqmin and Lindzen (1985) employed an approach similar to that of Lin, but arrived at quite different conclusions. They found that the stationary wave response was relatively insensitive to changes in the mean zonal wind. They attributed Lin's result to insufficient resolution in his numerical model. However, even Jacqmin and Lindzen find that the stratospheric wave response was considerably more sensitive to changes in the mean zonal wind than the tropospheric response. Although they were more concerned with investigating the sensitivity of the wave response than with trying to reproduce the

observed wave structure, Jacqmin and Lindzen's model does give a stratospheric wave pattern qualitatively similar to that observed.

It is remarkable that the above models are able to reproduce the observed wave structure so well, even though the models are linear. The amplitude of the waves is not small compared to the mean zonal wind, so linearization should not be a valid approximation. However, Derome (1984) showed that if the zonal basic state satisfies certain criteria, then linear solutions of the steady-state equations of motion will also be solutions of the full nonlinear equations. The observed basic state does approximately satisfy the required criteria, thus explaining why linear solutions are such good approximations, in spite of the large wave amplitudes. It should be noted that Derome's result is obtained in the framework of quasi-geostrophic theory, and ignores the effects of transients and dissipation. This result does not hold in the more general case where ageostrophic motion, transients, and dissipation are significant.

Early works on nonlinear models of stationary waves include those of Egger (1976) and Ashe (1979). Both models determined tropospheric responses at only two height levels. Egger's model was forced only by topography at the lower boundary, and had a simple analytic basic state wind. Transients were neglected. He found that the inclusion of nonlinear interactions significantly affected the amplitude but not the phase of the wave response. Ashe's model included forcing by both topography and diabatic heating, and used a zonal mean state taken from observations. Transients were not included explicitly, but dissipation terms provided a rough parameterization of their effect. With this model, it was found that the inclusion of nonlinearities could produce

a significant shift in the phase of the response to diabatic heating, but that nonlinearities were less important for topographically forced waves. In general, inclusion of nonlinearities produced a more realistic solution, though the linear and nonlinear model solutions were much more similar to each other than either was to the observed wave field.

Robinson (1986) employed a quasi-geostrophic beta-plane model with a simple basic-state wind profile and lower-boundary forcing to study wave-wave interactions in the stratosphere. The basic state satisfies Derome's non-interaction criteria, so wave-wave interaction occurs only in the presence of dissipation. Dissipation can lead to significant nonlinear interactions. Because of the simplified nature of the model, detailed comparisons with observations or other models are not possible.

A more realistic nonlinear atmospheric model is that of McLandress and Derome (1990, 1991). This is a steady-state quasi-geostrophic model with spherical geometry, with the basic-state wind field and lower-boundary forcing taken from observations. A linear version of this model gave wave solutions in qualitative agreement with observations, but the model's waves have too small amplitudes and too much phase tilt with height. Inclusion of nonlinear interactions in the model increased the wave amplitudes and reduced the phase tilt, so the nonlinear results were closer to the observed wave pattern, but the inclusion of wave-wave interactions had a relatively small effect on the model results. The waves remained too weak and too tilted in the vertical, compared to the observed waves. Since the model's basic state approximately satisfied

the Derome noninteraction criteria, the small effect of wave-wave interactions is not surprising.

It will be recalled that this result of Derome (1984) is valid only for steady-state quasi-geostrophic equations. When ageostrophic motions and transient are included, the nonlinear interactions may be significant even though the basic state satisfies the quasi-geostrophic noninteraction criteria. It is therefore of interest to study a nonlinear primitive-equations model of the stratosphere, to see whether the presence of ageostrophic motion has a significant effect on wave-wave interactions. It is also of interest to calculate the time means of transient momentum and heat fluxes, as determined from observations. These can then be included in the model as forcing terms in addition to the stationary wave forcing at the lower boundary of the model, in order to determine which mechanisms are significant for the maintenance of the quasi-stationary waves in the stratosphere.

In this thesis, Chapter 2 describes the data set used in this study, and the observed behaviour of the January stratosphere as evidenced in that data set. Chapter 3 contains a description of the model used in this work, with a derivation of the model equations. In an effort to make this section more readable, some of the lengthier steps in the derivation have been relegated to Appendix A, while the numerical methods used to solve the model equations are described in Appendix B. Chapter 4 deals with the results of numerical experiments performed for different years and with different versions of the model. The results of these experiments are compared to the observed behaviour of the stratospheric stationary waves. Conclusions and discussion follow in Chapter 5.

CHAPTER 2

OBSERVATIONS

(2.1) Introduction

This chapter describes the data set used in this study and the observed behaviour of the stratosphere as reflected in these data. Section 2.2 describes the data set, which consists of five years of daily height and temperature fields at nine levels. These data are used to compute mean zonal winds, as explained in Section 2.3. The zonal mean state is used as an input in the numerical model used in this work.

The zonal mean state is also important because it influences the propagation of planetary waves. In linear theory, this control of wave propagation by the zonal mean circulation can be expressed in terms of an index of refraction. This concept is discussed briefly in Section 2.4.

The observed stationary waves in the monthly mean geopotential height field have been computed from the data, and are presented in Section 2.5. The observed structure of the waves at 100 hPa is used as a lower boundary condition in the model, and provides the forcing for the waves throughout the model domain. The observed wave structure also serves as a standard against which the performance of the various versions of the model is to be measured.

(2.2) Data set

This study uses a stratospheric data set compiled by Hamilton (1987, personal communication), and used in the previous study by McLandress and Derome (1991). It consists of daily values of geopotential heights at eight levels, from 100 hPa to 1 hPa, on a 5° latitude \times 10° longitude grid covering the entire globe, for the time period 1982 to 1986. The data set was constructed using 100 hPa height fields taken from the ECMWF geopotential analysis, and NMC temperature data at 70, 50, 20, 10, 5, 2, and 1 hPa, obtained by satellite soundings using infrared radiometry. Height fields at the different levels were constructed by integrating upward from 100 hPa using the hypsometric equation and the NMC temperature data.

Data for a few days are missing from this set. The present study is restricted to the month of January, for which the data set has 31 days of observations for 1982, 29 days of observations for 1983 (January 1 and 10 missing), 31 days of observations for 1984, and 24 days of observations for 1986 (January 1-4, 11, 13, and 23 missing). The year 1985 has been excluded from the study for reasons discussed below. No attempt has been made to reconstruct data for the missing days by interpolation or extrapolation. When we refer to a January monthly mean, this will indicate a mean of the data for the available days.

Daily values of the 0.4 hPa geopotential height field, taken from NMC analyses, have been added to the data set described in the previous paragraph. Although these two data sets are not perfectly consistent, McLandress and Derome (1991) found that mean

zonal winds in the 70 hPa to 1 hPa region calculated from the Hamilton data set differed by only a few percent from those obtained using the NMC data set. Inclusion of these additional data therefore appears justified, in order to extend the observations as high as possible.

(2.3) Mean zonal wind

Monthly mean height fields have been calculated from this data set for January 1982-84 and 1986. The mean zonal wind was then calculated using the gradient wind equation

$$af[u] + [u]^2 \tan \theta + \frac{\partial [\Phi]}{\partial \theta} = 0, \quad (2.1)$$

where the square brackets represent the zonal average. Other symbols are standard and are defined in the List of Symbols. It is assumed that there is no mean meridional circulation, so the mean flow is purely zonal. These calculations were performed for each pressure level in the data set, then cubic spline interpolation was used to project the wind fields onto an equally-spaced vertical grid in log-pressure coordinates.

Equation (2.1) differs from the geostrophic wind equation by the presence of the $[u]^2 \tan \theta$ term. Several previous studies (Elson, 1986; Boville, 1987; Randel, 1987) have found that use of the geostrophic approximation may lead to significant errors when computing stratospheric winds from height fields. At 70°N latitude, inclusion of this

additional term in the gradient wind equation gives values of the mean zonal wind, computed from the data set used in the present study, which are typically 10-15% smaller than those computed geostrophically. This is consistent with the differences among gradient and geostrophic zonal mean winds found by Randel (1987). Randel found that, while gradient winds were a better approximation than geostrophic winds, a slightly better approximation was provided by what he termed "balance winds," though the difference was small in most cases. The latter, however, also yield a non-zero mean meridional circulation. In the model used for the present study, it is assumed that the mean flow is purely zonal, with no mean meridional circulation. The gradient wind equation with the mean meridional circulation set to zero therefore provides an appropriate level of approximation for computing the zonal mean circulation for use in this model.

The stratospheric circulation for the winter of 1984-85 was highly anomalous. A major sudden warming occurred early in the winter, resulting in a reversal of the zonal mean winds to an easterly direction in the lower stratosphere near the North Pole. The monthly mean zonal wind field for January 1985 has a zero-wind line at high latitudes. This produces a near-singularity in the model equations, and causes severe numerical difficulties. This case has therefore been excluded from the present work, which deals with January 1982-84 and 1986.

The mean zonal winds for these four months are shown in Figure 2.1. Note that the vertical coordinate used here and throughout this work is the log-pressure height, defined by

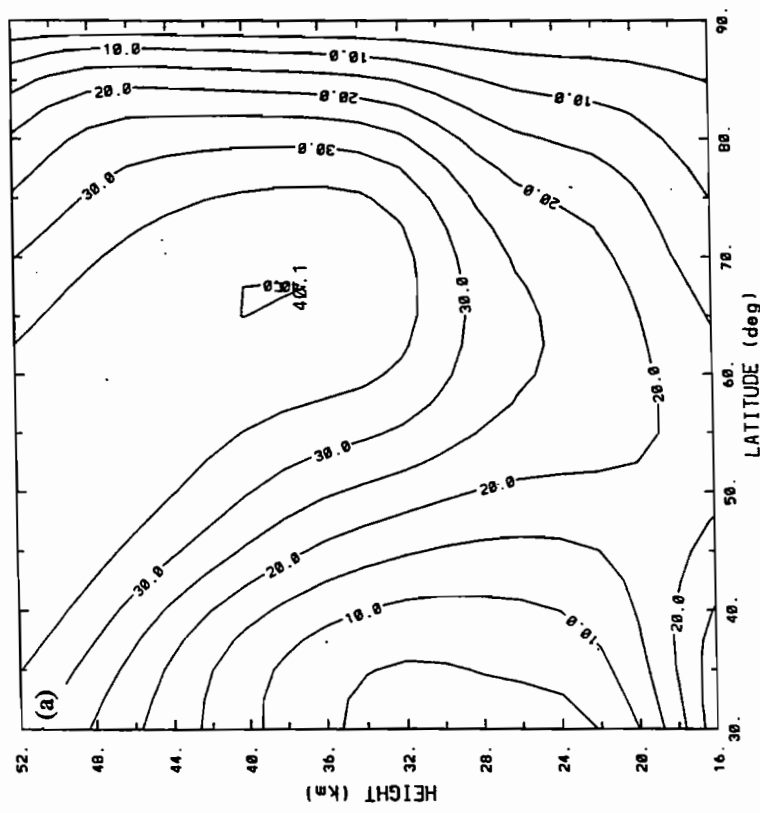
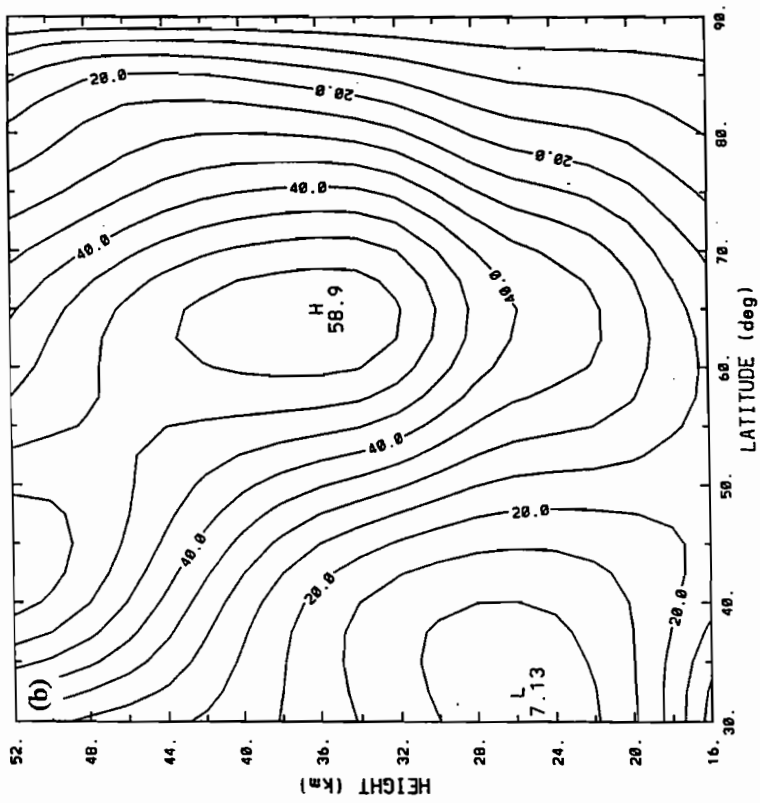


Fig. 2.1 Zonal mean wind. Monthly mean for January (a) 1982, (b) 1983, (c) 1984, and (d) 1986. Contour interval 5 m s⁻¹.

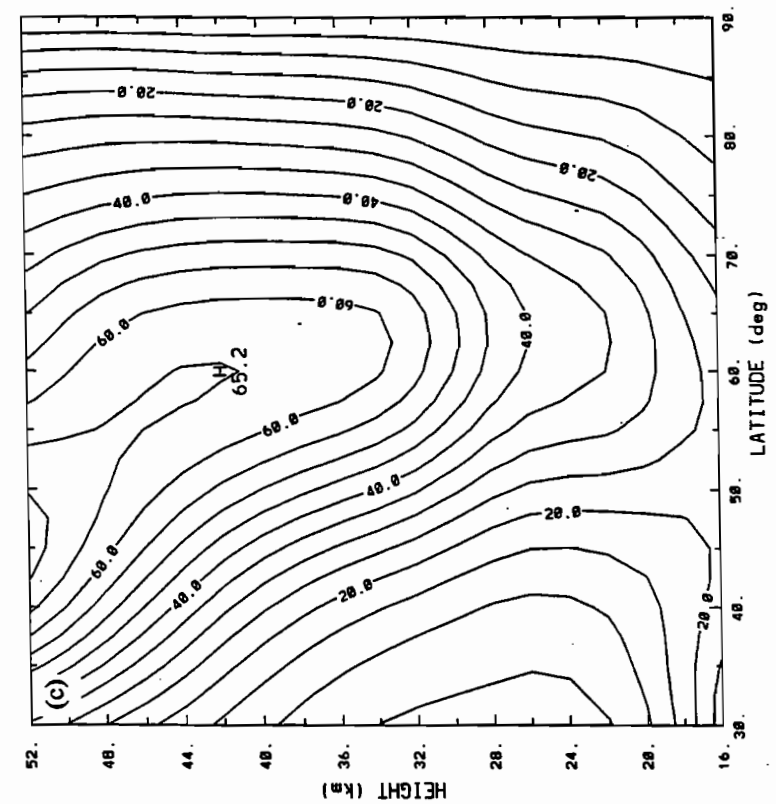
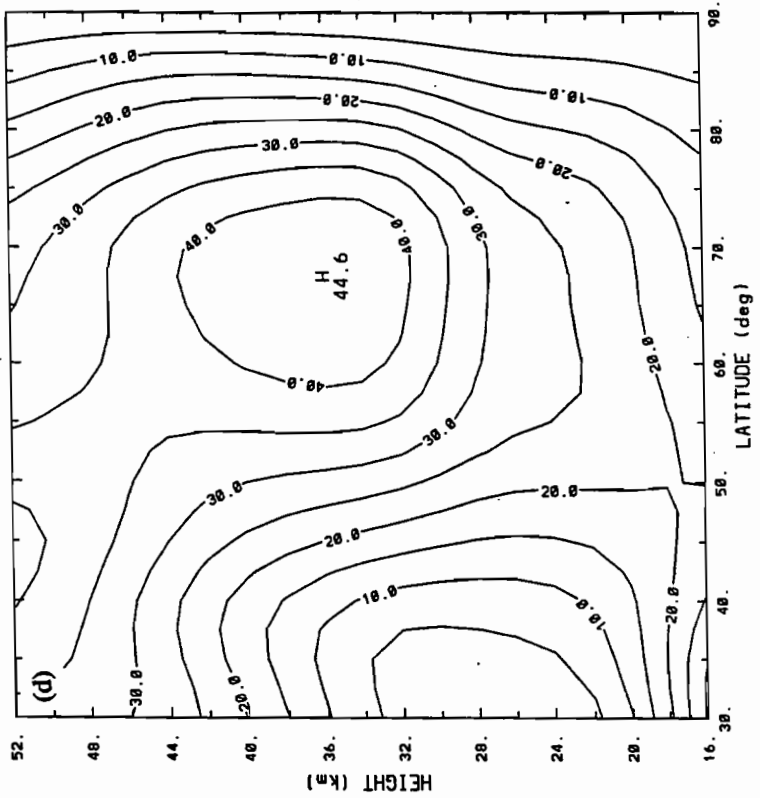


Fig. 2.1 Continued.

$$z = -H \log \frac{P}{P_s}, \quad (2.2)$$

where p_s is a reference pressure of 1000 hPa, and H is the mean scale height, taken to be 7000 m.

One may note that the qualitative features of the mean zonal circulation are broadly similar for all years. The winds are westerly throughout the domain of interest. There is a local maximum of wind velocity near latitude 60-65° N and altitude 36-42 km. Below this level, the jet axis is approximately vertical, but at higher altitudes the axis tilts equatorward, with the greatest velocities at the highest observed level and near latitude 40-45° N.

Although the qualitative structure of the monthly mean zonal circulation is similar for all the years studied, the quantitative values of the wind velocities show very significant interannual variability, of over 50 %.

There is also significant day-to-day variability in the zonal mean circulation. This is reflected in Figure 2.2, which shows the zonal mean wind velocity for each day at 65°N latitude and 32 km height. (As mentioned in Section 2.2 above, data are missing for some days in 1983 and 1986.) The variability is especially large for 1982, when there were large fluctuations in the zonal mean wind velocity throughout the month, and for 1983, when the zonal mean circulation was very strong early in the month, but became weak near the end of the month. The variability is less in 1984 and 1986, but

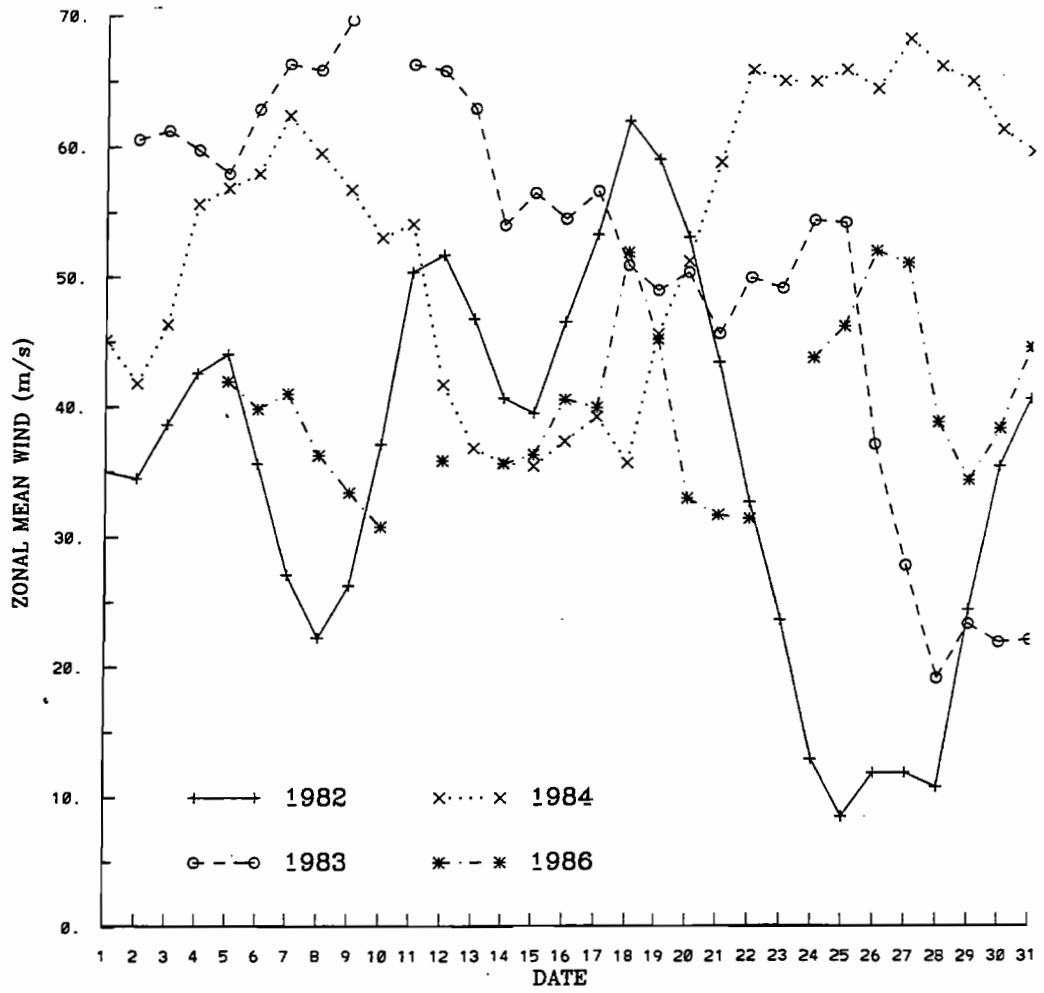


Fig. 2.2 Daily value of zonal mean wind speed at 65°N latitude and 32 km height.

still not negligible. The standard deviation of the zonal mean wind speed at 65°N and 32 km is 15 m s⁻¹ for 1982 and 1983, 11 m s⁻¹ for 1984, and 6 m s⁻¹ for 1986.

(2.4) Refractive index

The structure of the mean flow controls the propagation of waves in the stratosphere. This behaviour can be quantified by use of the squared refractive index Q_k for zonal wavenumber k , as defined by Matsuno (1970) within the context of a quasi-geostrophic model:

$$Q_k = \bar{\omega}^{-1} \left\{ 2(\Omega + \bar{\omega}) - \frac{\partial^2 \bar{\omega}}{\partial \theta^2} + 3 \tan \theta \frac{\partial \bar{\omega}}{\partial \theta} - \left(\frac{2 \Omega a \sin \theta}{N} \right)^2 \left(\frac{\partial^2 \bar{\omega}}{\partial z^2} - \frac{1}{H} \frac{\partial \bar{\omega}}{\partial z} \right) \right\} - \left(\frac{\Omega a \sin \theta}{NH} \right)^2 - \frac{k^2}{\cos^2 \theta}. \quad (2.2)$$

Waves can propagate only in regions where Q_k is positive, and are evanescent in regions where this quantity is negative. Figure 2.3 shows Q_k as computed from the monthly mean winds for each of the four Januaries studied in this work. Q_k becomes strongly negative at high latitudes, because of the $-k^2/\cos^2\theta$ term in Equation (2.2), so waves vanish at the pole. The refractive index is also observed to take on low values in the lower stratosphere around 40°N, above the midlatitude tropospheric jet, so waves do not propagate upwards at these latitudes. The stationary waves in the stratosphere are thus largely confined to the region between 50°N and 80°N. The refractive index decreases with increasing height in the upper stratosphere, as the zonal westerlies increase in

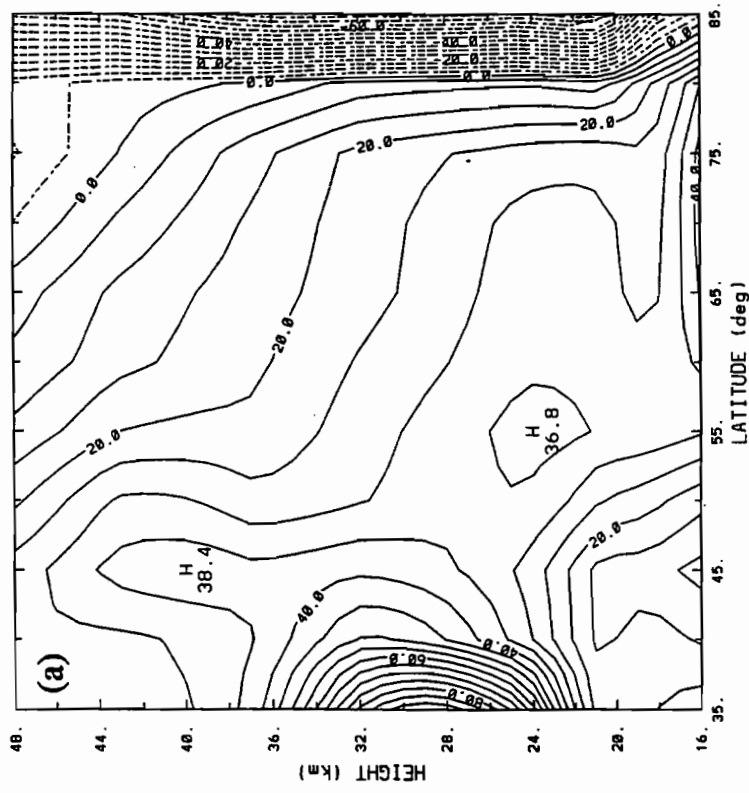
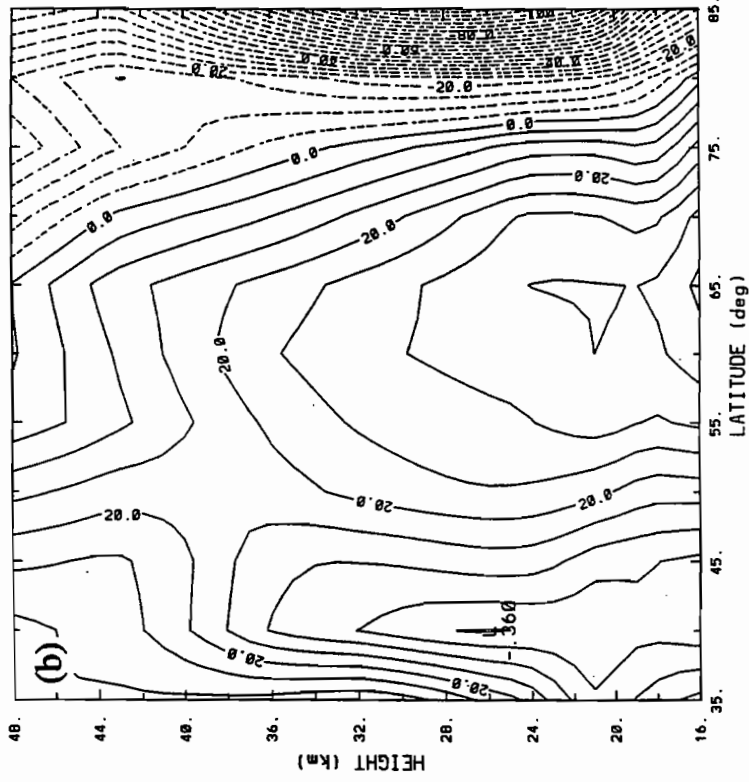


Fig. 2.3 Refractive index Q_1 computed from monthly mean of zonal mean wind for January (a) 1982, (b) 1983, (c) 1984, and (d) 1986. Contour interval 5.

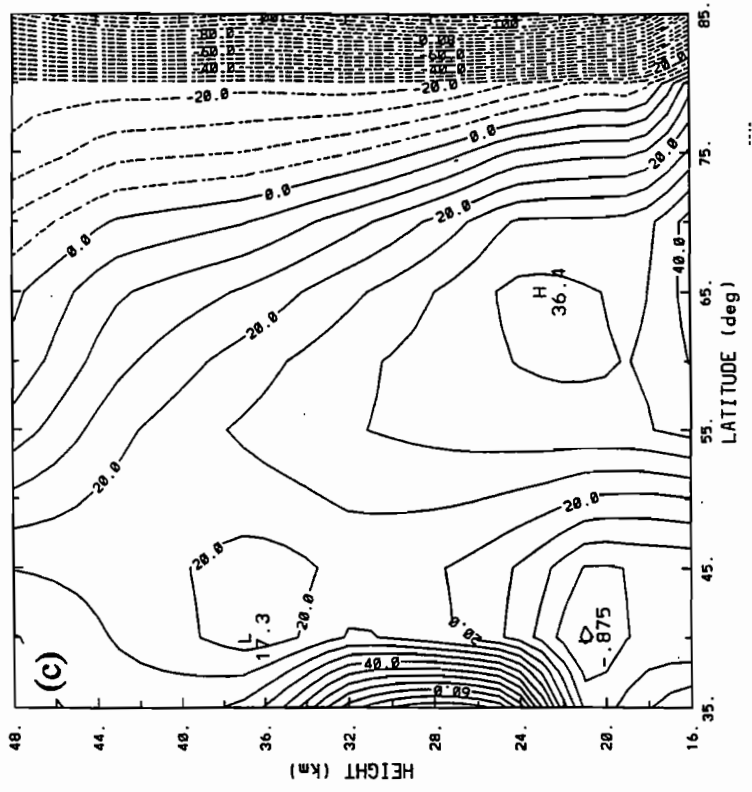
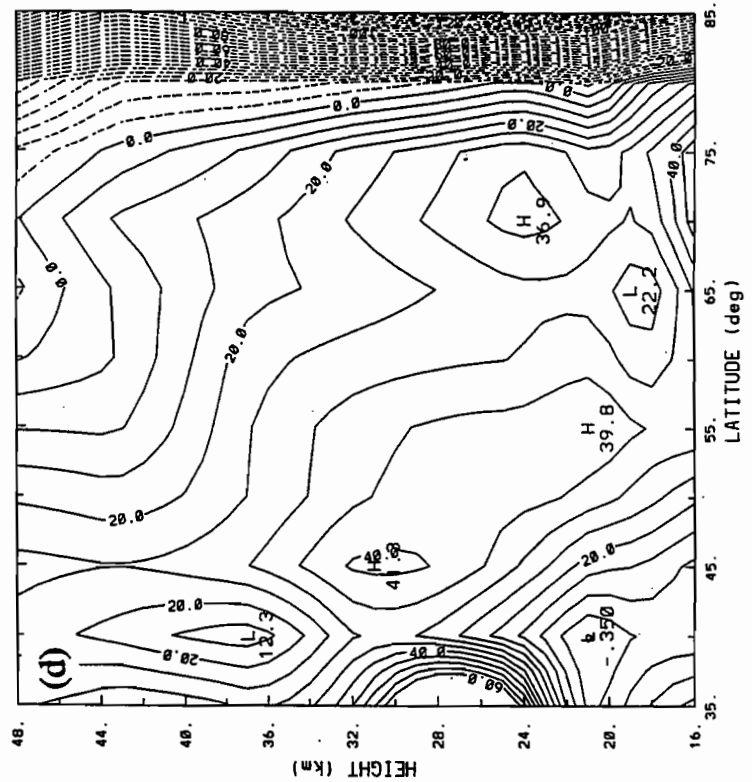


Fig. 2.3 Continued.

strength, so even the longest waves are trapped. Wave reflection off this barrier can produce standing wave patterns, giving amplitude maxima in the interior of the stratosphere, even if the waves are forced entirely from below.

(2.5) Stationary planetary waves

The amplitudes and phases of the stationary planetary waves of the monthly mean geopotential height field have been calculated from the observed data for each of the four Januaries being studied. We can write zonal wave k of the geopotential height as

$$Z_k = A_k e^{\frac{z-z_0}{2H}} \cos(k\lambda + \varphi_k), \quad (2.3)$$

where λ is longitude and z_0 is a reference height, chosen to correspond to a pressure of 100 hPa. We define the amplitude and phase to be A_k and φ_k , respectively. Note that A_k is the amplitude as usually defined, divided by $\exp((z-z_0)/2H)$. The exponential term is included in our definition of amplitude in order that A_k be proportional to the wave kinetic energy density.

Note also that the phase φ_k is not defined as the longitude of the wave crest, a definition used in some works. With our definition, there is a wave crest at longitude $-\varphi_k/k$. Thus an increase in phase with height corresponds to a wave tilting westward with height.

Figure 2.4 shows the structure of zonal wavenumbers 1 through 3 as a function of latitude and height for January 1983. One sees that wave 1 is able to propagate into the stratosphere, and has an amplitude maximum near 30 km, while waves 2 and 3 are trapped at lower levels, and have amplitudes which decrease monotonically with height. Wave 3 is seen to be more strongly trapped than wave 2. Similar behaviour is observed for the other years studied.

Figure 2.5 shows the sum of the zonal wavenumber 1 - 3 components of the monthly mean height field at a log-pressure height of 32 km (approximately 10 hPa) for January, for each of the four years studied. Note that for this figure the wave amplitudes have not been divided by a factor of $\exp((z-z_0)/2H)$. Wave 1 clearly dominates, though there is a significant wave 2 component as well, as shown by the asymmetry between the amplitudes of the high and the low. The position of the high varies little from year to year, being always located near the Bering Strait, while that of the low is much more variable, being in some years as far east as northwestern Russia, and in other years as far west as Davis Strait.

Figure 2.6 shows the structure of wave 1 for each of the four Januaries considered in this work. One notes that the behaviour of this wave is broadly similar from year to year, with an amplitude maximum near latitude 65° N and altitude 30 km. The case of January 1984 is an exception to this behaviour, with the maximum wave amplitude for that year being significantly weaker and located at a lower altitude.

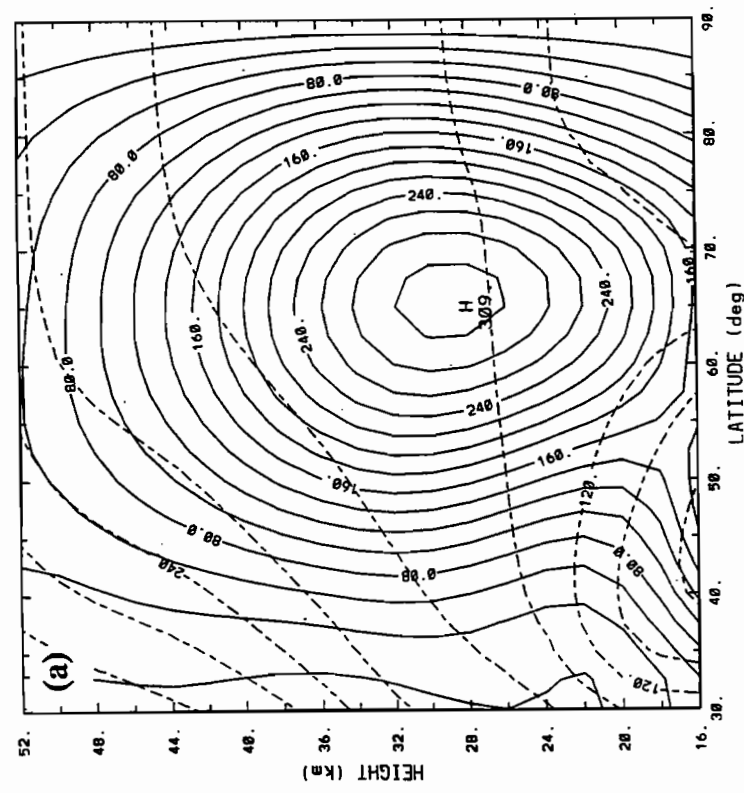
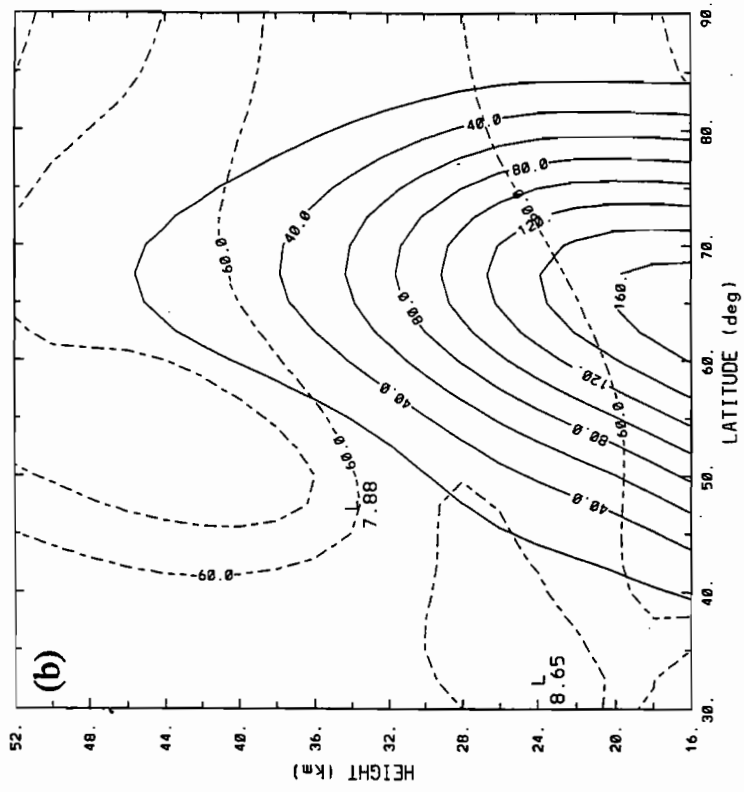


Fig. 2.4 January 1983 monthly mean stationary waves, from observations. Solid lines are amplitude (contour interval 20 m), broken lines are phase (contour interval 30°). Note that amplitudes are divided by factor of $\exp((z-z_0)/2H)$. (a) zonal wavenumber $k=1$, (b) $k=2$, (c) $k=3$.

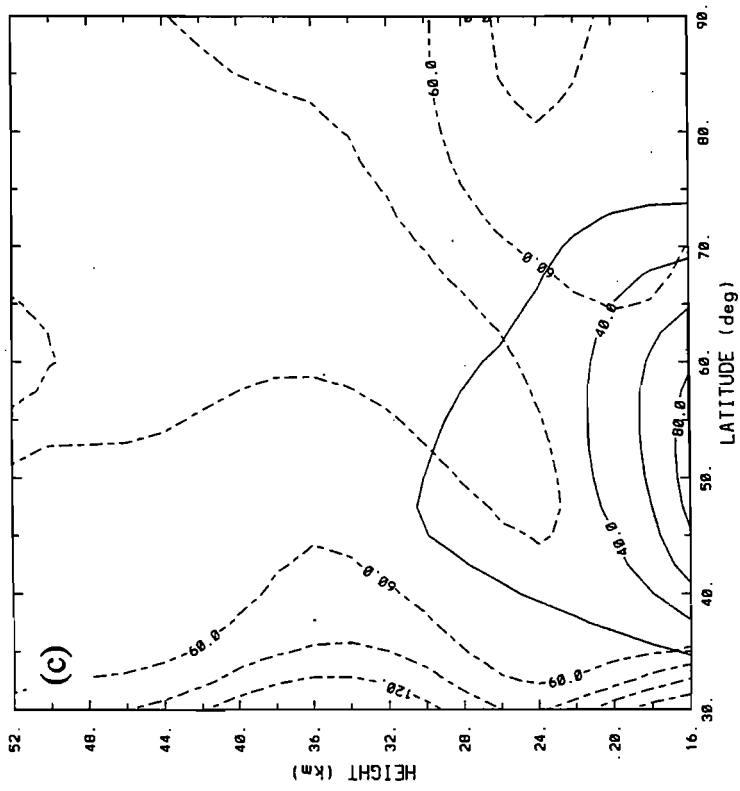


Fig. 2.4 Continued.

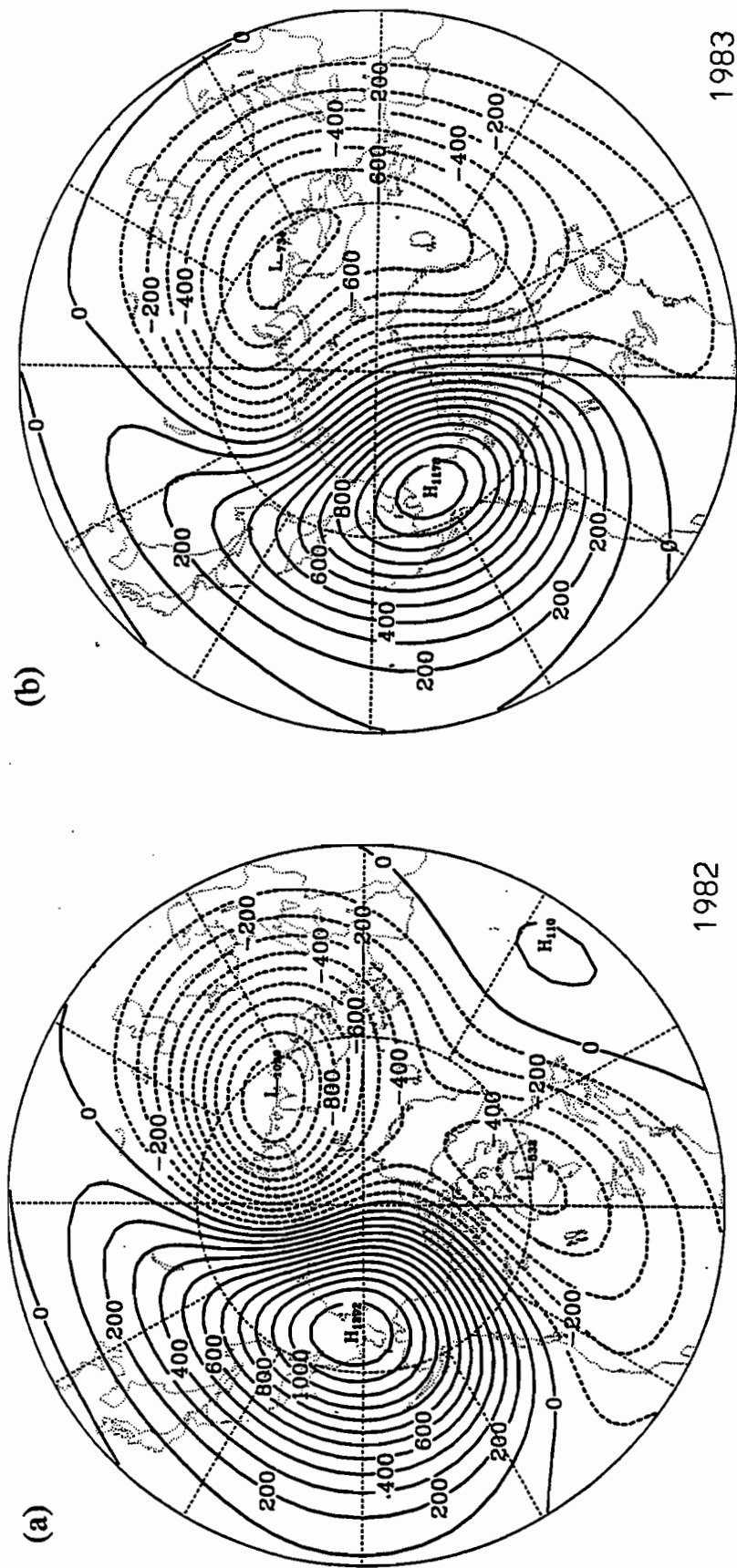


Fig. 2.5 January monthly mean geopotential height field (sum of zonal waves 1-3), from observations, for log-pressure height 32 km. Contour interval 100 m. (a) 1982, (b) 1983, (c) 1984, (d) 1986.

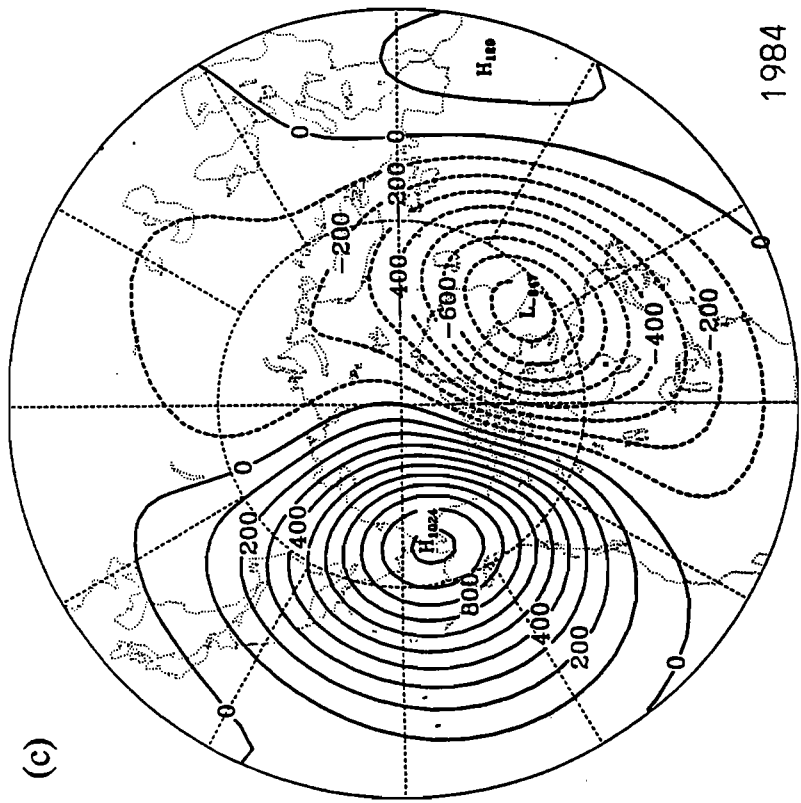
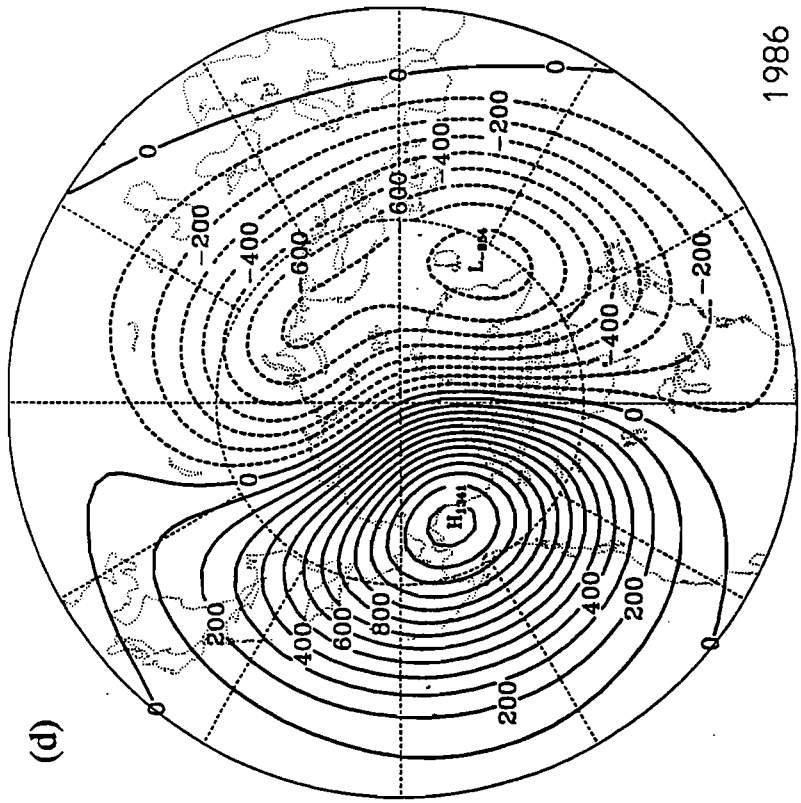


Fig. 2.5 Continued.

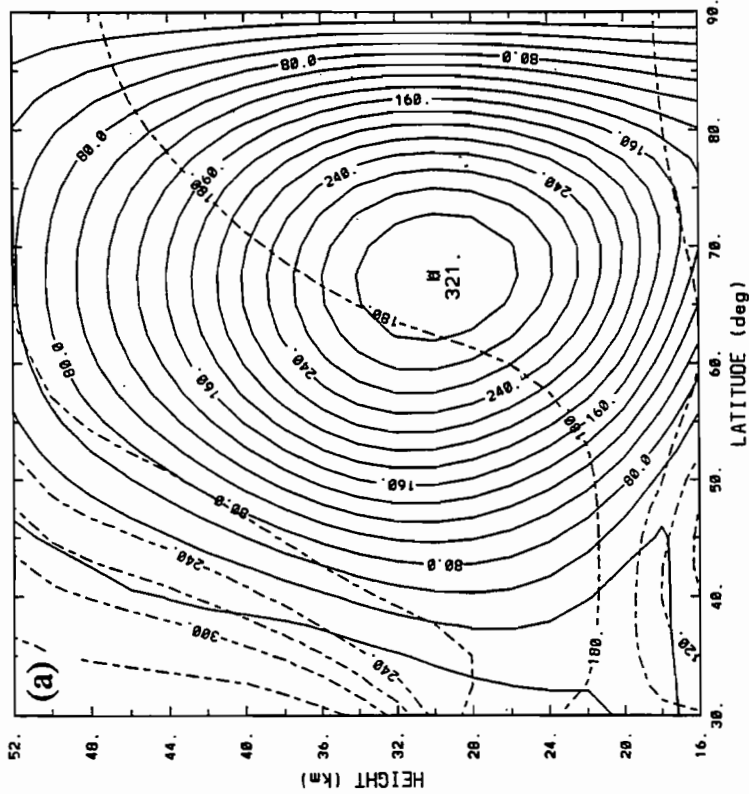
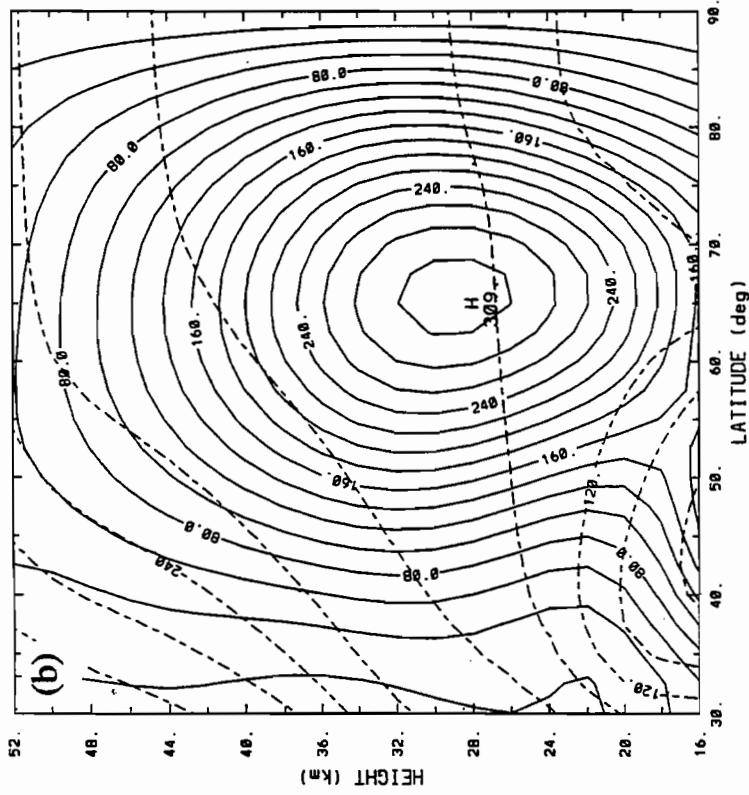


Fig. 2.6 January monthly mean stationary zonal wave $k=1$, from observations. Solid lines are amplitude (contour interval 20 m), broken lines are phase (contour interval 30°). Note that amplitudes are divided by factor of $\exp((z-z_0)/2H)$. (a) 1982, (b) 1983, (c) 1984, (d) 1986.

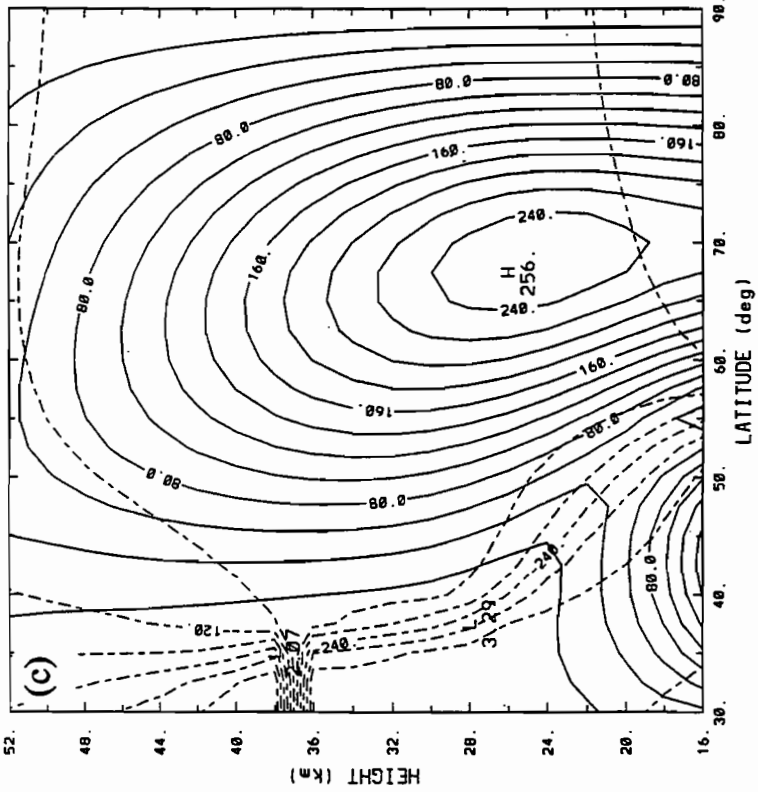
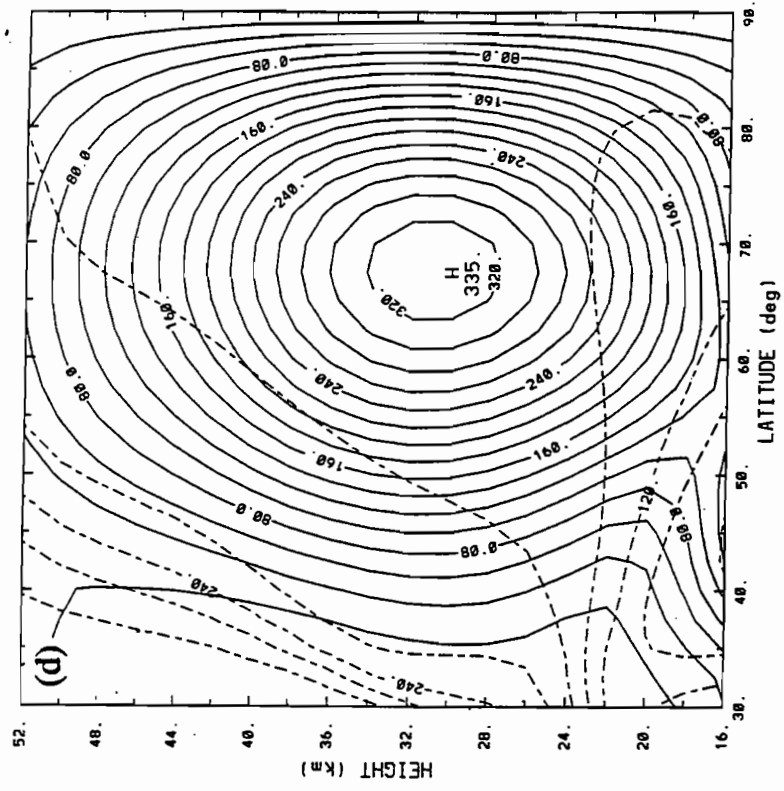


Fig. 2.6 Continued.

At the lowest level (100 hPa), however, the maximum amplitude of wave 1 is much greater in 1984 than in the other years studied, being 229 m in 1984, as compared to 150 m in 1982, 164 m in 1983, and 128 m in 1986.

The phase structure of wave 1 is also generally similar from year to year, with the wave tilting westward with height. The slope is greater at midlatitudes than at Arctic latitudes. This tilt is more pronounced in 1983 than in 1982 and 1986. Again 1984 is anomalous, showing a slight eastward tilt with height.

In the horizontal, wave 1 tends to slope eastward with increasing latitude, *i.e.* from southwest to northeast. This slope is greatest at midlatitudes and higher altitudes (above 30 km), and is weaker in the lower stratosphere and nearer the North Pole. Here too, the behaviour of wave 1 for January 1984 is anomalous. It shows very little horizontal tilt through most of the region where the amplitude is significant, and there is a southeast to northwest tilt at midlatitudes in the upper stratosphere, above 37 km.

Figure 2.7 shows the structure of wave 2 for each of the four Januaries considered in this work. Again, the behaviour of this wave is generally similar from year to year. The amplitude is a maximum at the lower boundary and at a latitude of 60-65°N. The maximum amplitude of wave 2 at 100 hPa is 228 m in 1982, 173 m in 1983, 252 m for 1984, and 181 m for 1986. For all the years studied, the amplitude decreases monotonically with height. In most cases the wave tilts westward with height. The vertical tilt of wave 2 is very weak for January 1983.

Figure 2.8 shows the sum of the zonal wavenumber 1 - 3 components of the monthly mean height field at 100 hPa, the lowest level in the data set, for January of

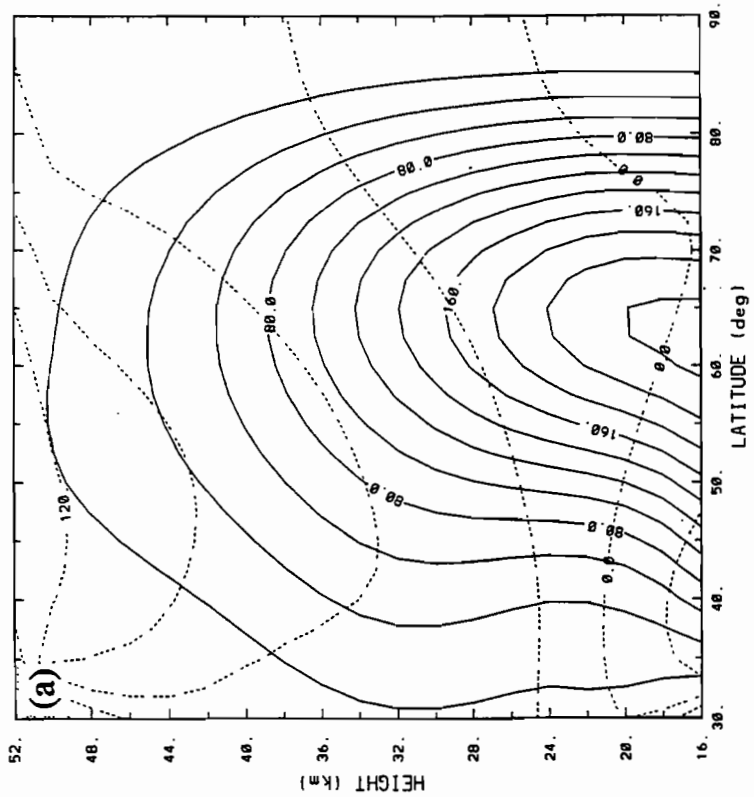
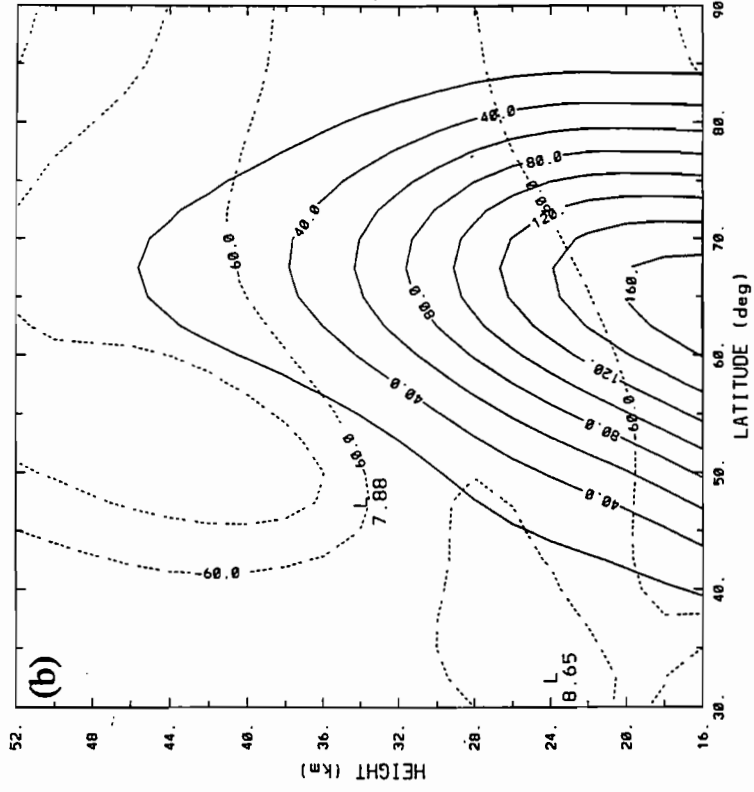


Fig. 2.7 As in Fig. 2.6, but for zonal wave $k=2$.

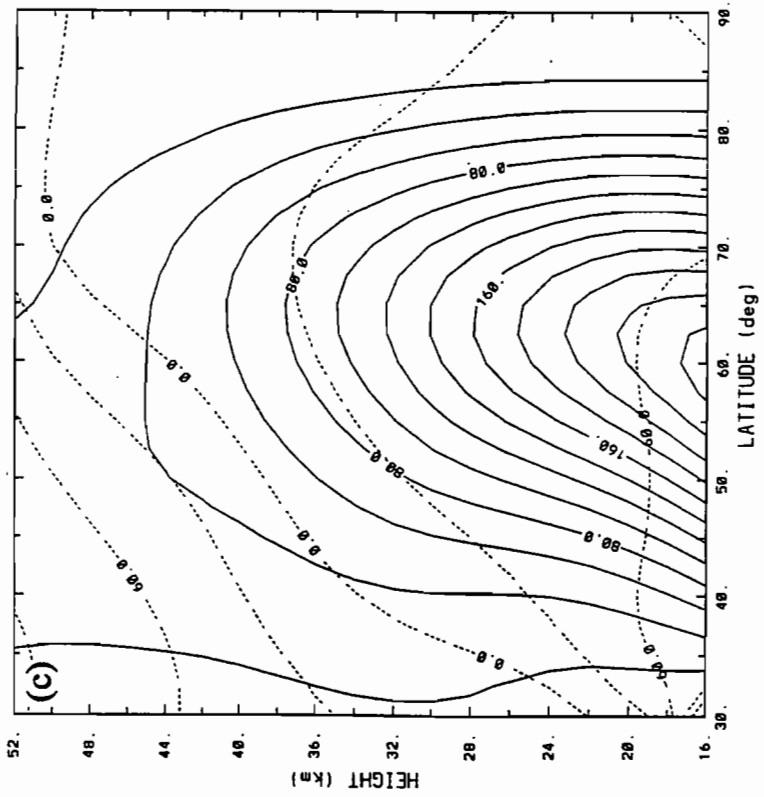
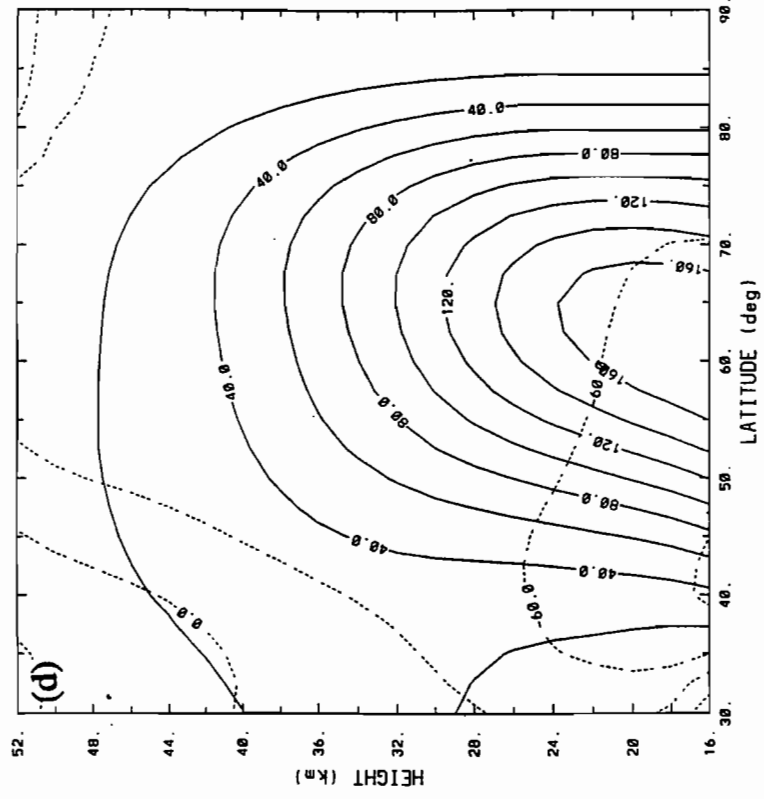


Fig. 2.7 Continued.

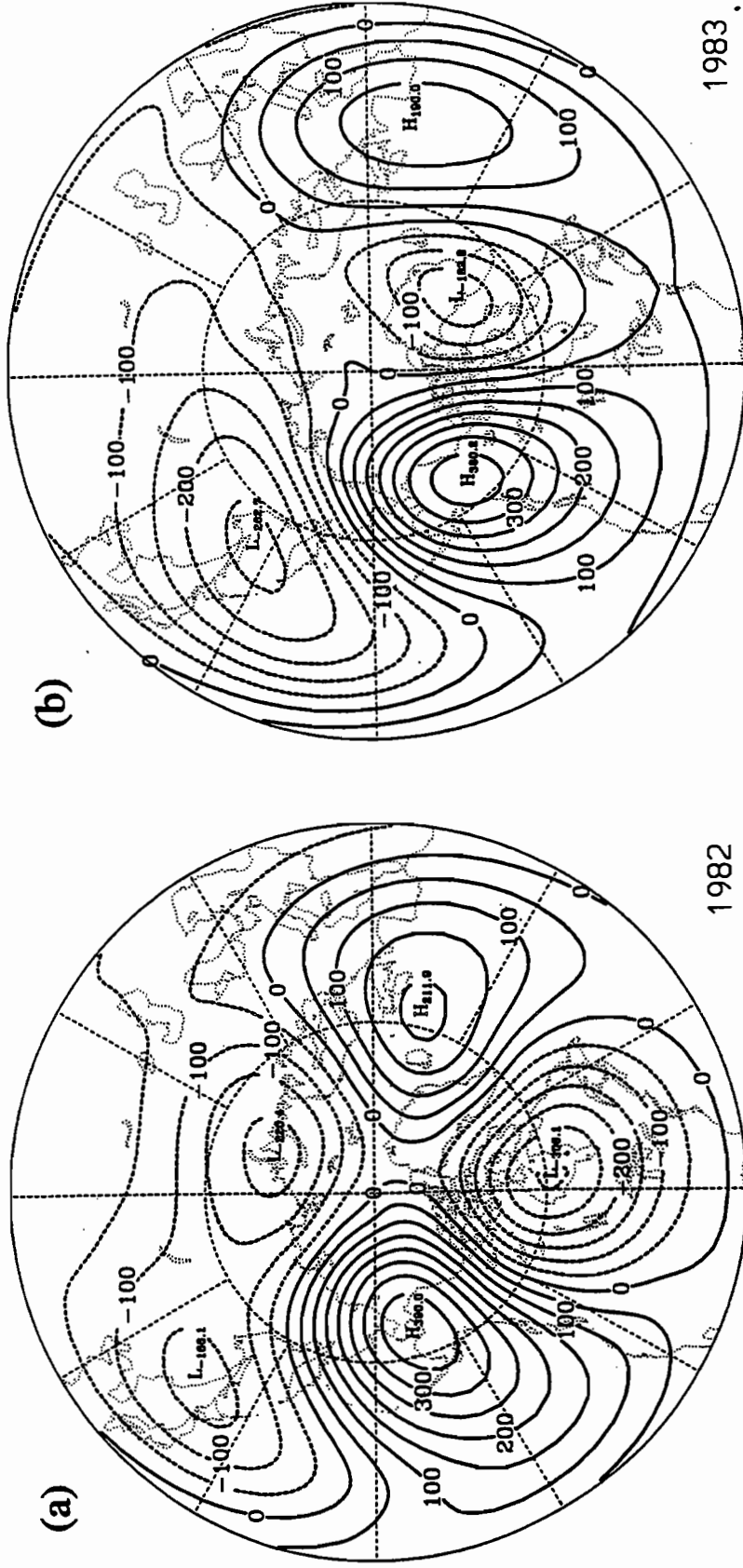


Fig. 2.8 January monthly mean geopotential height field (sum of zonal waves 1-3), from observations, for 100 hPa surface. Contour interval 50 m. (a) 1982, (b) 1983, (c) 1984, (d) 1986.

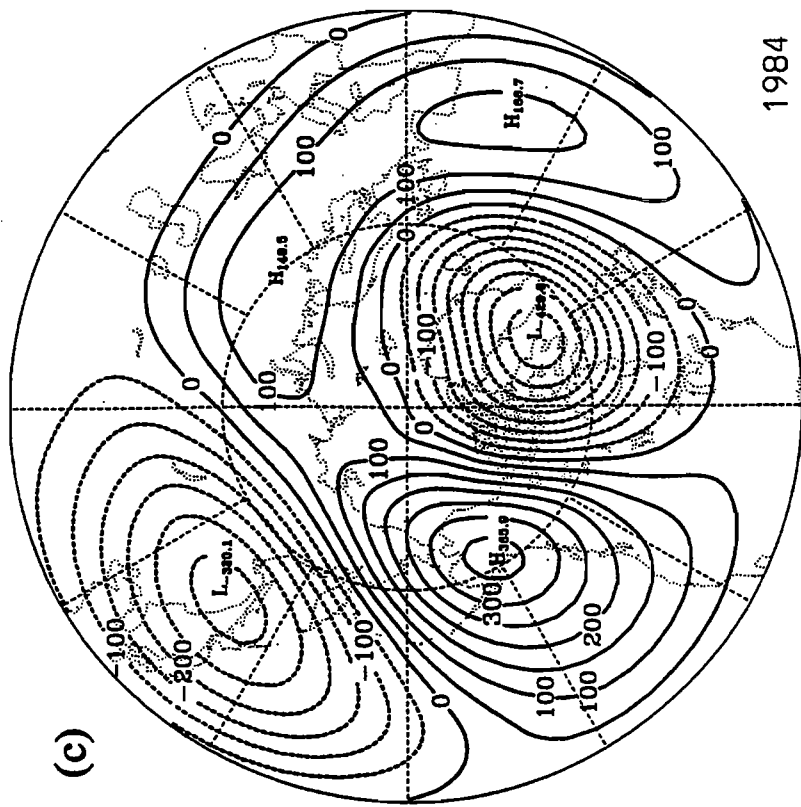
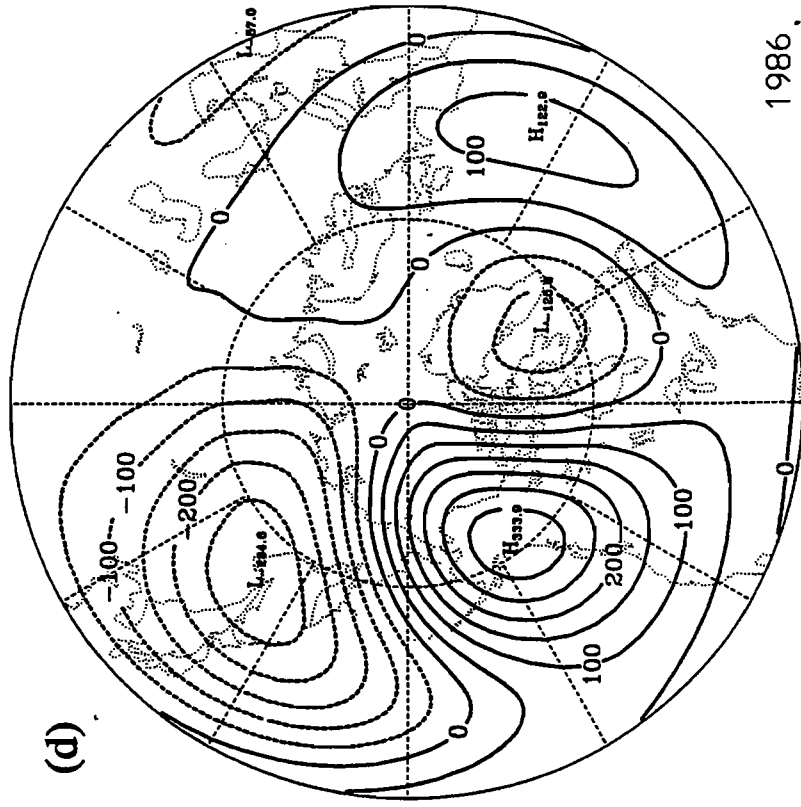


Fig. 2.8 Continued.

each of the four years studied. The high over Alaska is a nearly constant feature, with a similar position and amplitude in all the years studied. The lows vary somewhat in position, and vary greatly in amplitude, from year to year. Unlike the 32-km surface, whose pattern is dominated by wavenumber 1, this lower surface shows a strong wavenumber 2 component. These 100 hPa height fields are used as the lower boundary condition in the model described in the next chapter, and act as the principal forcing mechanism for the waves computed by this model.

CHAPTER 3

DESCRIPTION OF MODEL

(3.1) Introduction

This chapter commences with a derivation of the equations to be used in this model, beginning from the primitive equations. Because the expressions for some of the coefficients which arise in this derivation are very long, they have been placed in Appendix A. The numerical method of solution of the model equations is described in Appendix B. The choice of the model domain and the conditions imposed at the boundaries of that domain are discussed in Section 3.3.

The model requires that the zonal mean state be specified. The zonal mean wind is computed from observed data, as discussed in Chapter 2 above. A number of other parameters, such as the buoyancy frequency and the Newtonian cooling and Rayleigh friction coefficients, must also be specified. The choice of these parameters is discussed in Section 3.4.

For certain zonal mean states, the model equations reduce to the Laplace tidal equations. Since the solution to these equations is known, one can perform a partial test of the model. This testing is described in Section 3.5.

As part of this study, forcing fields due to the monthly mean of the transient momentum and heat fluxes were computed from observations. The derivation in Section 3.2 gives equations for this forcing. However, numerical difficulties arose when these

equations were used to compute the forcing due to transients. A quasi-geostrophic approximation has therefore been used to simplify the computation of these forcing fields. This question is discussed in Section 3.6.

In another portion of this study, solutions are found to the model equations for the case where nonlinear interactions between the stationary waves are included. Inclusion of these nonlinearities renders the solution of the model equations substantially more difficult. An iterative technique, described in Section 3.7, has been employed to solve the system of nonlinear equations.

The calculations required for this iterative procedure generate spurious small-scale structure in the geopotential field calculated by the model. If these structures are not removed, they will cause the model solution to diverge. In order to prevent this, smoothing has been applied to the model fields at each iteration, as explained in Section 3.8.

(3.2) Derivation of model equations

The model is based upon the primitive equations in log-pressure coordinates on the sphere:

$$\frac{Du}{Dt} - \left[f + \frac{u \tan \theta}{a} \right] v + \frac{\Phi_\lambda}{a \cos \theta} = X, \quad (3.1)$$

$$\frac{Dv}{Dt} + \left[f + \frac{u \tan \theta}{a} \right] u + \frac{\Phi_\theta}{a} = Y, \quad (3.2)$$

$$\Phi_z = H^{-1}RT, \quad (3.3)$$

$$\frac{DT}{Dt} + \frac{\kappa T w}{H} = \frac{J}{c_p}, \quad (3.4)$$

$$\frac{[u_\lambda + (v \cos \theta)_\theta]}{a \cos \theta} + \frac{(\rho_0 w)_z}{\rho_0} = 0, \quad (3.5)$$

(e.g. Andrews *et al.*, 1987). These are, respectively, the zonal momentum, meridional momentum, hydrostatic, thermodynamic, and continuity equations. Most symbols have their conventional meanings and are defined in the list of symbols. Subscripts λ , θ , and z denote partial derivatives. X , Y , and J are, respectively, the zonal and meridional components of the friction force and the diabatic heating rate, whose forms are as yet unspecified.

Eliminating T between (3.3) and (3.4), expanding the material derivative D/Dt , and performing some algebraic manipulation gives the system of equations:

$$a \frac{\partial u}{\partial t} + \frac{u}{\cos \theta} \frac{\partial u}{\partial \lambda} + \frac{v}{\cos \theta} \frac{\partial}{\partial \theta} (u \cos \theta) + w^* \frac{\partial u}{\partial z} - f^* v + \frac{\Phi_\lambda}{\cos \theta} = aX, \quad (3.6)$$

$$a \frac{\partial v}{\partial t} + \frac{u}{\cos \theta} \frac{\partial v}{\partial \lambda} + v \frac{\partial v}{\partial \theta} + w^* \frac{\partial v}{\partial z} + u^2 \tan \theta + f^* u + \Phi_\theta = aY, \quad (3.7)$$

$$a \frac{\partial \Phi_z}{\partial t} + \frac{u}{\cos \theta} \frac{\partial \Phi_z}{\partial \lambda} + v \frac{\partial \Phi_z}{\partial \theta} + w^* N^2 = \frac{a\kappa J}{H}, \quad (3.8)$$

$$\frac{1}{\cos \theta} \frac{\partial u}{\partial \lambda} + \frac{1}{\cos \theta} \frac{\partial}{\partial \theta} (v \cos \theta) + \frac{\partial w^*}{\partial z} - \frac{w^*}{H} = 0, \quad (3.9)$$

where $w^* = aw$ and $f^* = af$.

We write the variables u , v , w^* , and Φ as the sum of time-mean and transient parts (e.g. $u(\lambda, \theta, z, t) = \bar{u}(\lambda, \theta, z) + u'(\lambda, \theta, z, t)$), then take the time mean of (3.6)-(3.9).

This results in the following system of equations:

$$\frac{\bar{u}}{\cos \theta} \frac{\partial \bar{u}}{\partial \lambda} + \frac{\bar{v}}{\cos \theta} \frac{\partial}{\partial \theta} (\bar{u} \cos \theta) + \bar{w}^* \frac{\partial \bar{u}}{\partial z} - f^* \bar{v} + \frac{\bar{\Phi}_\lambda}{\cos \theta} = a\bar{X} + (Tr)_u, \quad (3.10)$$

$$\frac{\bar{u}}{\cos\theta} \frac{\partial \bar{v}}{\partial \lambda} + \bar{v} \frac{\partial \bar{v}}{\partial \theta} + \bar{w} \cdot \frac{\partial \bar{v}}{\partial z} + \bar{u}^2 \tan\theta + f^* \bar{u} + \bar{\Phi}_\theta = a \bar{Y} + (Tr)_{v,} \quad (3.11)$$

$$\frac{\bar{u}}{\cos\theta} \frac{\partial \bar{\Phi}_z}{\partial \lambda} + \bar{v} \frac{\partial \bar{\Phi}_z}{\partial \theta} + \bar{w} \cdot \bar{N}^2 = \frac{a \kappa \bar{J}}{H} + (Tr)_{T,} \quad (3.12)$$

$$\frac{1}{\cos\theta} \frac{\partial \bar{u}}{\partial \lambda} + \frac{1}{\cos\theta} \frac{\partial}{\partial \theta} (\bar{v} \cos\theta) + \frac{\partial \bar{w}^*}{\partial z} - \frac{\bar{w}^*}{H} = 0, \quad (3.13)$$

where the transient terms are included in $(Tr)_{u,}$, $(Tr)_{v,}$, and $(Tr)_{T,}$, which are detailed in Appendix A.

We now separate the time means into zonal mean and stationary wave parts. We also neglect the mean meridional circulation, so

$$\begin{aligned} \bar{u}(\lambda, \theta, z) &= [\bar{u}] (\theta, z) + \hat{u}(\lambda, \theta, z) \\ \bar{v}(\lambda, \theta, z) &= \hat{v}(\lambda, \theta, z) \\ \bar{w}^*(\lambda, \theta, z) &= \hat{w}(\lambda, \theta, z) \\ \bar{\Phi}(\lambda, \theta, z) &= [\bar{\Phi}] (\theta, z) + \hat{\Phi}(\lambda, \theta, z) \end{aligned} \quad (3.14)$$

Then (3.10)-(3.13) give, after subtraction of the zonal mean part:

$$\omega \frac{\partial \hat{u}}{\partial \lambda} + \beta^* \hat{v} + \frac{\partial [u]}{\partial z} \hat{w} + \frac{1}{\cos \theta} \frac{\partial \hat{\Phi}}{\partial \lambda} = -a\nu \hat{u} + (St)_u + (Tr)_u, \quad (3.15)$$

$$\xi^* \hat{u} + \omega \frac{\partial \hat{v}}{\partial \lambda} + \frac{\partial \hat{\Phi}}{\partial \theta} = -a\nu \hat{v} + (St)_v + (Tr)_v, \quad (3.16)$$

$$Z^* \hat{v} + [N^2] \hat{w} + \omega \frac{\partial \hat{\Phi}_z}{\partial \lambda} = -a\alpha \hat{\Phi}_z + (St)_T + (Tr)_T, \quad (3.17)$$

$$\frac{1}{\cos \theta} \frac{\partial \hat{u}}{\partial \lambda} + \frac{1}{\cos \theta} \frac{\partial}{\partial \theta} (\hat{v} \cos \theta) + \frac{\partial \hat{w}}{\partial z} - \frac{\hat{w}}{H} = 0, \quad (3.18)$$

where the nonlinear interactions between the stationary wave terms are found in $(St)_u$, $(St)_v$, and $(St)_T$, which are detailed in Appendix A. The coefficients ω , β^* , ξ^* , and Z^* are functions of the zonal mean state, and are also detailed in Appendix A. The friction (X, Y) and the diabatic heating J are assumed to take the form of Rayleigh friction with coefficient ν and Newtonian cooling with coefficient α .

Note that in deriving (3.16) from (3.11) we have used the fact that for steady, purely zonal flow with no friction or diabatic heating, we have

$$f^* [u] + [u]^2 \tan \theta + [\Phi]_\theta = 0. \quad (3.19)$$

Now we let

$$\begin{bmatrix} \hat{u}(\lambda, \theta, z) \\ \hat{v}(\lambda, \theta, z) \\ \hat{w}(\lambda, \theta, z) \\ \hat{\Phi}(\lambda, \theta, z) \end{bmatrix} = \sum_{\substack{m=-M \\ m \neq 0}}^M \begin{bmatrix} \tilde{u}_m(\theta, z) \\ i \tilde{v}_m(\theta, z) \\ i \tilde{w}_m(\theta, z) \\ \tilde{\Phi}_m(\theta, z) \end{bmatrix} \exp \left[im\lambda + \frac{z-z_0}{2H} \right], \quad (3.20)$$

and note that since the left hand side of (3.20) is real, we have $\tilde{u}_{-m} = \tilde{u}_m^*$, $\tilde{v}_{-m} = -\tilde{v}_m^*$, $\tilde{w}_{-m} = -\tilde{w}_m^*$, $\tilde{\Phi}_{-m} = \tilde{\Phi}_m^*$, where the asterisk denotes the complex conjugate.

Substituting (3.20) in (3.15)-(3.18), multiplying the resulting equations by $\exp(-ik\lambda - (z-z_0)/2H)$, and integrating around a latitude circle, our system of

equations takes the form

$$\Delta_k \tilde{u}_k + \beta^* \tilde{v}_k + \frac{\partial [u]}{\partial z} \tilde{w}_k + \frac{k}{\cos \theta} \tilde{\Phi}_k = P_k^S + P_k^T, \quad (3.21)$$

$$\xi^* \bar{u}_k - \Delta_k \bar{v}_k + \frac{\partial \bar{\Phi}_k}{\partial \theta} = Q_k^S + Q_k^T, \quad (3.22)$$

$$Z^* \bar{v}_k + [N^2] \bar{w}_k + \Gamma_k \left[\frac{\partial}{\partial z} + \frac{1}{2H} \right] \bar{\Phi}_k = R_k^S + R_k^T, \quad (3.23)$$

$$\frac{k}{\cos \theta} \bar{u}_k + \frac{1}{\cos \theta} \frac{\partial}{\partial \theta} (\bar{v}_k \cos \theta) + \left[\frac{\partial}{\partial z} - \frac{1}{2H} \right] \bar{w}_k = 0, \quad (3.24)$$

where $\Delta_k = k\omega - i\nu$, $\Gamma_k = k\omega - i\alpha$, and where P_k^j , Q_k^j , and R_k^j ($j = S$ or T), detailed in Appendix A, include the nonlinear interactions among the stationary waves and among the transients, respectively.

We can solve (3.21)-(3.23) to give \bar{u}_k , \bar{v}_k , and \bar{w}_k as functions of $\bar{\Phi}_k$, giving

$$\tau \begin{bmatrix} \bar{u}_k \\ \bar{v}_k \\ \bar{w}_k \end{bmatrix} = \begin{bmatrix} -\Delta_k [N^2] & Z^* \frac{\partial [u]}{\partial z} - \beta^* [N^2] & \Delta_k \frac{\partial [u]}{\partial z} \\ -\xi^* [N^2] & \Delta_k [N^2] & -Z^* \\ \xi^* Z^* & -Z^* \Delta_k & -\epsilon \end{bmatrix} \begin{bmatrix} \frac{k \bar{\Phi}_k}{\cos \theta} - P_k^S - P_k^T \\ \frac{\partial \bar{\Phi}_k}{\partial \theta} - Q_k^S - Q_k^T \\ \Gamma_k \left[\frac{\partial \bar{\Phi}_k}{\partial z} + \frac{\bar{\Phi}_k}{2H} \right] - R_k^S - R_k^T \end{bmatrix}, \quad (3.25)$$

where ϵ and τ are functions of the zonal mean state, detailed in Appendix A.

Finally, we substitute (3.25) into (3.24) to obtain the single equation

$$A \frac{\partial^2 \tilde{\Phi}_k}{\partial z^2} + B \frac{\partial^2 \tilde{\Phi}_k}{\partial z \partial \theta} + C \frac{\partial^2 \tilde{\Phi}_k}{\partial \theta^2} + D \frac{\partial \tilde{\Phi}_k}{\partial z} + E \frac{\partial \tilde{\Phi}_k}{\partial \theta} + F \tilde{\Phi}_k = G^S + G^T, \quad (3.26)$$

where the coefficients $A-G$ are detailed in Appendix A.

We wish to solve (3.26) to determine the structure of the stationary planetary waves $\tilde{\Phi}_k$. In principle, one needs to do so for all values of the zonal wavenumber k in order to completely determine the state of the atmosphere. In practice, it is found that small-scale waves are trapped in the troposphere and cannot propagate into the stratosphere. We therefore need only retain the largest scale waves in our model. We choose to retain zonal wavenumbers 1 through 3. This gives us three equations of the form of (3.26) to be solved.

Note that G^S is a nonlinear function of $\tilde{\Phi}_k$, and its presence in (3.26) gives a system of three coupled nonlinear differential equations to be solved. Setting $G^S = 0$ reduces the system to one of three uncoupled linear differential equations.

(3.3) Model domain and boundary conditions

The model equations are solved on a hemispheric domain extending from the equator to the North Pole. A global domain would seem the most natural choice, but as noted in the introduction, the easterly zonal mean circulation in the summer stratosphere prevents propagation of planetary waves into this region, so the flow is almost purely zonal and is not of interest for the present study. The domain can therefore be restricted to the winter hemisphere.

At the North Pole, we impose the boundary condition

$$\tilde{\Phi}_k \sim (\pi/2 - \theta)^k, \quad (3.27)$$

while the boundary condition at the equator is that the wave be symmetric about the equator. The boundary condition at the pole is a consequence of the geometry of the model (Matsuno, 1970). At the equator, the physical justification for this boundary condition is less obvious. However, as will be discussed in more detail below, the model is not expected to produce realistic results for tropical latitudes, due to the presence of a critical layer on which the mean zonal wind vanishes. These latitudes can be taken to be a computational region, in which a simple boundary condition may be chosen, motivated by convenience.

The vertical domain of the model is taken to extend from 16 to 80 km. At the lower boundary, the observed stationary wave structure is imposed as a boundary condition. This constitutes the principal forcing mechanism in the model, and represents mainly the effect of waves generated at the earth's surface by topography and by land-sea thermal contrast, which propagate upward into the stratosphere.

The location of the upper boundary and the choice of an upper boundary condition are somewhat arbitrary, since the real atmosphere does not have an upper boundary. It is observed that the westerly zonal flow, whose strength increases with height, tends to trap the wave energy in the stratosphere and prevent propagation in the mesosphere. This can be reproduced in the model by imposing the condition that the waves vanish at the upper boundary, and including a "sponge layer" with large dissipation in the upper

portion of the model. This sponge layer is a computational region, where the model is not expected to generate realistic results.

In order to test the effect of this upper boundary condition, the model has been run with the upper boundary raised from 80 to 100 km. The solution obtained with the upper boundary at 100 km is found to differ significantly from that obtained with the upper boundary at 80 km only at altitudes above 65 km. Below this height, in the region of interest for this study, the two models give virtually identical results. This suggests that the choice of an upper boundary at 80 km is adequate for the purposes of this study.

(3.4) Zonal mean state

The coefficients A-F in (3.26) are functions of the mean zonal state only. $[u]$ is calculated using (3.19). Beginning with a data set, described in Chapter 2, made up of daily values of height fields, we calculate the zonal and time mean geopotential $[\Phi]$. We replace the derivative in (3.19) by a centred finite difference, and compute $[u]$ on each pressure surface and at each gridpoint in latitude for the observed data set. Bicubic spline interpolation is then used to project the mean zonal wind field onto the latitude-height grid to be used in the model. Given the mean zonal wind field $[u]$, the derived quantities ω , β^* , ξ^* , and Z^* can be computed using (A.7)-(A.10), where again derivatives have been replaced by centred finite differences.

Previous investigators (e.g Schoeberl and Geller, 1977) have found that the stationary wave structure is relatively insensitive to the value of the buoyancy frequency. We therefore take $[N^2]$ to have a constant value of $4 \times 10^{-4} \text{ s}^{-1}$.

The frictional force in the horizontal momentum equations and the diabatic term in the thermodynamic equation are assumed to take the form of Rayleigh friction and Newtonian cooling, respectively. The Newtonian cooling coefficient is taken from Holton and Mass (1976). It is a function of height only, and varies from about $(20 \text{ days})^{-1}$ at the bottom of the model domain to $(4.6 \text{ days})^{-1}$ at the top. The Newtonian cooling coefficient, in $(\text{seconds})^{-1}$, is given by

$$\alpha = (1.5 + \tanh(z/H - 5)) \times 10^{-6}, \quad (3.28)$$

where z is the log-pressure height and H is the scale height, taken to have a constant value of 7000 m. Below 50 km, this profile is very similar to that of Dickinson (1973). At higher altitudes, the Newtonian cooling rate remains large, and serves to absorb wave energy.

Below 50 km, the Rayleigh friction coefficient, in $(\text{seconds})^{-1}$, is given by the equation

$$\nu = 5 \times 10^{-7} \{ 200 - 199 \tanh^2(4\theta) \}, \quad (3.29)$$

where θ is the latitude in radians. Above 50 km, this coefficient is increased by the additional term

$$5 \times 10^{-6} \{e^{(z/40-1.25)} - 1\}, \quad (3.30)$$

where z is the height in kilometres.

Equation (3.29) gives a value of $(23 \text{ days})^{-1}$ for the Rayleigh friction coefficient at the North Pole and below 50 km. Above 50 km, the inclusion of the additional term (3.30) causes the Rayleigh friction coefficient to increase in value, to a maximum of $(2 \text{ days})^{-1}$ at the upper limit of the model. This serves as a sponge layer to prevent reflection from the upper boundary.

Without thermal and frictional damping, the model equation (3.26) would be singular at points where the mean zonal wind vanishes. Inclusion of damping serves to remove this singularity, but with weak damping the equation is nearly singular in this critical layer region, and the model does not perform well in reproducing the observed stationary wave structure. It is found to be necessary to introduce strong Rayleigh friction damping at low latitudes, where the mean zonal wind is weak, in order to obtain realistic results from the model. This is the justification for the latitudinal dependence of the Rayleigh friction, as given in (3.29) above. The choice of the functional dependence of the damping on latitude and the values of the coefficients in the (3.28) are somewhat arbitrary. It has been found by trial and error that the nonlinear model does not converge to a solution when smaller values of the Rayleigh friction coefficient are used at low latitudes. Because the damping is unrealistically large at low latitudes, we do not expect the model to produce realistic results south of 30°N .

(3.5) Test of model using Hough functions

In the case where there is no dissipation ($\alpha = \nu = 0$), a constant buoyancy frequency [N^2], a mean zonal state in solid-body rotation ($\omega = \text{constant}$), and no nonlinear interactions ($G^s = G^T = 0$), the model equation (3.26) reduces to the Laplace tidal equation. In this case, the solutions are separable into horizontal and vertical parts. The horizontal structure equation has an infinite number of eigensolutions known as Hough functions, described in detail by Longuet-Higgins (1968). The vertical structure equation has a solution which is either a sinusoidal function of height or an exponential decaying with increasing height. The functional form of the vertical solution and its wavelength (for a sinusoidal solution) or rate of decay (for an exponential solution) depend on the eigenvalue of the corresponding horizontal solution.

To test the model, it has been run with a mean zonal state in solid-body rotation, no dissipation, and no nonlinear interactions. The wave structure at the lower boundary is specified to be a Hough function, and the model run to determine the wave structure in the interior of the model domain. This procedure has been repeated using several different values of the rotation rate ω and for different Hough modes. All of the modes tested represented vertically trapped waves.

The Laplace tidal equation is singular at a latitude θ given by

$$\theta = \sin^{-1} \frac{k\omega}{2(a\Omega + \omega)}, \quad (3.31)$$

where k is the zonal wavenumber, ω the zonal wind velocity at the equator for the atmosphere in solid-body rotation, and Ω the angular velocity of Earth. For the low zonal wavenumbers used in this study, and for values of ω which approximate observed mean zonal winds, the singular latitude is found near the equator. In order to perform these tests, the model was modified slightly to exclude the singular latitude from the domain.

In all cases, the numerical solution is found to agree very well with the analytic solution, *i.e.* the horizontal structure of the model solution is, throughout the model domain, that of the Hough function specified as the lower boundary condition, with the amplitude of the waves decaying exponentially with height at the rate predicted by the analytic solution. Near the top levels of the model, the rate of decay of the amplitude is slightly larger than that predicted analytically, since the upper boundary condition forces the solution to go to zero at a finite height, instead of extending to infinity. The ability of the model to reproduce the analytic result for this special case provides a partial test that model derivation and computer coding have been performed correctly.

(3.6) Computation of transient forcing fields

G^T is to be computed from observations. Our data set consists only of geopotential height fields, while G^T depends on the wind fields, through (A.1)-(A.3). An attempt was made to compute G^T using the model equations given in the appendix. In (A.1)-(A.3), the terms involving the vertical velocity were ignored. Daily values of the transient horizontal winds u' and v' were computed from the height fields, assuming geostrophy. The transient forcing field G^T was then computed using (A.1)-(A.3), (A.14)-(A.16), (A.26)-(A.28), and (A.25). This method did not yield satisfactory results, with G^T taking on very large values near the North Pole.

Note that some terms in (A.25) contain a factor of $\cos \theta$ in the denominator. G will remain finite at the pole only if $kX - Y \sin \theta$ goes to zero at least as fast as $\cos \theta$. It can be shown analytically that this condition is indeed satisfied. However, when G^T is calculated numerically, this condition does not hold, either due to errors in the data set or to inaccuracies due to the finite resolution of the grid used for the calculations. This results in the computed values of G^T blowing up near the pole.

In order to determine whether this problem resulted from insufficient accuracy of the geostrophic winds, the calculations were repeated using "balance winds," as defined by Randel (1987). This failed to resolve the difficulty.

We have therefore resorted to a quasi-geostrophic formulation of the forcing field due to transients, rather than one derived from the primitive equations. It can be shown that for quasi-geostrophic flow, the forcing due to transients in (3.26) takes the form

$$G^T = \frac{if^3 N^2}{2\pi} e^{-\frac{z_0-z}{2H}} \int_{-\pi}^{\pi} \left\{ aN^2 \nabla \cdot \overline{V'_g \zeta'_g} + \frac{Rf^*}{H} \left(\frac{\partial}{\partial z} - \frac{1}{H} \right) \nabla \cdot \overline{V'_g T'} \right\} e^{-ik\lambda} d\lambda, \quad (3.32)$$

where $\nabla \cdot$ is the horizontal divergence operator on the unit sphere, V'_g is the transient geostrophic wind, and ζ'_g the transient geostrophic vorticity, computed from

$$\zeta'_g = \frac{1}{f} \nabla^2 \Phi'. \quad (3.33)$$

With this formulation, the computed values of G^T remain well-behaved near the pole.

(3.7) Iterative solution technique for nonlinear model

The values of G^T are computed from observations. In contrast, the values of G^S , the term representing the nonlinear interactions among the stationary waves, are a function of the model solutions $\tilde{\Phi}_k$. An iterative method is used to solve the model equation (3.26). Let $\tilde{\Phi}_k^j$ be the solution found on the j th iteration. The model equation (3.26) may be written in the form

$$L(\tilde{\Phi}_k) = G^S(\tilde{\Phi}_m, \tilde{\Phi}_n) + G^T, \quad (3.34)$$

where $L(\tilde{\Phi}_k)$ represents the left-hand side of (3.26) and is a linear function of $\tilde{\Phi}_k$, G^S is a nonlinear function of $\tilde{\Phi}_k$ for the different values of the wavenumber k , while G^T is independent of the solution $\tilde{\Phi}_k$. For the first iteration, we set G^S to zero and solve

$$L(\tilde{\Phi}_k^1) - G^T. \quad (3.35)$$

For subsequent iterations we solve

$$L(\tilde{\Phi}_k^j) - G^S(\tilde{\Phi}_m^{j-1}, \tilde{\Phi}_n^{j-1}) + G^T. \quad (3.36)$$

As a measure of the convergence of this method to a solution of (3.26), we may compute the residual

$$L(\tilde{\Phi}_k^j) - G^S(\tilde{\Phi}_m^j, \tilde{\Phi}_n^j) - G^T. \quad (3.37)$$

This will tend to zero if the iterative method is converging to a solution. Using (3.36), the residual (3.37) is equivalent to

$$\delta G_k^S - G^S(\tilde{\Phi}_m^{j-1}, \tilde{\Phi}_n^{j-1}) - G^S(\tilde{\Phi}_m^j, \tilde{\Phi}_n^j). \quad (3.38)$$

In order to obtain a single number to serve as a measure of convergence, we transform δG_k^S from Fourier space to real space in longitude, via

$$\delta \tilde{G}(\lambda, \theta, z) = 2 \sum_{k=1}^3 \operatorname{Re} \{ \delta G_k^S(\theta, z) e^{ik\lambda} \}. \quad (3.39)$$

We similarly transform the nonlinear forcing field G_k^S via

$$\tilde{G}(\lambda, \theta, z) = 2 \sum_{k=1}^3 \operatorname{Re} \{ G_k^S(\theta, z) e^{ik\lambda} \}. \quad (3.40)$$

We then integrate the square of the residual over the domain of validity of the model, taken to extend from 16 to 50 km and from 30°N to 90°N, and normalize by the square of the nonlinear forcing field integrated over the same domain, *i.e.* we compute

$$\Delta G = \frac{\int_{16}^{50} \int_{\pi/6}^{\pi/2} \int_{-\pi}^{\pi} \{ \delta \tilde{G}(\lambda, \theta, z) \}^2 \cos \theta \, d\lambda \, d\theta \, dz}{\int_{16}^{50} \int_{\pi/6}^{\pi/2} \int_{-\pi}^{\pi} \{ \tilde{G}(\lambda, \theta, z) \}^2 \cos \theta \, d\lambda \, d\theta \, dz}. \quad (3.41)$$

We shall consider the iteration process to have converged to a solution when the value of ΔG falls below 10^{-3} .

For several cases, we have continued the iterative process after this criterion has been met, in an effort to determine whether this criterion corresponds well to an intuitive notion of convergence. In one case, for example, the criterion of $\Delta G < 10^{-3}$ was met after 14 iterations. Calculations were continued for a total of 40 iterations. It was found that ΔG continued to decrease monotonically at each iteration, that the values of $\tilde{\Phi}_k$ at a given gridpoint varied by less than 0.3% from the 14th to the 40th iteration, and that

graphs of Φ_k as a function of latitude and height show no variation upon visual inspection for all of the iterations from 14 to 40. Similar results were obtained for other cases. It therefore appears that this criterion for convergence is a reasonable one.

In some cases, this criterion is never attained. ΔG is found to decrease for a finite number of iterations, then to increase with further iterations until the model eventually blows up. In these cases, we cannot claim to have found an exact nonlinear solution to the model equation (3.26). In such cases, however, the residuals of (3.26), as defined by (3.37), are typically significantly smaller for the solution Φ_k^j that minimizes ΔG than they are for the solution Φ_k^l of the linear system. It is therefore of interest to examine that solution which minimizes ΔG , as a best approximation to the exact solution to the nonlinear equation (3.26).

It is found (Robinson, 1986) that the system is more likely to converge to a solution if the value of G^s to be used for the $(j+1)$ -th iteration is computed, not from the solution Φ_k^j of the j th iteration, but from a linear combination

$$\eta \Phi_k^{j-1} + (1 - \eta) \Phi_k^j \quad (3.42)$$

of solutions from the last two iterations. By trial and error, a value of $\eta = 0.5$ has been found to yield satisfactory results in most cases. (Note that in computing the residual δG_k^s , as defined in (3.38), in order to test for convergence, we use the solution obtained at the last iteration, not a linear combination of the last two solutions).

A series of experiments has shown that, in the cases where the nonlinear system converges to a solution, the solution is not strongly dependent on η . If the value of η

chosen is too small, the system may not converge. If η is greater than some critical value, which may vary from one case to another, the system converges to a solution which is virtually independent of the value of η , though the rate of convergence will depend on η .

(3.8) Smoothing of model fields

Multiplication of two fields in a gridpoint model will lead to the generation of spurious small-scale structure. In order to filter out such small scales, smoothing is performed after each multiplication. The smoothed field \tilde{f}_j at gridpoint j is related to the unsmoothed field f_j by

$$\tilde{f}_j = \frac{1}{4}(f_{j-1} + 2f_j + f_{j+1}). \quad (3.43)$$

Two such smoothings are performed in latitude and two in height after each multiplication of fields.

In order to filter out spurious small-scale structure in the model solutions, the fields $\tilde{\Phi}_k$ are projected onto associated Legendre functions P_k after each iteration. We let

$$\tilde{\Phi}_k(\theta, z) = \sum_{l=k}^L \Phi_l(z) P_{lk}(\sin \theta), \quad (3.44)$$

and truncate the resulting expansion at $L = 16$. G^S is filtered by a similar procedure at each iteration. Since G^S is a more highly differentiated field than $\tilde{\Phi}_k$, it will have more small-scale structure. Smoothing of G^S is thus performed with truncation at $L = 18$.

CHAPTER 4

RESULTS OF MODEL SIMULATIONS

(4.1) Introduction

Three series of experiments have been performed using the numerical model described in Chapter 3. In the first series, both the nonlinear interaction among stationary waves, G^S , and the monthly mean of the nonlinear interaction among transients, G^T , have been set to zero in the model equation (3.26). We refer to this as the linear model without transients. Because the model equation is linear in $\tilde{\Phi}_k$, the existence and uniqueness of a solution are assured, and computation of this solution is straightforward. The results of these experiments are presented in Section 4.2.

In the second series, G^T is computed from the observed data set and included as a forcing term in the model, while G^S is set to zero. We refer to this as the linear model with transients. Note that the term G^T represents the monthly mean of the nonlinear interaction among transients. Though we refer to this as a "model with transients," the model remains time-independent. The transients only enter the model through G^T , which is taken from observations and input into the model, not computed by the model. Note also that, although G^T represents a nonlinear interaction, the model equation (3.26) is linear in $\tilde{\Phi}_k$ when G^S is set to zero. It is for this reason that we refer to this case as a linear model. As in the previous series of experiments, the linearity of the model equation ensures that there exists a unique solution, which can be computed in a

straightforward manner. The results of this series of experiments are presented in Section 4.3.

In the third series, G^T is set to zero, while G^S is computed iteratively, as described in Chapter 3. We call this the nonlinear model without transients. In this case, one must solve a system of coupled nonlinear differential equations. This is a much more difficult computational problem than that of the previous sections. The results of these experiments are presented in Section 4.4.

One would like to perform a fourth series of experiments, with a nonlinear model with transients. G^T would be computed from the observed data set, and G^S computed iteratively. Such experiments have been attempted, but it was found to be difficult to obtain convergence to a solution of the system of nonlinear equations.

In each series of experiments, calculations have been performed for the January monthly means of each of four years, 1982-84 and 1986. For a given year, the mean zonal state and the lower boundary forcing are unchanged from one series of experiments to another. Recall that the mean zonal wind and the lower boundary forcing (*i.e.* the stationary waves at 100 hPa) are taken from observations, as described in Chapter 2.

(4.2) Linear model without transients

Figure 4.1 shows the amplitude and phase of each of the first three zonal wavenumbers as a function of latitude and height, computed by the linear model without transients, for January 1983. Note that the amplitudes are scaled by a factor

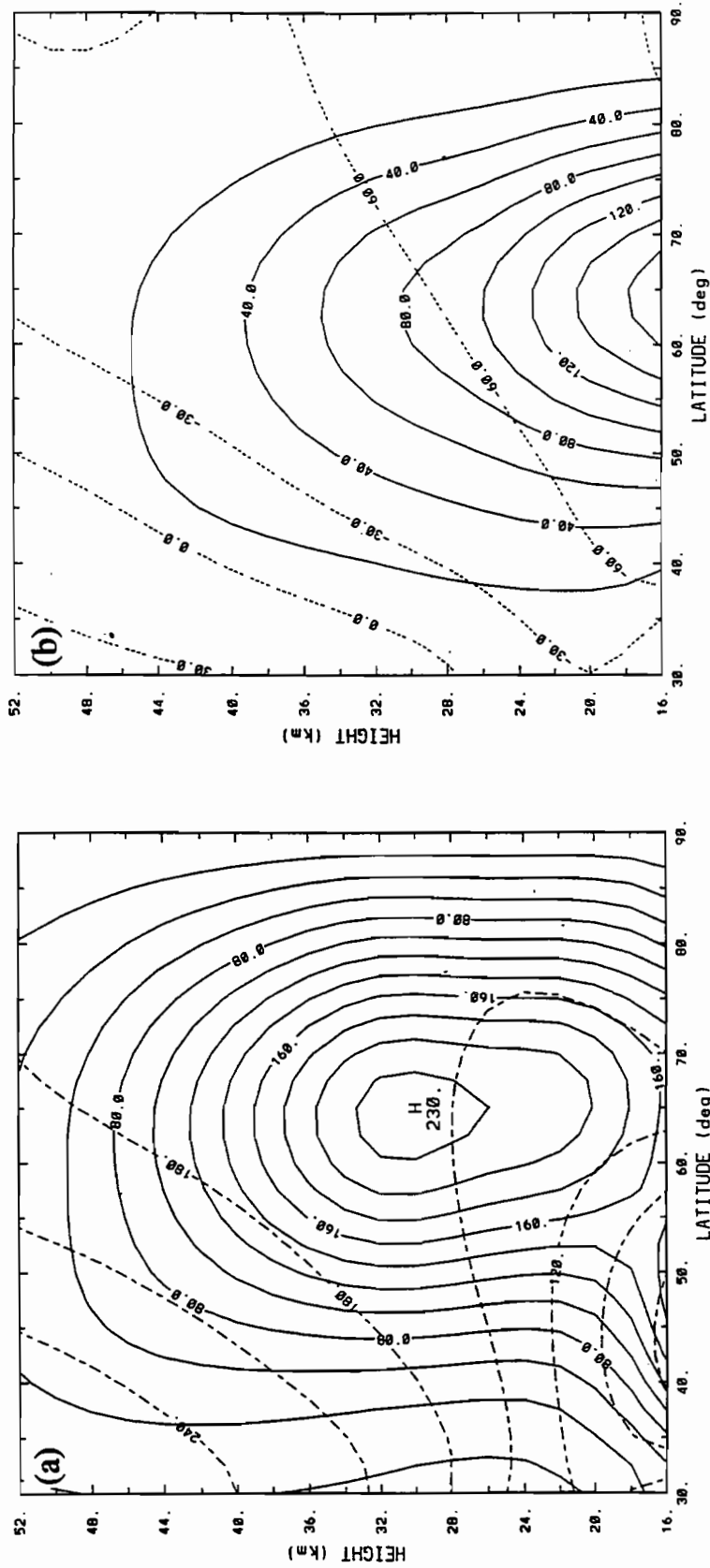


Fig. 4.1 Stationary waves for January 1983, from linear model without transients. Solid lines are amplitude (contour interval 20 m), broken lines are phase (contour interval 30°). Note that amplitudes are divided by factor of $\exp((z-z_0)/2H)$. (a) zonal wavenumber $k=1$, (b) $k=2$, (c) $k=3$.

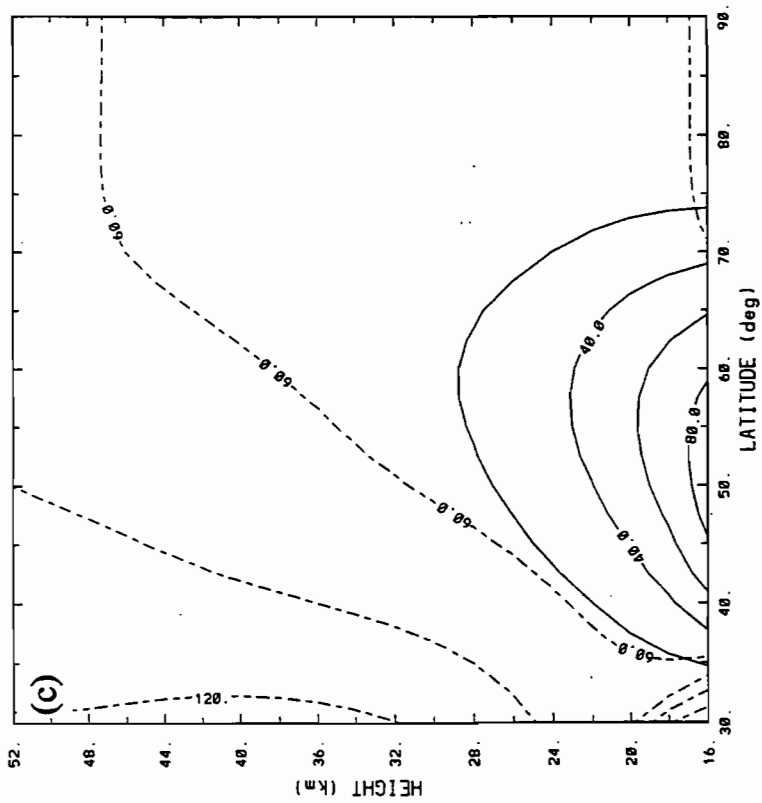


Fig. 4.1 Continued.

$\exp(-(z-z_0)/2H)$, so that an increase in amplitude corresponds to an increase in wave kinetic energy. We note that wavenumber 1 has an amplitude maximum in the interior of the model domain, while wavenumbers 2 and 3 have amplitudes which decrease monotonically with height, with wavenumber 3 decaying more rapidly than wavenumber 2. This is in accord with theory, which predicts that only the largest scale waves will be able to propagate into the stratosphere.

Comparing the observed stationary wave structure in Figure 2.4 and that computed by the linear model without transients in Figure 4.1, we note that the model reproduces the observed qualitative behaviour of the waves quite well for January 1983. For wave 1, the model correctly reproduces the position of the amplitude maximum near 65°N and 30 km. The maximum amplitude in the model is, however, only 73% of that which is observed. As noted above, waves 2 and 3 decay monotonically with height. The rate of decay is reasonably well simulated by the model, though the maximum amplitude of wave 2 at any given height tends to be somewhat farther south in the model than in the observations.

The model computes a zonal wave 3 which decays rapidly with height, in good agreement with the observed behaviour of this wave. Wave 3 has been retained throughout this study, in order to investigate the possibility that it could take on large values due to forcing by transients or due to nonlinear interactions among waves 1 and 2. It is found, however, that for all the years studied and with all versions of the model, wave 3 remains strongly trapped at lower levels and makes only a minor contribution to

the monthly mean stratospheric circulation. Wave 3 will therefore not be discussed further in this work.

Figure 4.2 shows the height field at 32 km (approximately 10 hPa) due to the sum of zonal waves 1-3, as computed by the linear model without transients, for each of the four Januaries in this study. This is to be compared with the observed monthly mean fields, as shown in Figure 2.5. For 1982, the position of the high over eastern Siberia is well-reproduced by the model, but the calculated amplitude is less than half that observed in reality. The low near Hudson Bay is simulated well. The low over northwestern Russia is positioned correctly, but is far too weak.

For 1983, the performance of the linear model without transients is considerably better than for the previous year. The high over Alaska is well-positioned, and its computed amplitude is 83% of that observed. The position of the low is fairly well reproduced, though the minimum is more elongated in longitude in the model than in reality. Again, the amplitude given by the model is too weak.

For 1984, the model performs very poorly. From Figure 2.5(c), one sees that the observed 32 km wave height field is dominated by zonal wavenumber 1, but the model output, as shown in Figure 4.2(c), displays a strong wavenumber 2 component. The model amplitudes are much weaker than those observed.

For 1986, the model is reasonably successful at reproducing the observed positions of both the high and the low, but the amplitudes are again much too weak, with the computed high being only 57% of that observed.

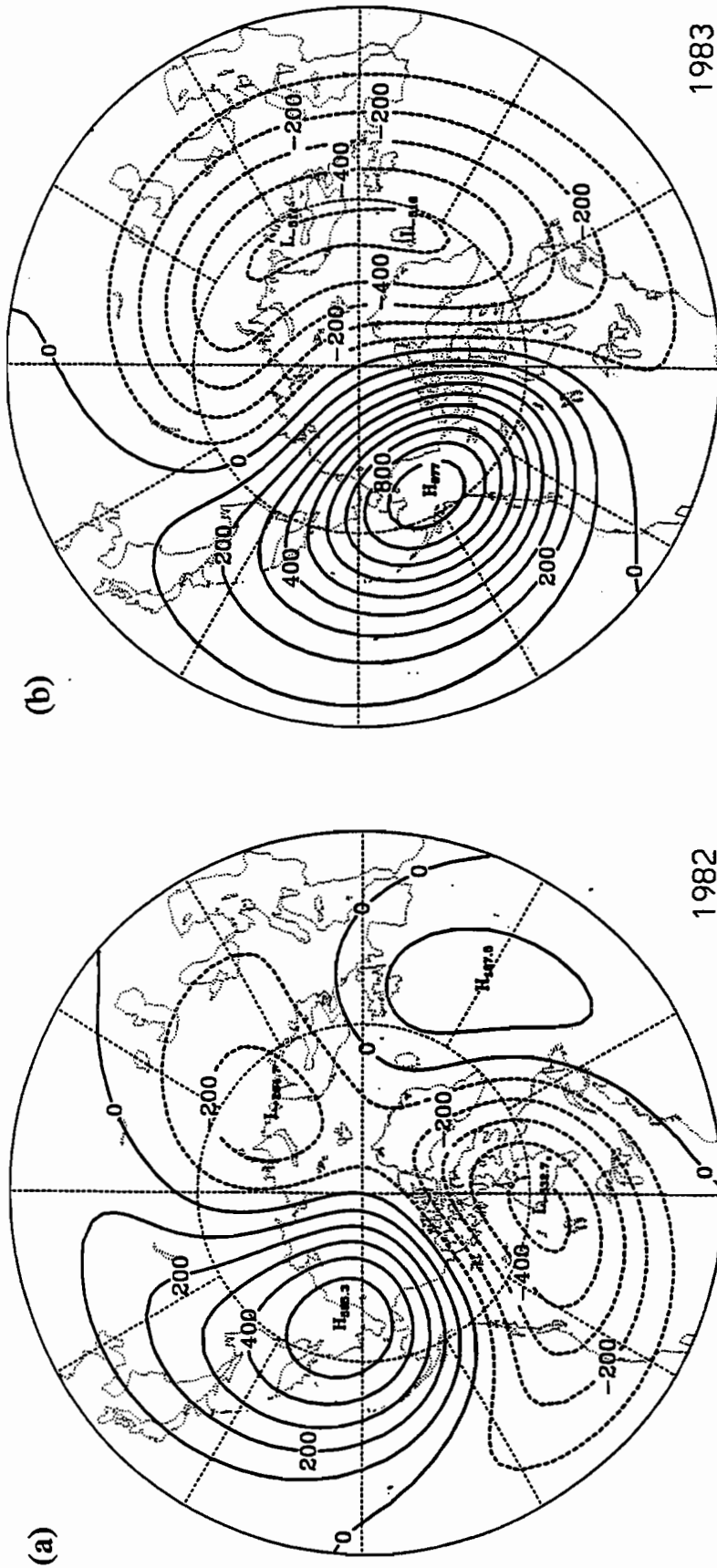


Fig. 4.2 Geopotential height field (sum of zonal waves 1-3), from linear model without transients, for log-pressure height 32 km. Contour interval 100 m. (a) 1982, (b) 1983, (c) 1984, (d) 1986.

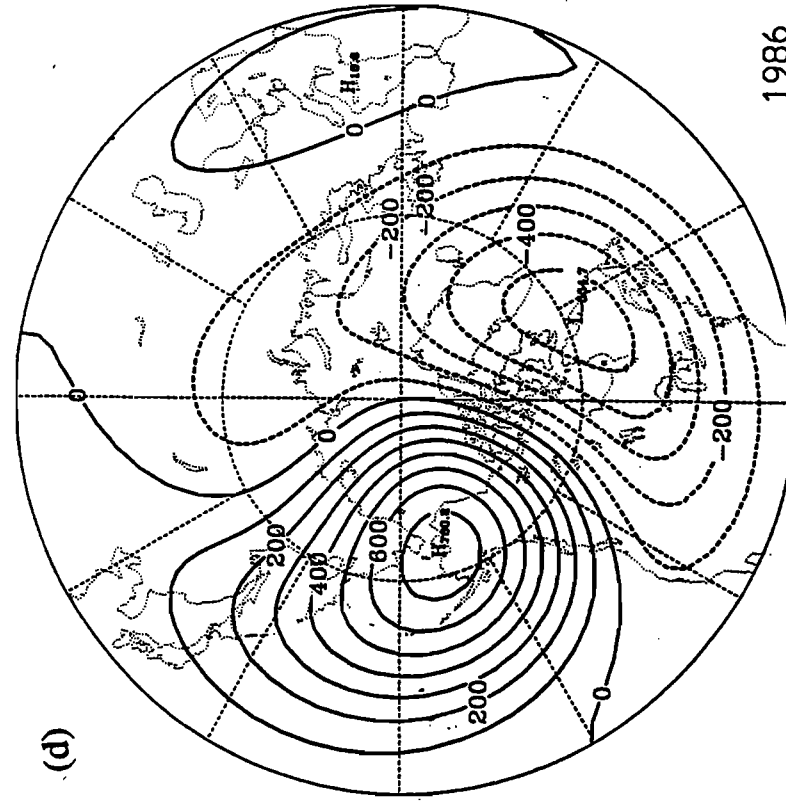
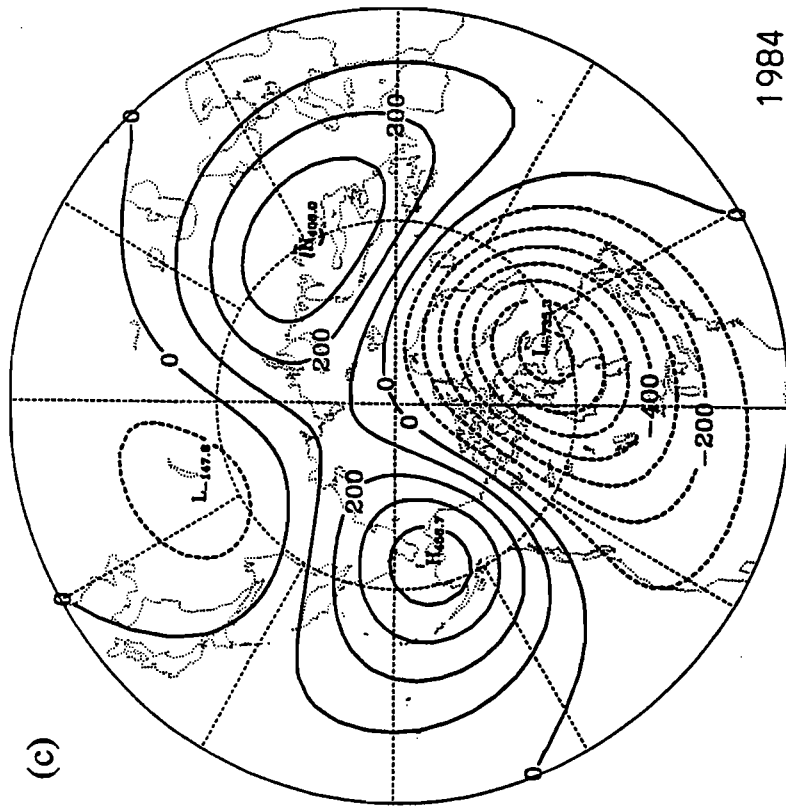


Fig. 4.2 Continued.

Figure 4.3 shows the structure of the January mean zonal wave 1 as calculated by the linear model without transients for each of the four years studied. This is to be compared to the observed structure of this wave, as shown in Figure 2.6. Recall that the amplitudes have been divided by a factor of $\exp((z-z_0)/2H)$, as discussed in Section 2.5.

We note that there is a very large interannual variability in the behaviour of wave 1 as computed by the model. For 1982 and 1984, the model generates a wave 1 which decays monotonically with height, while for 1983 and 1986 the amplitude of wave 1 is found to attain a maximum in the interior of the model domain. This contrasts with the observed behaviour of wave 1, which displays an amplitude maximum in the interior of the domain for all of the years studied. For 1983 and 1986, the model generates an amplitude maximum at the correct latitude and height, but in all four years, the model amplitudes are much less than those which are observed in the real atmosphere.

The linear model without transients reproduces the phase structure of wave 1 fairly well, in a qualitative sense. The waves tilt westward with increasing height, and eastward with increasing latitude (*i.e.* there is a southwest-northeast tilt in the horizontal). Quantitatively, there is, at the latitude of maximum amplitude, somewhat less phase tilt with height in the model output than in observations for 1983. For the other three years, however, the model generates a wave 1 with substantially more phase tilt with height than is observed in nature, at the latitude of maximum amplitude.

Figure 4.4 shows the structure of the January mean zonal wave 2 as calculated by the linear model without transients for each of the four years studied. This is to be compared to the observed structure of this wave, as shown in Figure 2.7. In all cases,

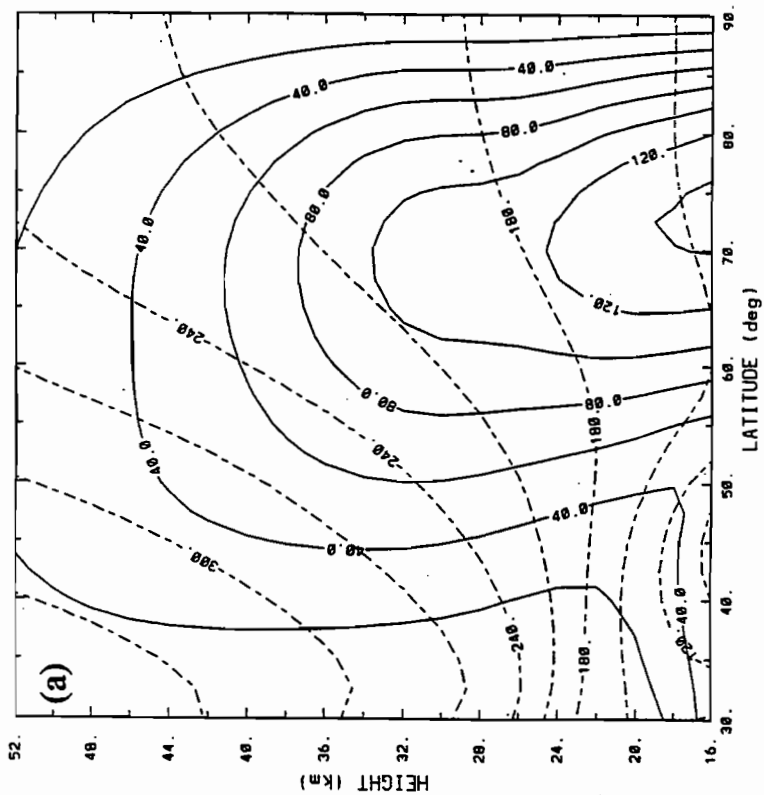
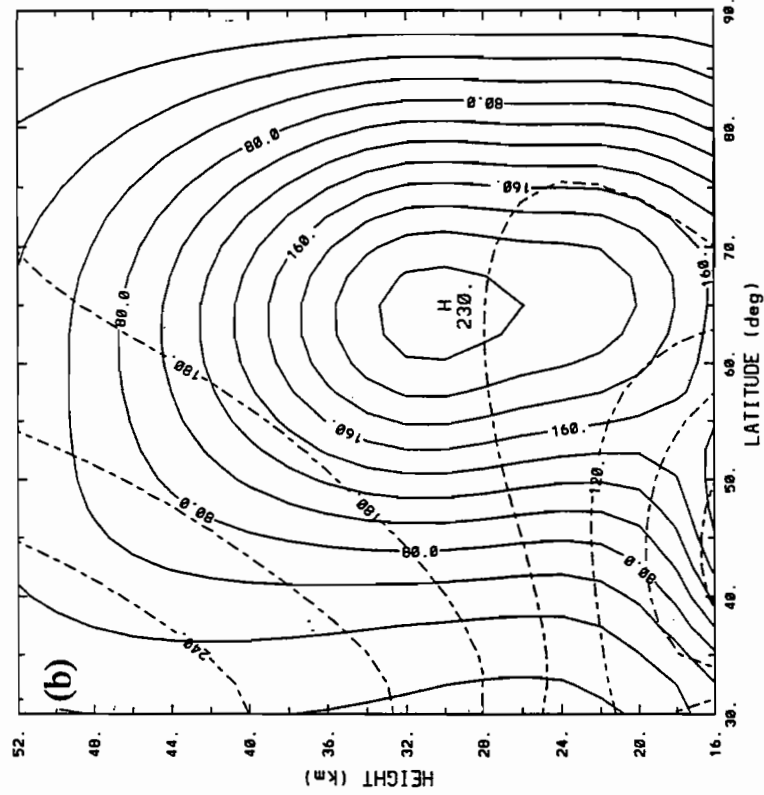


Fig. 4.3 Stationary zonal wave $k=1$, from linear model without transients. Solid lines are amplitude (contour interval 20 m), broken lines are phase (contour interval 30°). Note that amplitudes are divided by factor of $\exp((z-z_0)/2H)$. (a) 1982, (b) 1983, (c) 1984, (d) 1986.

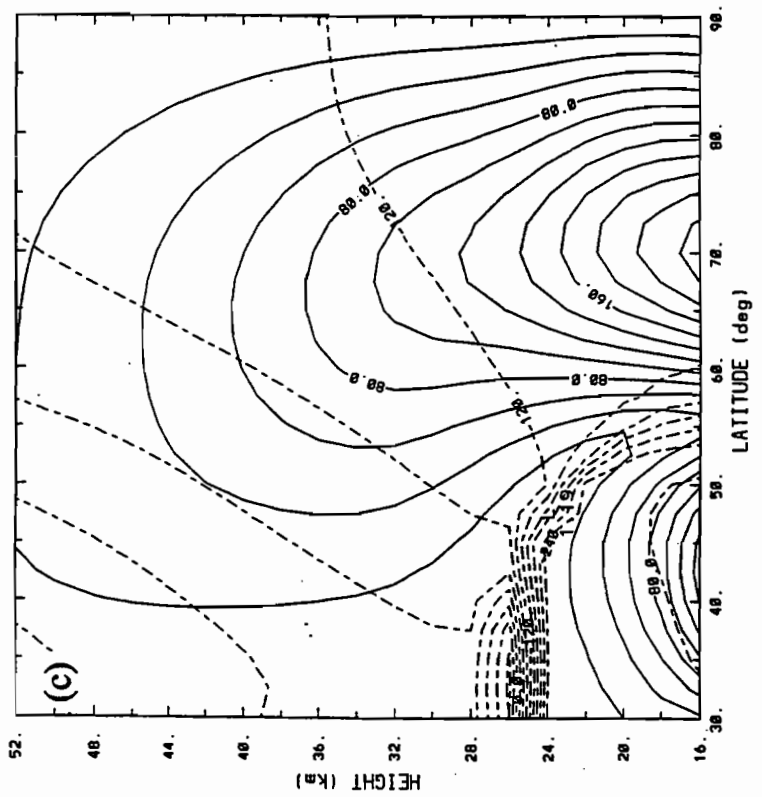
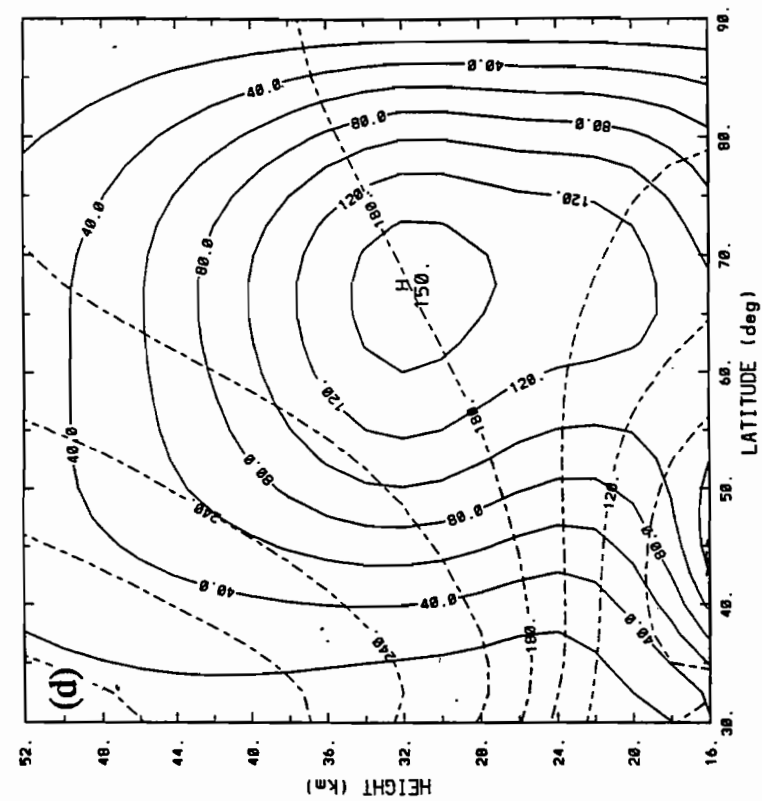


Fig. 4.3 Continued.

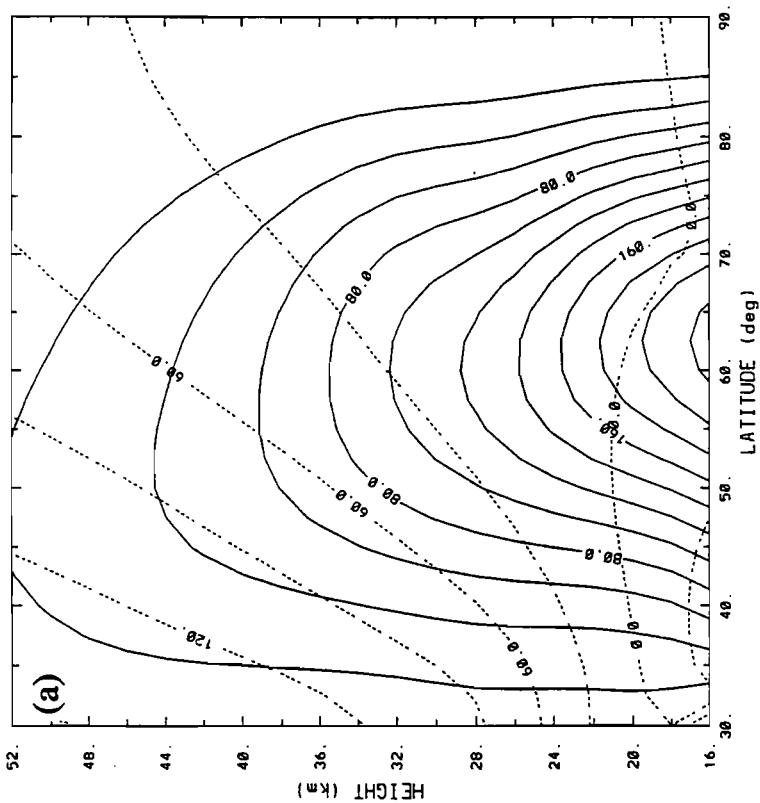
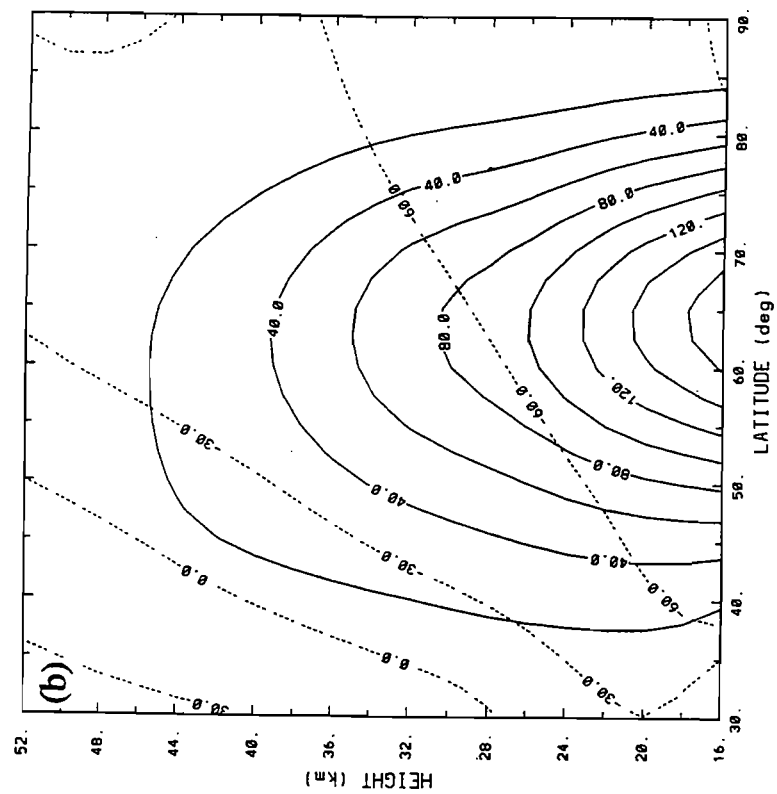


Fig. 4.4 As in Fig. 4.3, but for zonal wave $k=2$.

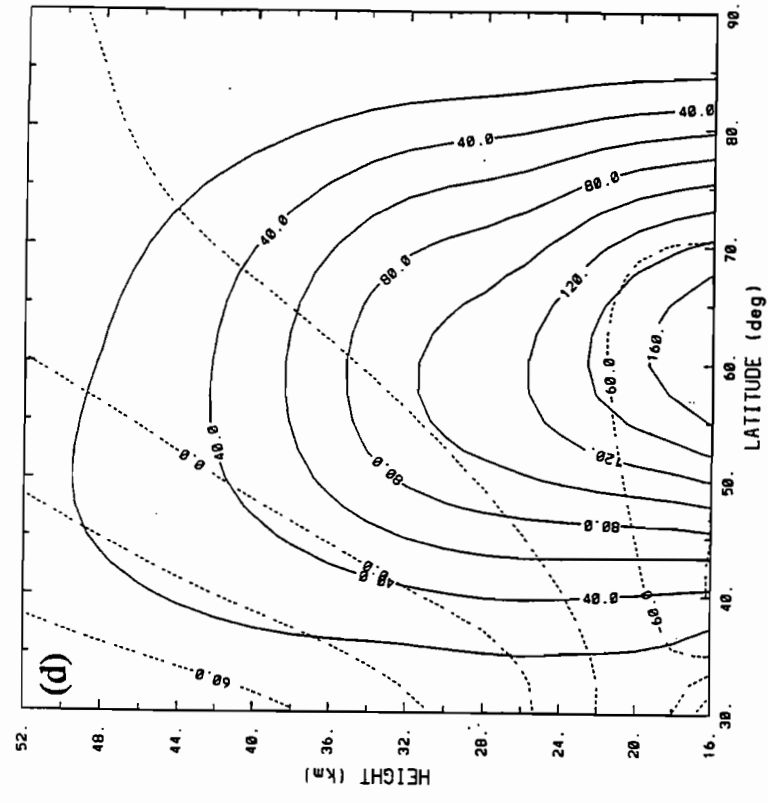
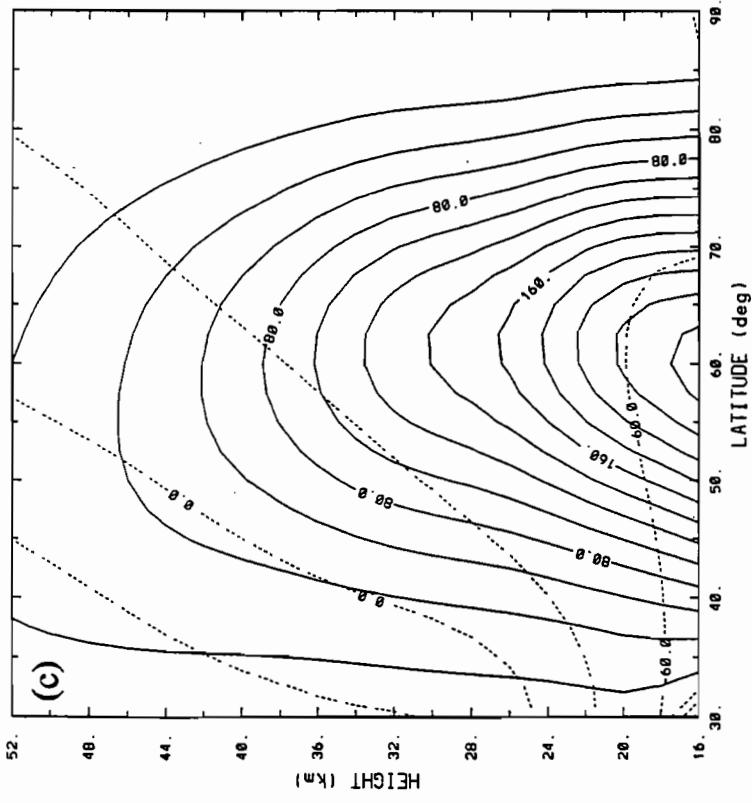


Fig. 4.4 Continued.

the model correctly reproduces the vertical trapping of this wave. The model's wave 2 tends to decay in amplitude with height somewhat more rapidly than is observed in nature. The model also places the maximum amplitude of wave 2 slightly too far south, for any given height. The model's wave 2 tilts westward with increasing height and with decreasing latitude. This is in general agreement with the observed behaviour of wave 2, though the model wave tends to display more tilt in both height and latitude than that of the real atmosphere. Note that the model's performance in simulating wave 2 is not significantly worse for 1984 than for other years, in sharp contrast with its performance in simulating wave 1.

In summary, the linear model without forcing by the monthly mean of the transient momentum and heat flux divergences is fairly successful at reproducing the gross features of the stationary planetary waves in the stratosphere. The positions of the highs and lows are reproduced reasonably well. However, the wave amplitudes calculated by the model are in all cases too weak, and in three of the four years there is too much phase tilt with height for wave 1, which makes the largest contribution to the wave structure. For two of the four years, the model computes a wave 1 whose amplitude decreases monotonically with height, in disagreement with observations.

(4.3) Linear model with transients

Figure 4.5 shows the height field at 32 km (approximately 10 hPa) due to the sum of zonal waves 1-3, as computed by the linear model with transients, for each of the four

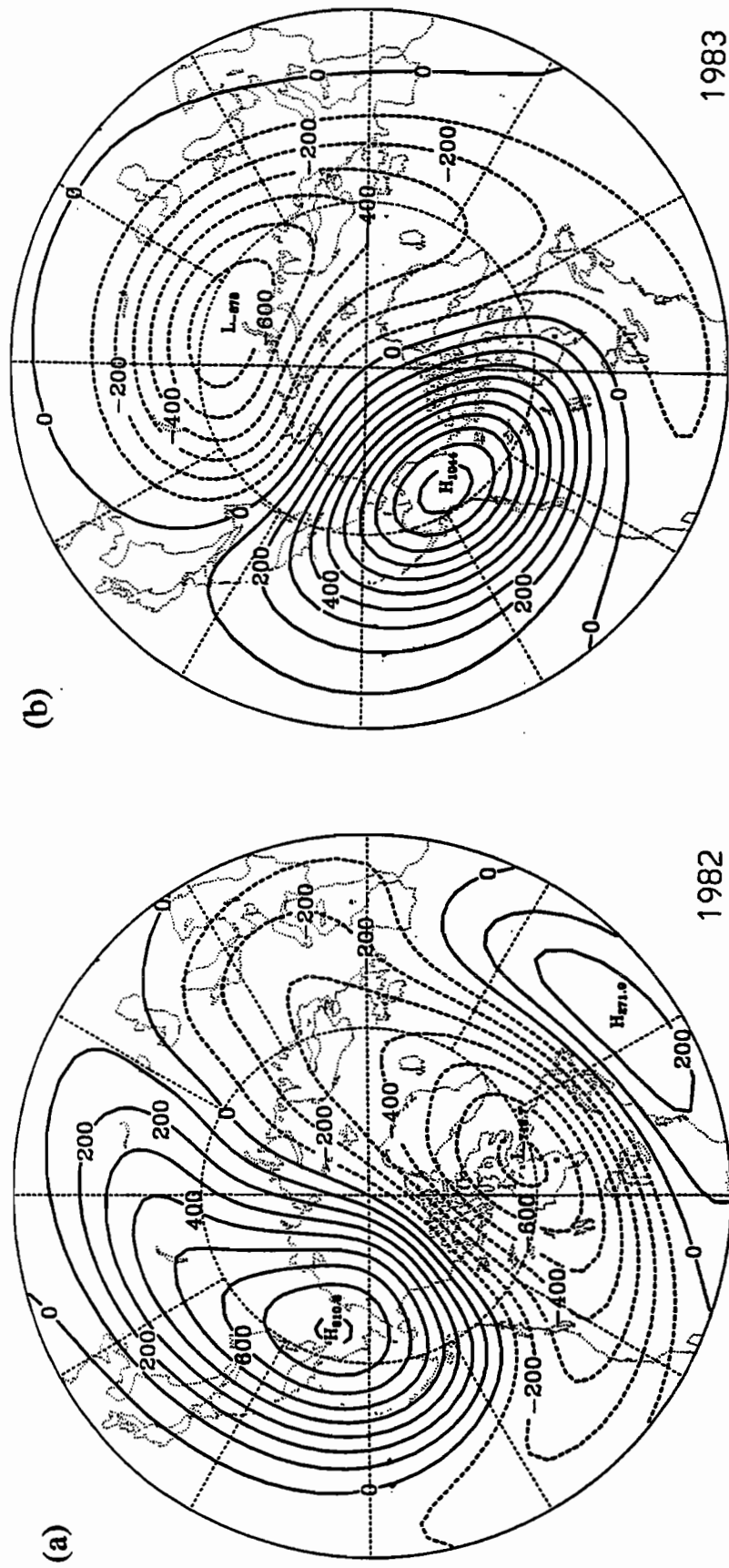


Fig. 4.5 Geopotential height field (sum of zonal waves 1-3), from linear model with transients, for log-pressure height 32 km. Contour interval 100 m. (a) 1982, (b) 1983, (c) 1984, (d) 1986.

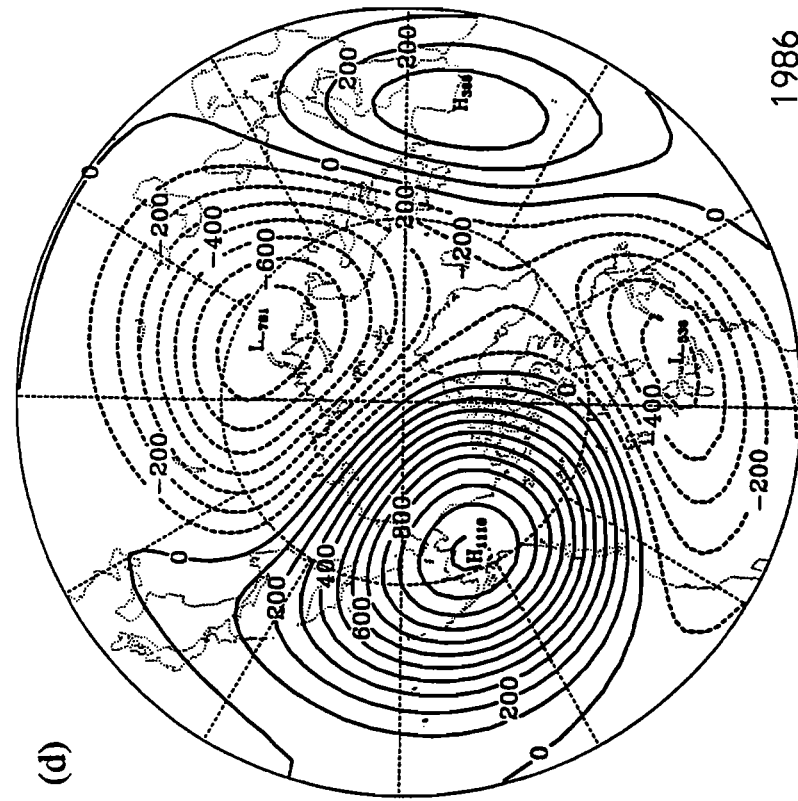
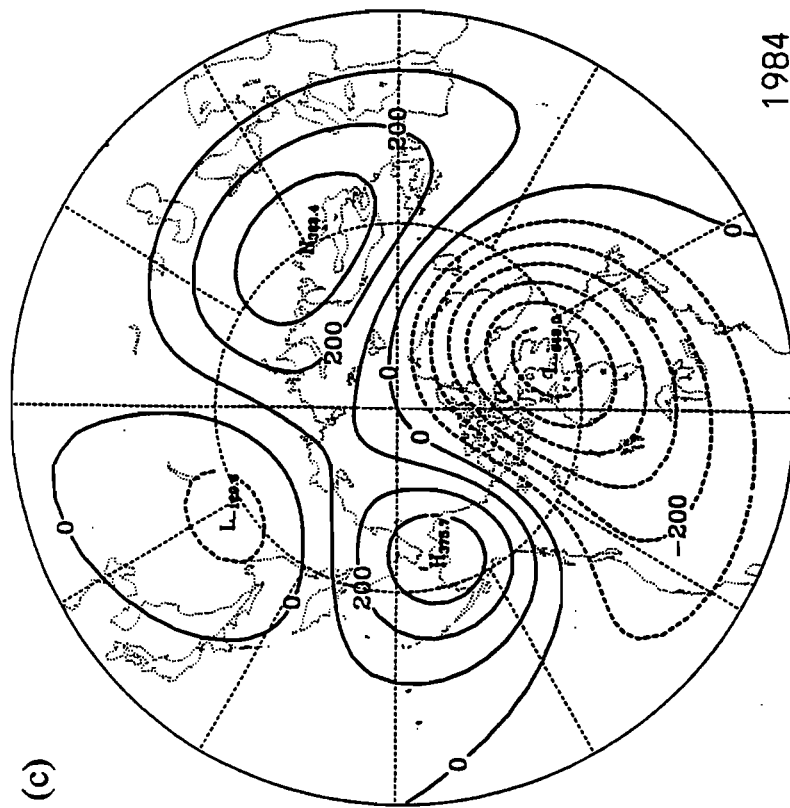


Fig. 4.5 Continued.

Januaries in this study. Comparing these with the output of the linear model without transients (Figure 4.2) and with observations (Figure 2.5), we see that inclusion of forcing by the monthly mean of the transients has a large effect on the model results for 1982 and 1986, but a much smaller effect for 1983 and 1984, and that the inclusion of forcing by transients tends to bring the model output into closer agreement with observations.

For 1982, the high over eastern Siberia is well-positioned in both versions of the model, but inclusion of forcing by transients increases its amplitude, giving better agreement with observations. The structure of the low is less well-reproduced for this year. The computed position of the low near Hudson Bay is closer to the observed location when transients are included, but its amplitude is too large. This model does not give another low centre near northwestern Russia, unlike both the observed atmosphere and the linear model without transients.

For 1983, inclusion of transients produces fewer changes in the 32 km map. The amplitude of both the high and the low are increased somewhat, bringing them into better agreement with observations. The high remains well-positioned. The low is less elongated than in the model without transients, giving better agreement with observations, but it is now positioned too far to the east.

For 1984, the model performs poorly both with and without transients. Inclusion of transients has little effect. Amplitudes at 32 km are reduced slightly, and the positions of the extrema are largely unchanged.

For 1986, inclusion of transients produces a large increase in the amplitude of the high over Alaska, giving better agreement with observations. The structure of the low is less well-reproduced, however. Instead of a single low over the north Atlantic, as seen in both the observations and the output of the linear model without transients, the model with transients gives two distinct lows.

Figure 4.6 shows the structure of the January mean zonal wave 1 as calculated by the linear model with transients for each of the four years studied. Comparing these with the output of the linear model without transients (Figure 4.3), we see that inclusion of forcing by the monthly mean of the transients has a large effect on the model results for 1982 and 1986, but a much smaller effect for 1983 and 1984.

For January 1982, the linear model without transients computes a wave 1 that is much weaker than that observed, and which decays with height instead of having a maximum in the interior of the model domain. Inclusion of transients gives a substantial increase in the amplitude of the waves. The model with transients gives an amplitude maximum in the interior of the model domain, at a slightly higher altitude and more southerly latitude than the observed maximum. The model with transients, like that without transients, produces considerably more phase tilt with height at the latitude of maximum amplitude than was observed for January 1982.

For January 1983, inclusion of transients has a relatively small effect on the structure of wave 1, as compared to the model without transients. The amplitude of this wave is somewhat greater in the model with transients, though it remains weaker than that which is observed in nature. The latitude and height of the amplitude maximum is

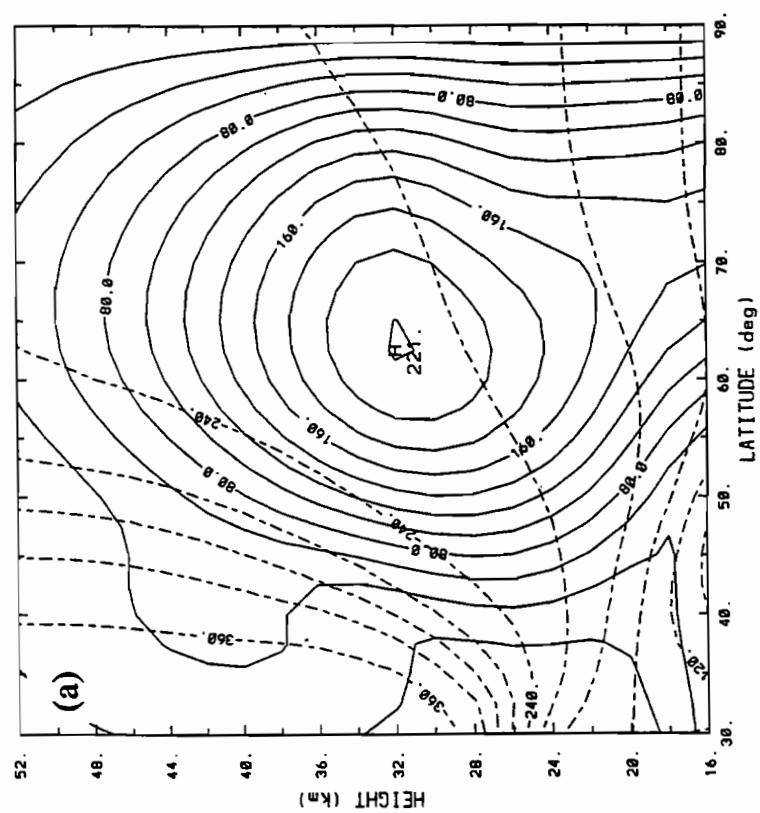
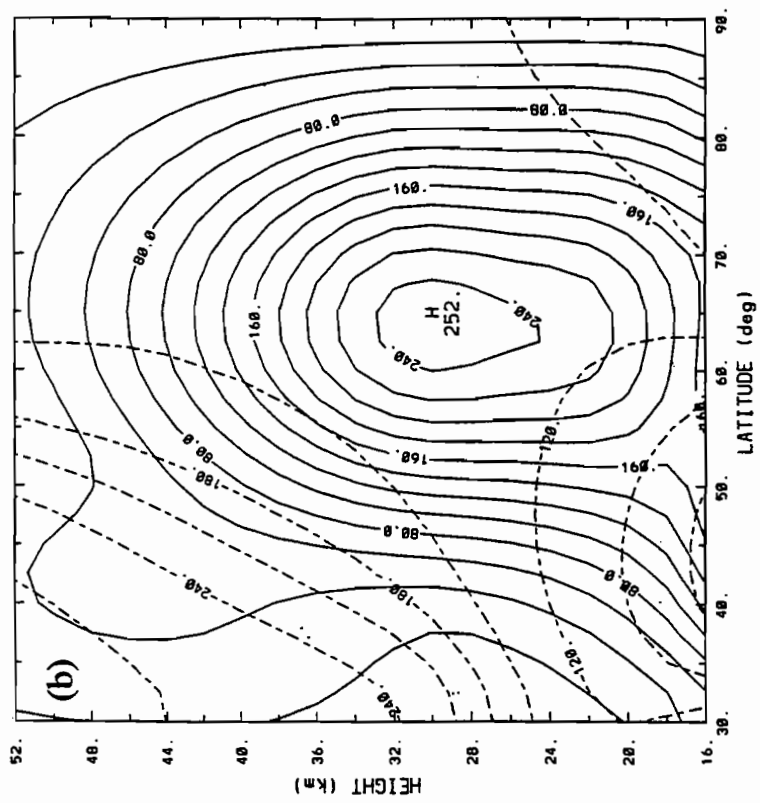


Fig. 4.6 Stationary zonal wave $k=1$, from linear model with transients. Solid lines are amplitude (contour interval 20 m), broken lines are phase (contour interval 30°). Note that amplitudes are divided by factor of $\exp((z-z_0)/2H)$. (a) 1982, (b) 1983, (c) 1984, (d) 1986.

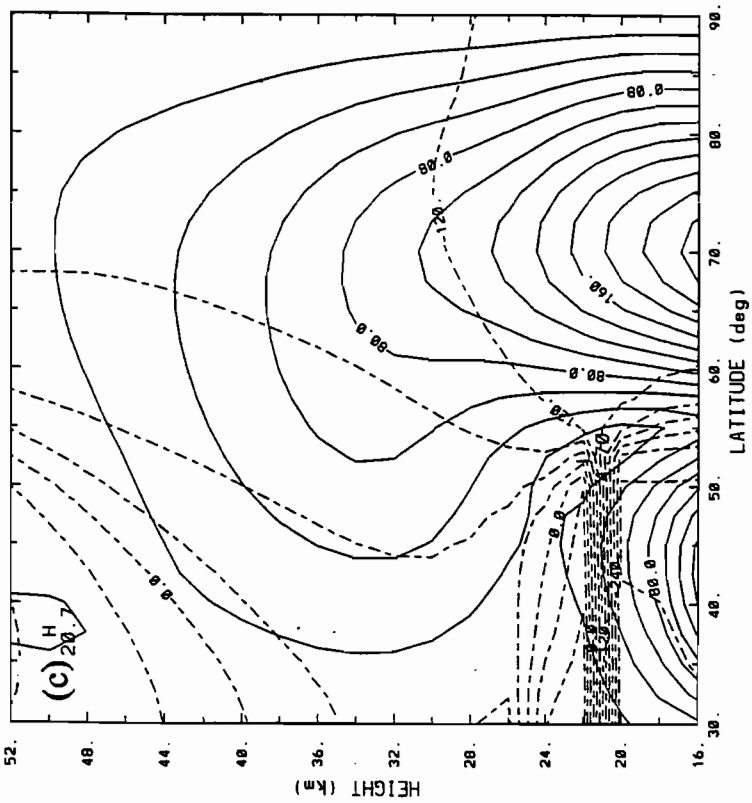
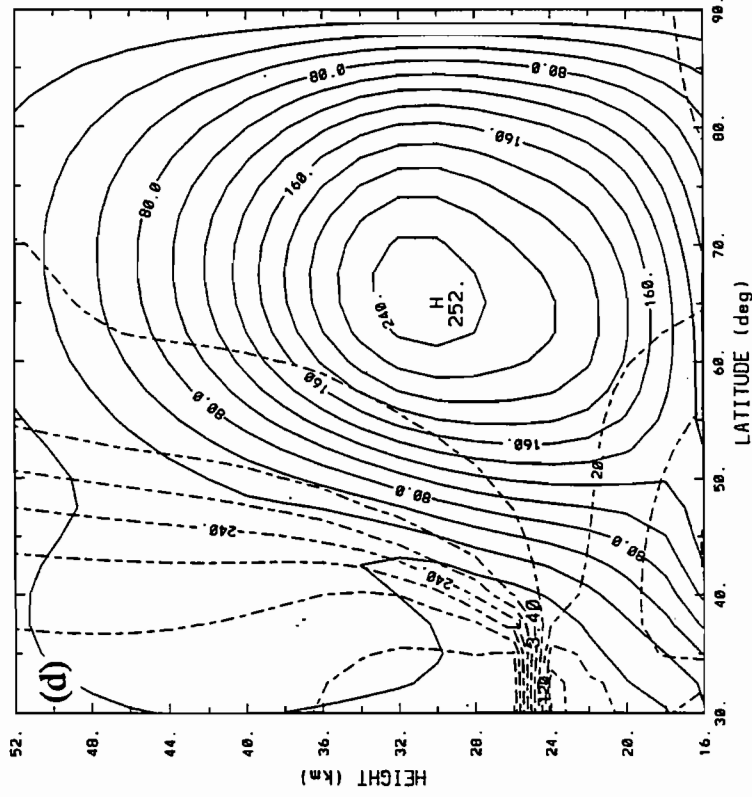


Fig. 4.6 Continued.

well reproduced in both models. Both models exhibit less phase tilt with height than is observed, with the model with transients performing slightly worse in this respect than that without transients.

For January 1984, the linear models, both with and without transients, compute a stationary wave 1 whose amplitude decreases monotonically with height. The wave decays slightly more rapidly with height in the model with transients than in that without transients. This behaviour is not in agreement with that observed in nature, where there is an amplitude maximum at an altitude of 26 km. The linear models with and without transients also compute very similar phase structures for wave 1, neither of which is in good agreement with the observed phase structure.

For January 1986, inclusion of forcing by transients produces a very large increase in the amplitude of wave 1 computed by the linear model, compared to that computed by the model without transients. The model without transients generates a maximum amplitude which is only 46% of that observed, while the model with transients gives a maximum amplitude 81% of that observed in the real atmosphere. The position of the amplitude maximum is at the correct altitude but slightly too far south in the model without transients, and at the correct latitude but slightly too low in altitude in the model with transients. Inclusion of transients also decreases the phase tilt with height, bringing the model results into better accord with the observations.

The linear model with transients is better able to reproduce the observed behaviour of stationary wave 1 than the linear model without transients for January 1982, 1983, and 1986. The improvement brought about by the inclusion of transients is large

for 1982 and 1986, and smaller for 1983. Neither the linear model without transients nor that with transients is able to reproduce well the observed behaviour of wave 1 for January 1984.

Figure 4.7 shows the amplitudes of the forcing fields G_1^T due to transients as computed from data for each January in this study and used as model input in Equation (3.26). The forcing due to transients is significantly weaker for 1984 than for the other years studied. (The wave 2 forcing due to transients, G_2^T , (not shown) is also significantly weaker for 1984 than for the other years studied.) Thus it is not surprising that the model solution is less affected by the inclusion of transients for this year than for other years. There is, however, not a simple linear relationship between the magnitude of the forcing by transients and its effect on the model solution, since the forcing due to transients in 1983 is comparable to that in 1982 and 1986, but the change in the model response is less in 1983 than in the other years.

Figure 4.8 shows the structure of the January mean zonal wave 2 as calculated by the linear model with transients for each of the four years studied. Comparing these with the output of the linear model without transients (Figure 4.4), we see that inclusion of forcing by transients has considerably less effect on wave 2 than on wave 1. Wave 2 remains trapped in all cases (with the exception of a local maximum in the interior of the model domain for 1982). Inclusion of transients increases the rate of decay of amplitude with height in two cases, 1982 and 1984, and decreases this rate of decay in the other two cases.

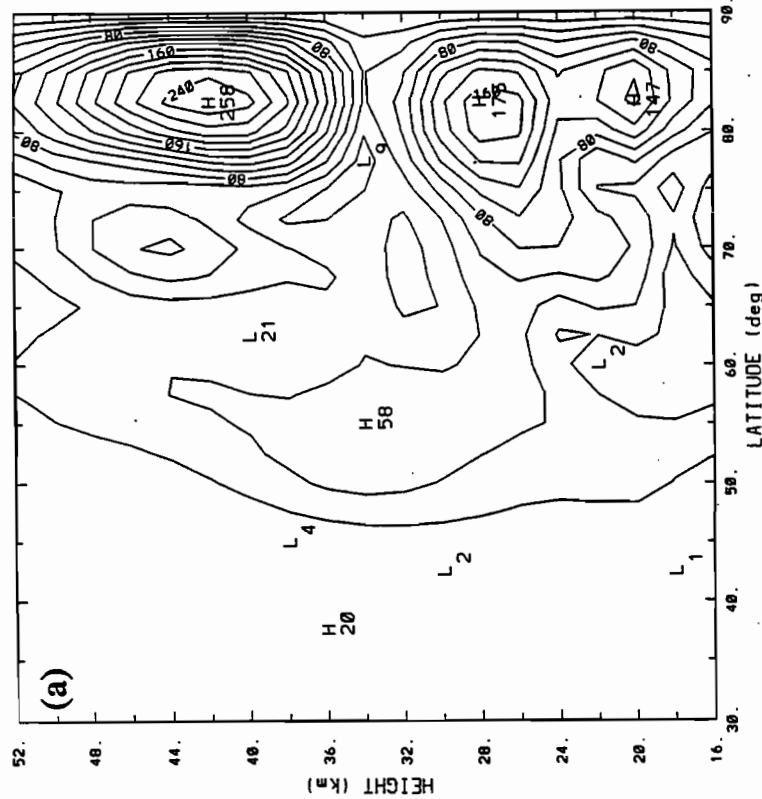
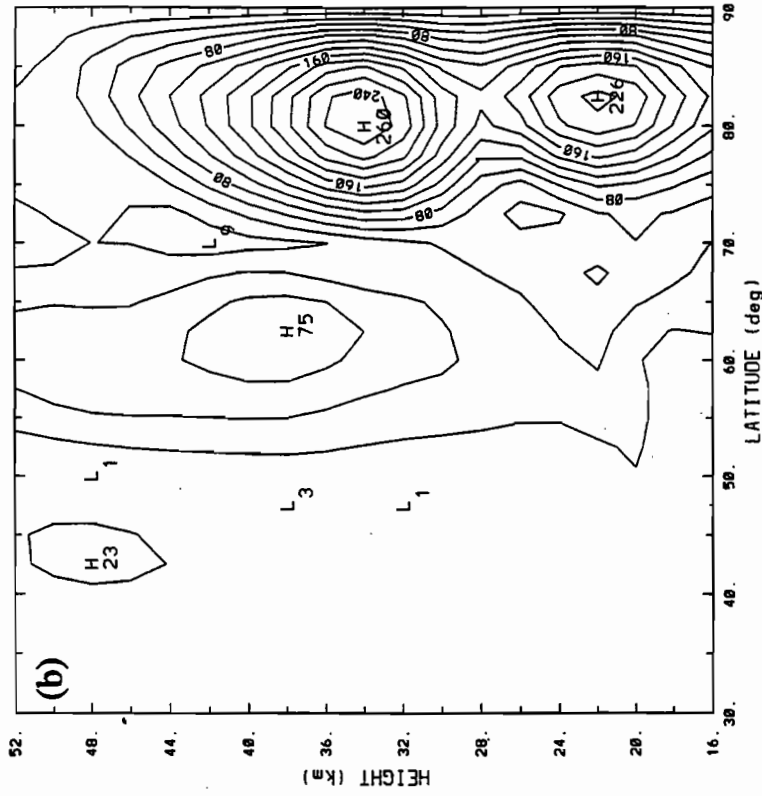


Fig. 4.7 Amplitude of forcing field G_T^T due to monthly mean of transient momentum and heat flux divergences, as computed from observations, for January (a) 1982, (b) 1983, (c) 1984, (d) 1986. Contour interval $2 \times 10^4 \text{ m}^3 \text{ s}^{-7}$.

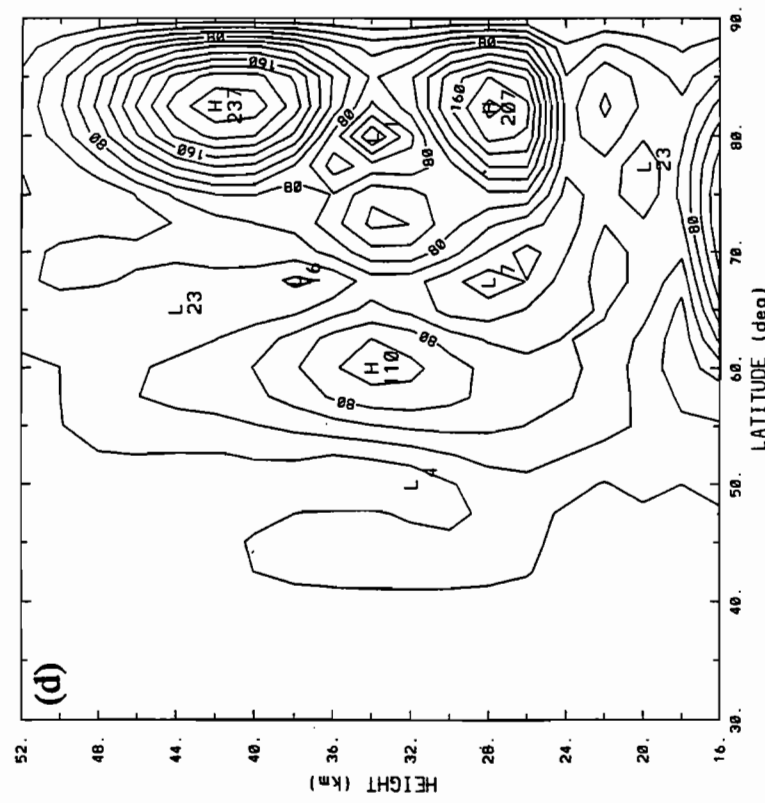
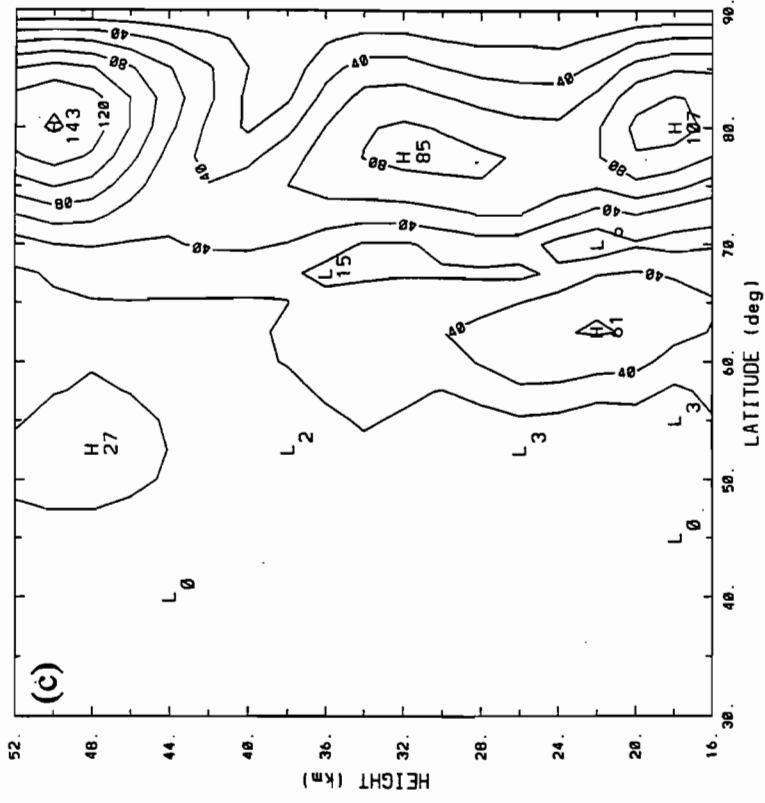


Fig. 4.7 Continued.

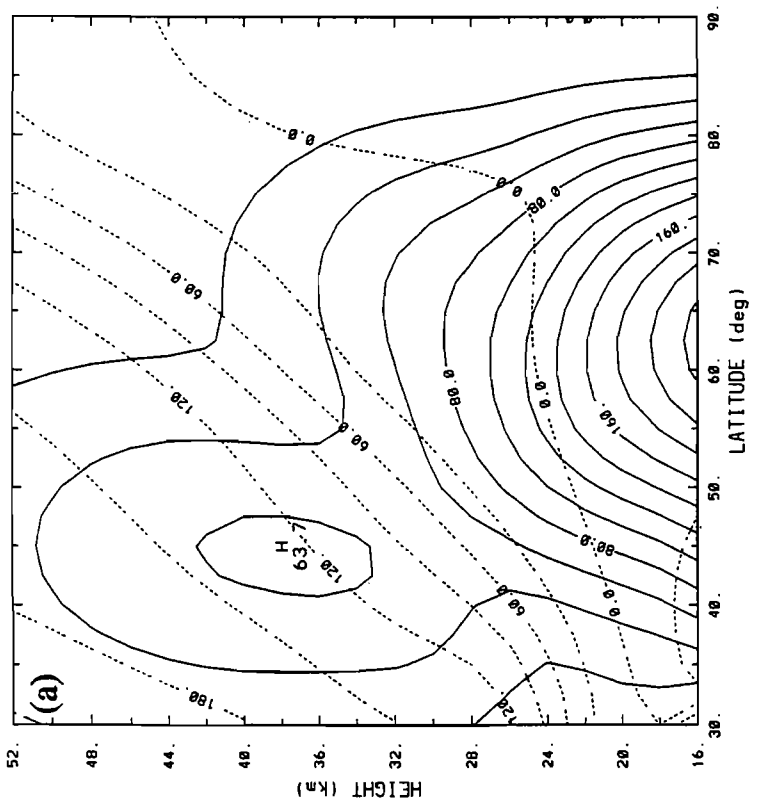
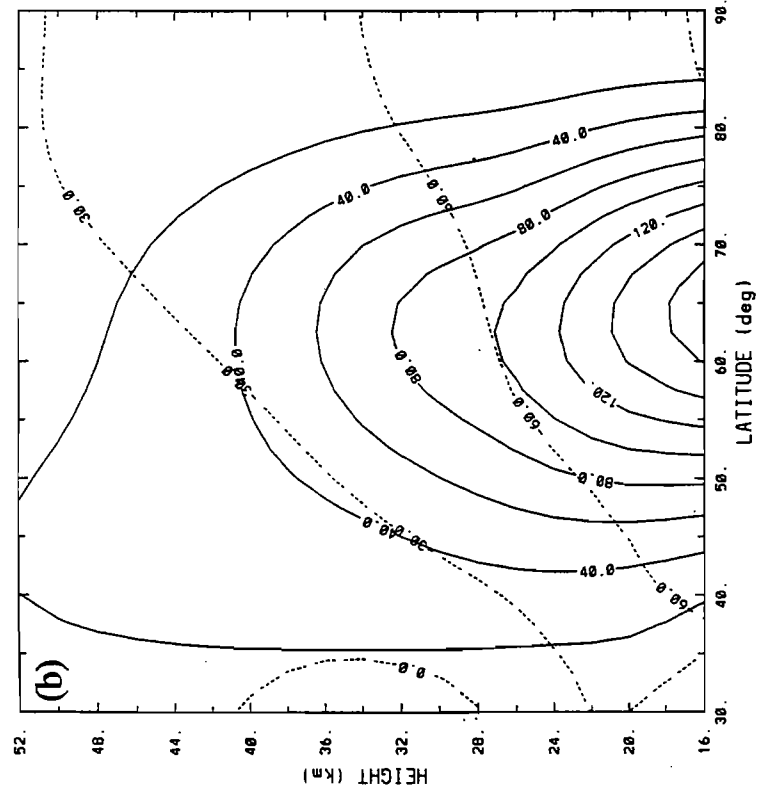


Fig. 4.8 As in Fig. 4.6, but for zonal wave $k=2$.

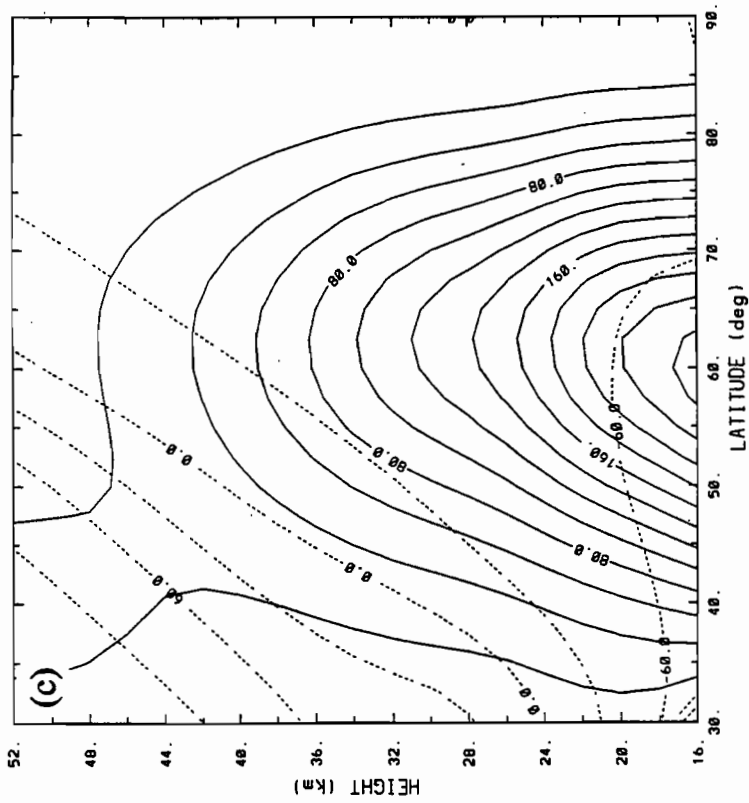
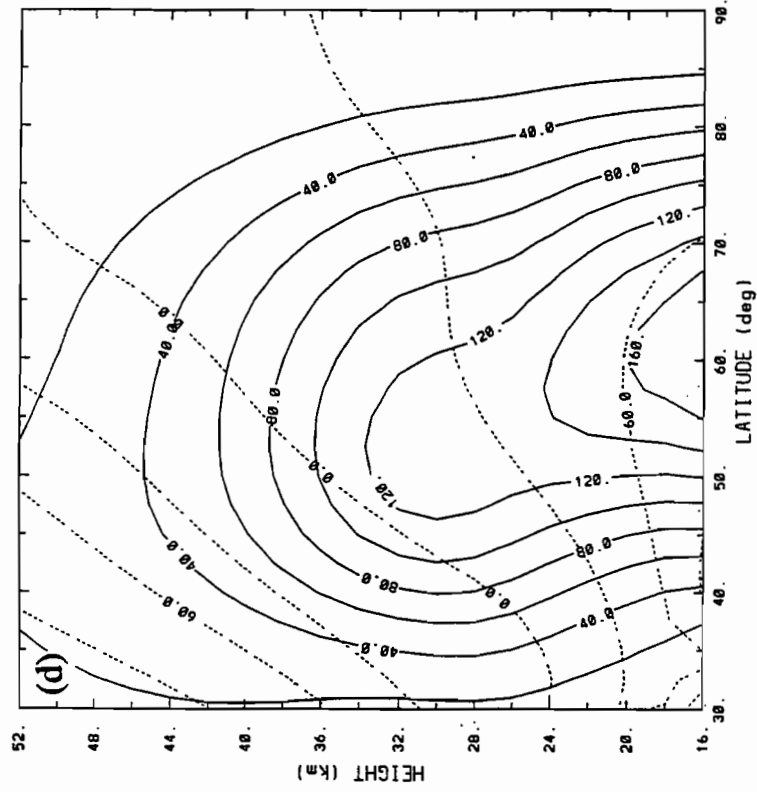


Fig. 4.8 Continued.

In summary, inclusion of forcing by the monthly mean of transient flux divergences results in generally better performance of the model, as compared to the model without transients. The model without transients computes waves which are much weaker than those observed in the real atmosphere; inclusion of transients gives significantly larger wave amplitudes, though the model's waves remain somewhat weaker than those observed. The improved performance of the model is due in large part to the greater amplitudes of wave 1, and is most pronounced for 1982 and 1986, and more modest for 1983. For 1984, the model performs poorly whether or not forcing by transients is included.

(4.4) Nonlinear model without transients

As noted in Section 4.1 above, solution of the coupled nonlinear differential equations of this version of the model is a more difficult computational problem than solution of the linear equations of the models used in Sections 4.2 and 4.3. The iterative solution technique described in Section 3.7 has been employed. As explained in that section, the model is considered to have converged to a solution when the value of ΔG , as defined by Equation (3.41), falls below 10^{-3} . Satisfactory convergence by this criterion was obtained for 1982, 1983, and 1984.

For 1986, the model did not converge. A solution was found for which $\Delta G = 0.0244$, but further iterations resulted in the solution diverging. As discussed in Section 3.7, this solution at the iteration which minimizes ΔG constitutes a best available

approximation to the exact solution to the nonlinear equation (3.26). This solution is presented below as that for 1986. It should be viewed with caution, however, since it is not the exact solution.

Figure 4.9 shows the height field at 32 km (approximately 10 hPa) due to the sum of zonal waves 1-3, as computed by the nonlinear model without transients, for each of the four Januaries in this study. Comparing these with the output of the linear model without transients (Figure 4.2), with the linear model with transients (Figure 4.5), and with observations (Figure 2.5), we find that inclusion of nonlinear interactions among the stationary waves has relatively little effect on the amplitude of the waves calculated by the model, but gives a phase structure in better agreement with observations.

For 1982, the linear model without transients positions the high and low centres correctly, but their amplitudes are much too weak, and the relative depths of the two lows are incorrect, with the Western Hemisphere low being deeper than the Eastern Hemisphere low in this version of the model. Inclusion of nonlinear interactions among the stationary waves has little effect on the amplitudes at 32 km, weakening them somewhat, but it does give a better simulation of the relative depths of the two lows. This contrasts with the effect of including transients in the model, which gives a large increase in the amplitudes of the waves at 32 km, giving better agreement with observations, but gives a less accurate simulation of the phase structure, with only a single low centre instead of the two observed in nature.

For 1983, inclusion of the nonlinear interactions among the stationary waves gives a slightly weaker high at 32 km, and a slightly deeper low, as compared to the linear

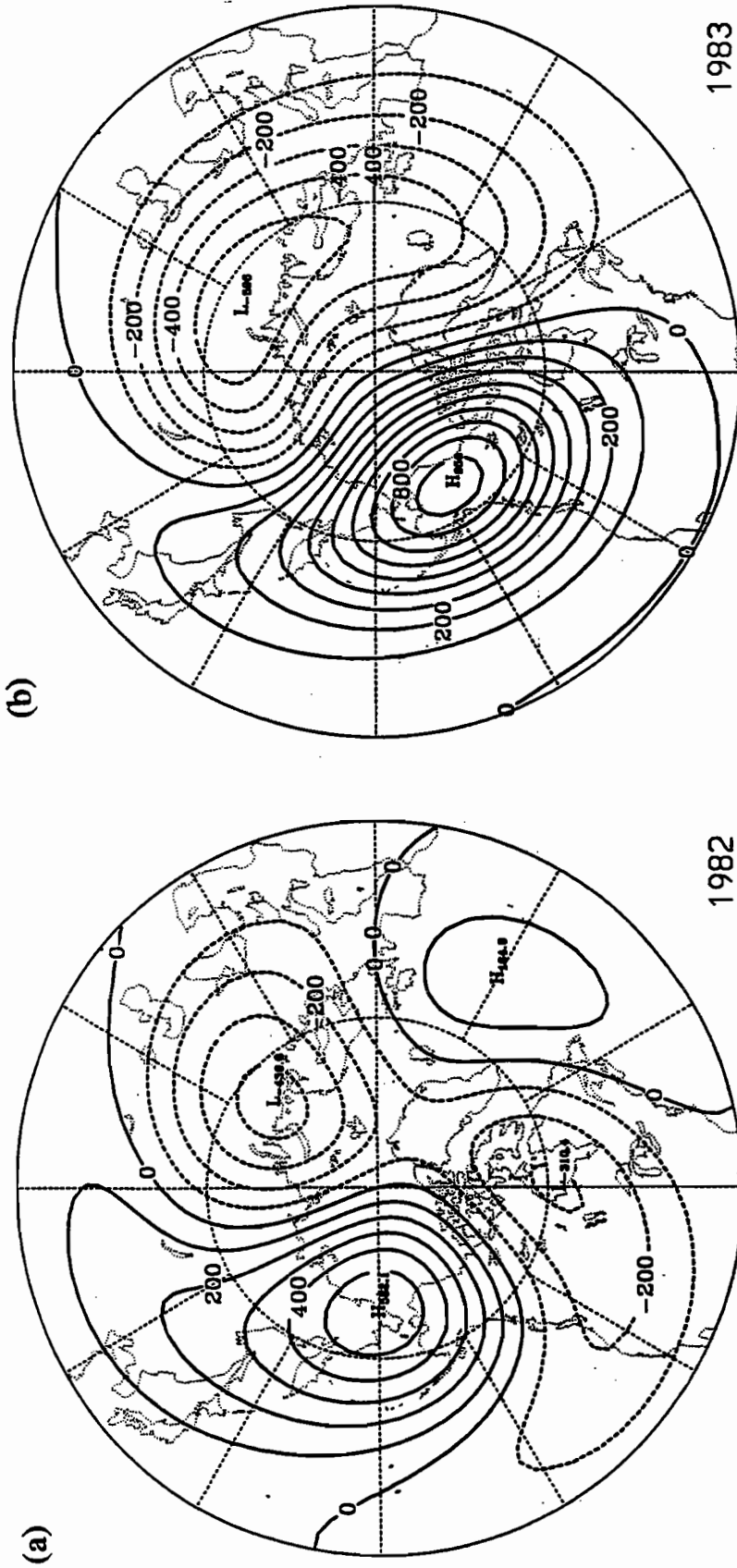


Fig. 4.9 Geopotential height field (sum of zonal waves 1-3), from nonlinear model without transients, for log-pressure height 32 km. Contour interval 100 m. (a) 1982, (b) 1983, (c) 1984, (d) 1986.

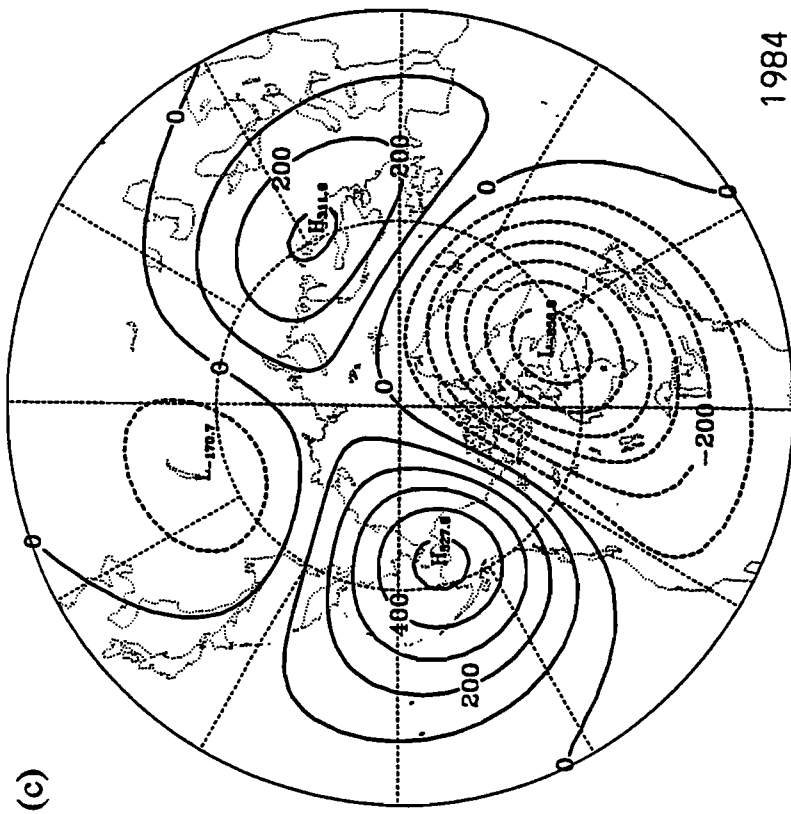
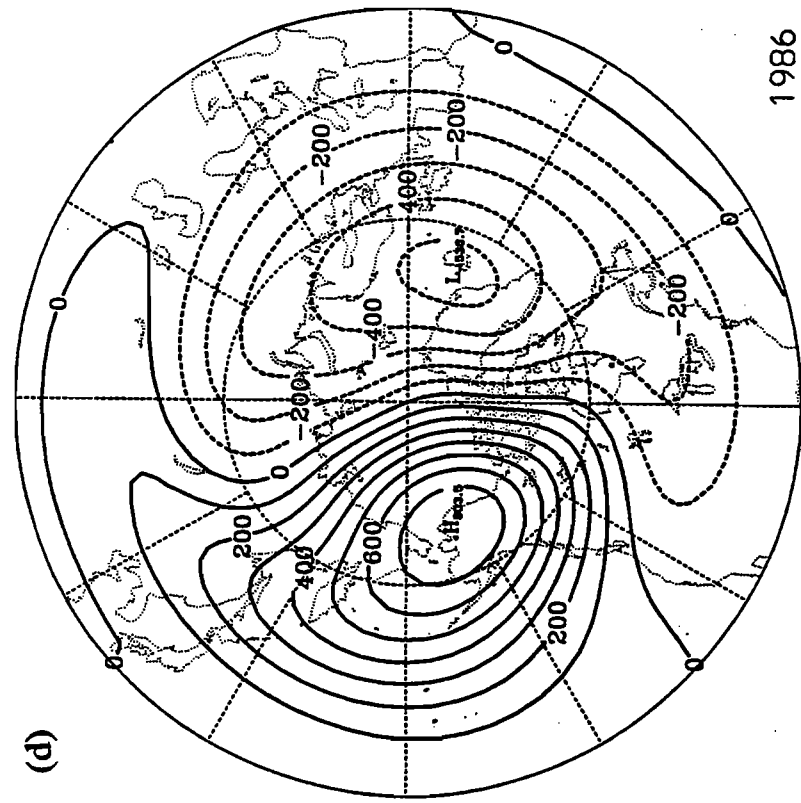


Fig. 4.9 Continued.

model without transients. The shape of the low is more accurately reproduced in the nonlinear model, without the excessive elongation to the west given by the linear model. Again, the change in amplitude due to the inclusion of the nonlinear interactions among the stationary waves is less than that given by the inclusion of forcing by transients.

For 1984, the nonlinear model performs only slightly better than the other versions of the model. The model results continue to show a strong wave 2 pattern at 32 km, in contrast to observations, which show a pattern dominated by wave 1. Inclusion of nonlinear interactions gives a slight improvement in that the high over the Bering Strait, which corresponds to an observed feature, is strengthened, while that over western Russia, which is spurious, is weakened.

For 1986, inclusion of the nonlinear interactions among the stationary waves gives a slightly stronger high at 32 km, in better agreement with observations. The low is weakened slightly, but its position near Iceland is in better agreement with observations than that in the linear model. Once again, inclusion of nonlinear interactions among the stationary waves has less effect on the wave amplitudes than does inclusion of forcing by transients. The linear model with transients gives a better approximation to the observed amplitudes, but the nonlinear model without transients better reproduces the observed phase structure.

Figure 4.10 shows the structure of the January mean zonal wave 1 as calculated by the nonlinear model without transients for each of the four years studied. Comparing these with the output of the linear model without transients (Figure 4.3), we see that inclusion of forcing by the nonlinear interaction among the stationary waves has a

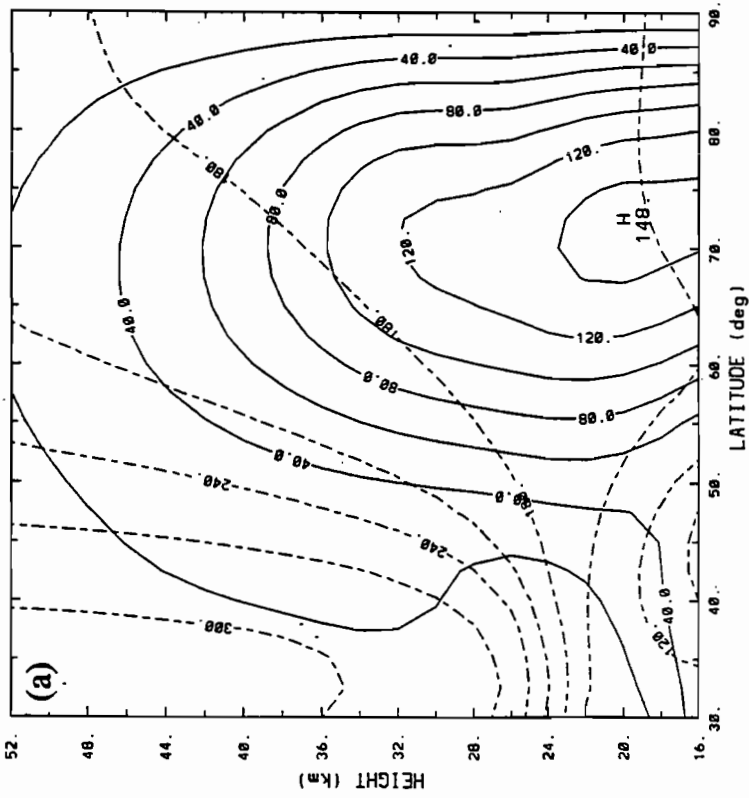
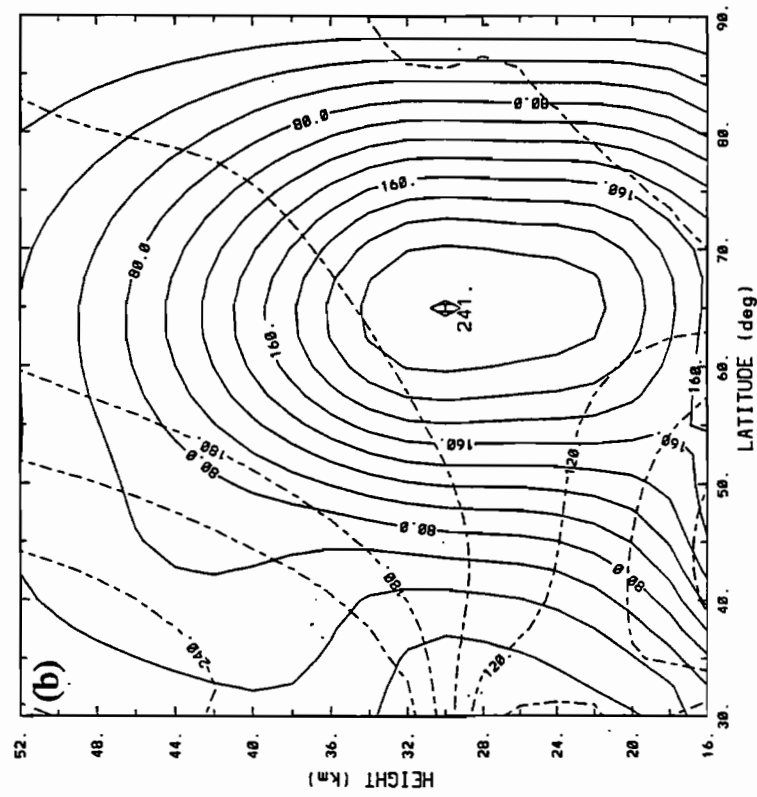


Fig. 4.10 Stationary zonal wave $k=1$, from nonlinear model without transients. Solid lines are amplitude (contour interval 20 m), broken lines are phase (contour interval 30°). Note that amplitudes are divided by factor of $\exp((z-z_0)/2H)$. (a) 1982, (b) 1983, (c) 1984, (d) 1986.

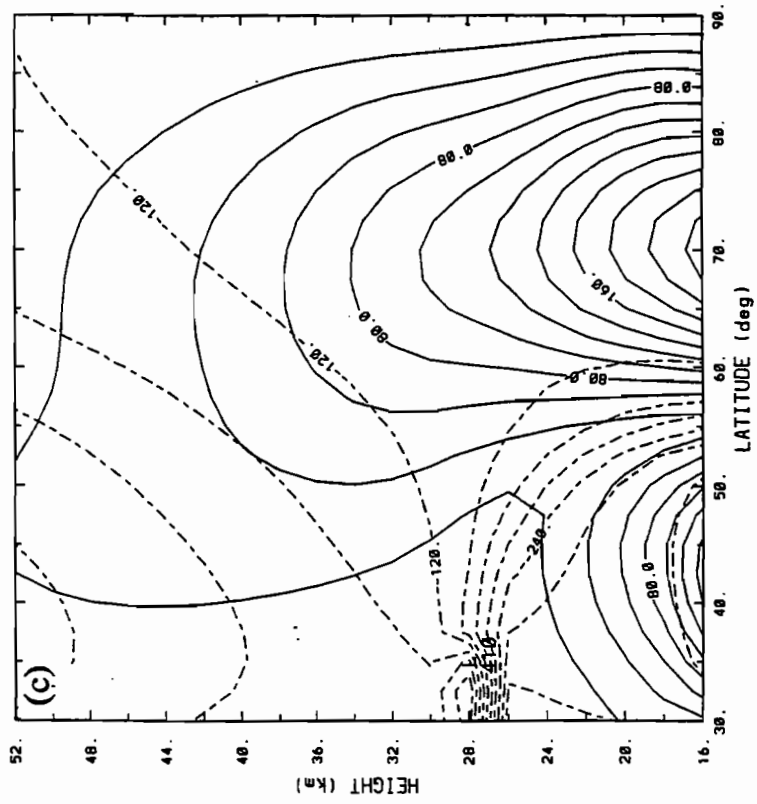
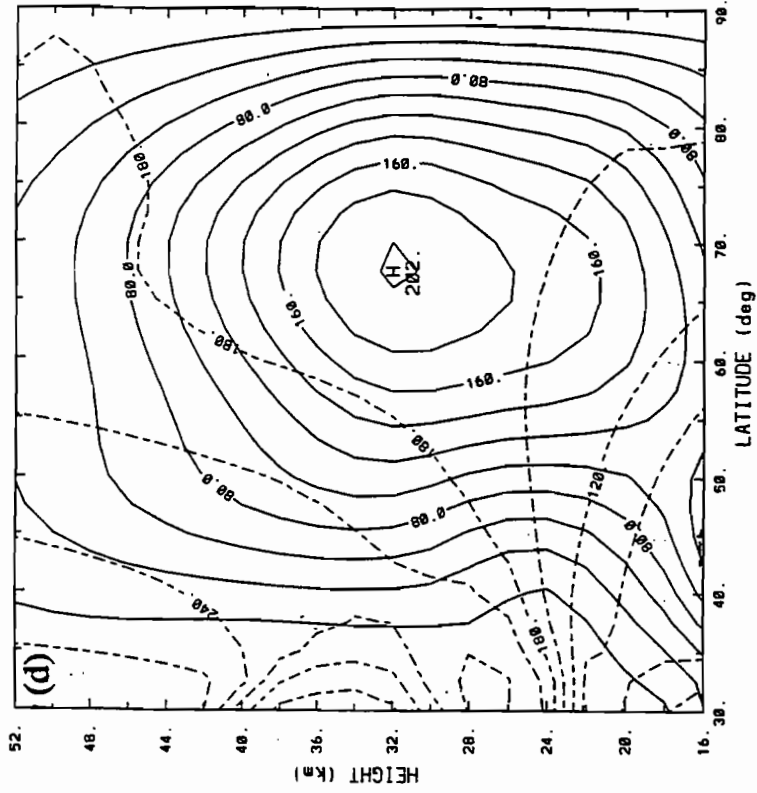


Fig. 4.10 Continued.

relatively small effect on the amplitude of stationary wave 1, except for 1986, where the maximum amplitude is increased by 35%. For 1982, this version of the model gives a wave 1 which has an amplitude maximum at 20 km. Although this is slightly better than the linear model without transients, which gives a monotonically decaying wave, the wave is still much too strongly trapped, in contrast with observations. Inclusion of forcing by transients gives much better results in this case, with a correctly-positioned amplitude maximum. Inclusion of nonlinear interactions among stationary waves does reduce the phase tilt of wave 1, giving better agreement with observations.

For 1983, the nonlinear model gives a slight increase in the amplitude of wave 1, compared to the linear model without transients, but the increase is less than that produced by the inclusion of forcing by transients. In all cases, the general structure of this wave is reproduced reasonably well, but the wave amplitude remains too weak.

For 1984, the nonlinear model gives a trapped wave, like the other versions of the model, but in contrast to the observed behaviour of the atmosphere. Both the nonlinear model without transients and the linear model with transients give a more rapidly decaying wave than the linear model without transients.

For 1986, the inclusion of nonlinear interactions among stationary waves gives a wave 1 with a substantially greater amplitude than that computed by the linear model without transients. The phase tilt with height is decreased. Both these changes bring the model output into better agreement with observations. The increase in amplitude is considerably less than that given by the linear model with transients.

Figure 4.11 shows the structure of the January mean zonal wave 2 as calculated by the nonlinear model without transients for each of the four years studied. Comparing these with the output of the linear model without transients (Figure 4.4), we see that inclusion of forcing by the nonlinear interaction among the stationary waves has a relatively small effect on wave 2, much less than that on wave 1. In both versions of the model, wave 2 tends to be somewhat more rapidly decaying with height than in nature. Inclusion of nonlinear interactions tends to shift the latitude of maximum amplitude slightly farther north, giving better agreement with observations.

In summary, the nonlinear model without transients reproduces the gross features of the stratospheric stationary waves fairly well, for three of the four years studied. The main shortcoming of this version of the model is that the amplitudes it generates are significantly too weak. Inclusion of forcing by the monthly mean of transient momentum and heat flux divergences results in a significant increase in the amplitude of wave 1, bringing the model into better agreement with observations, though the wave amplitudes remain somewhat too weak. There is much less change in waves 2 and 3 when forcing by transients is included. Inclusion of nonlinear interactions among the stationary waves has less effect on wave amplitudes than does the inclusion of forcing by transients, but the nonlinear model without transients is better able to reproduce the observed phase structure of the waves.

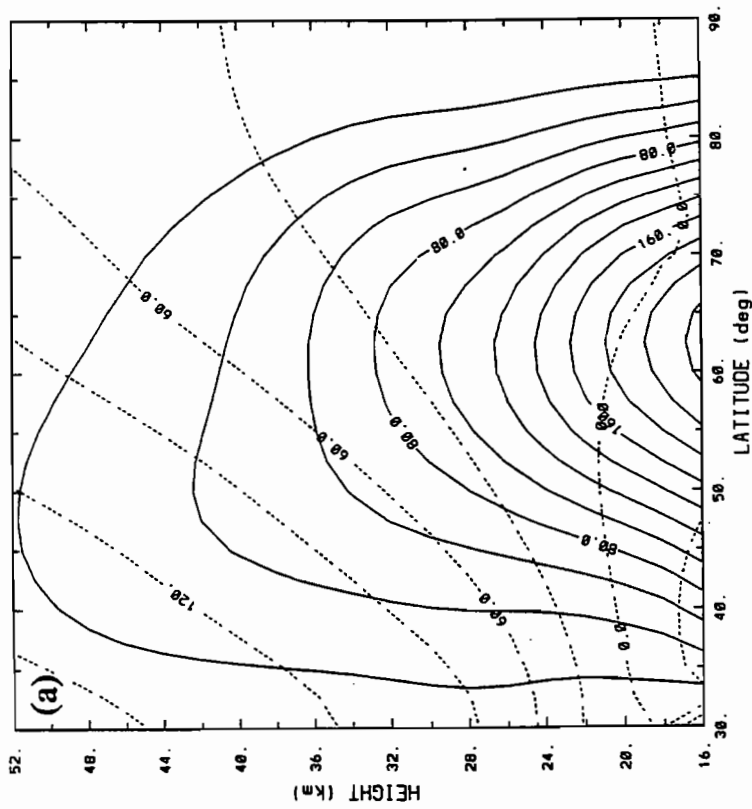
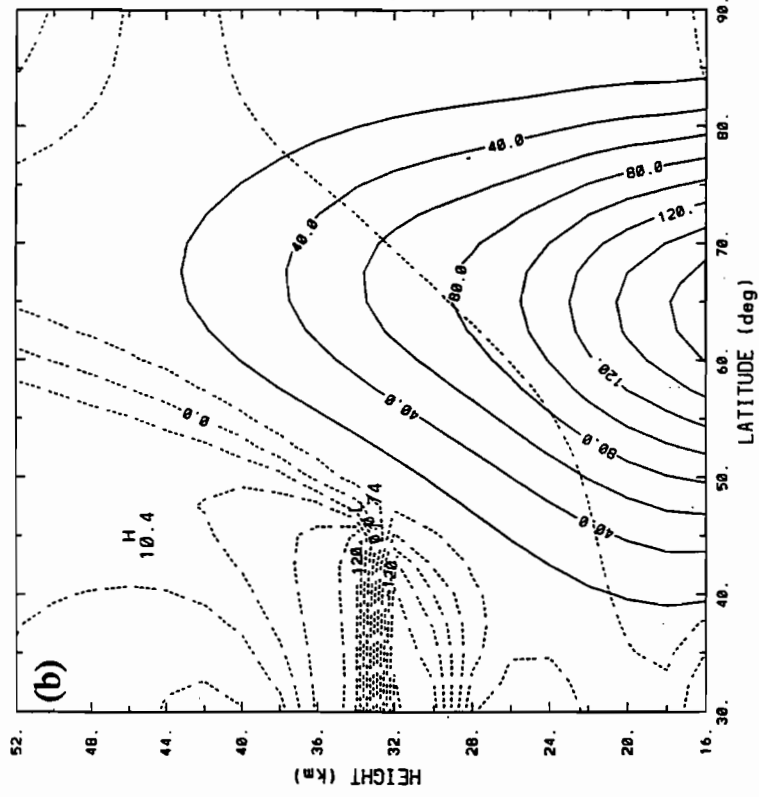


Fig. 4.11 As in Fig. 4.10, but for zonal wave $k=2$.

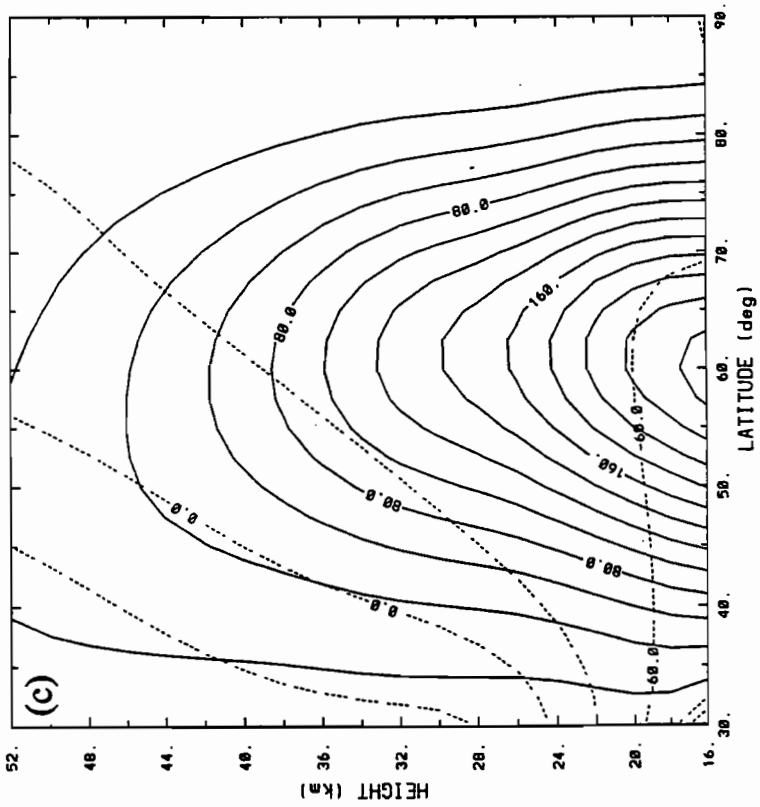
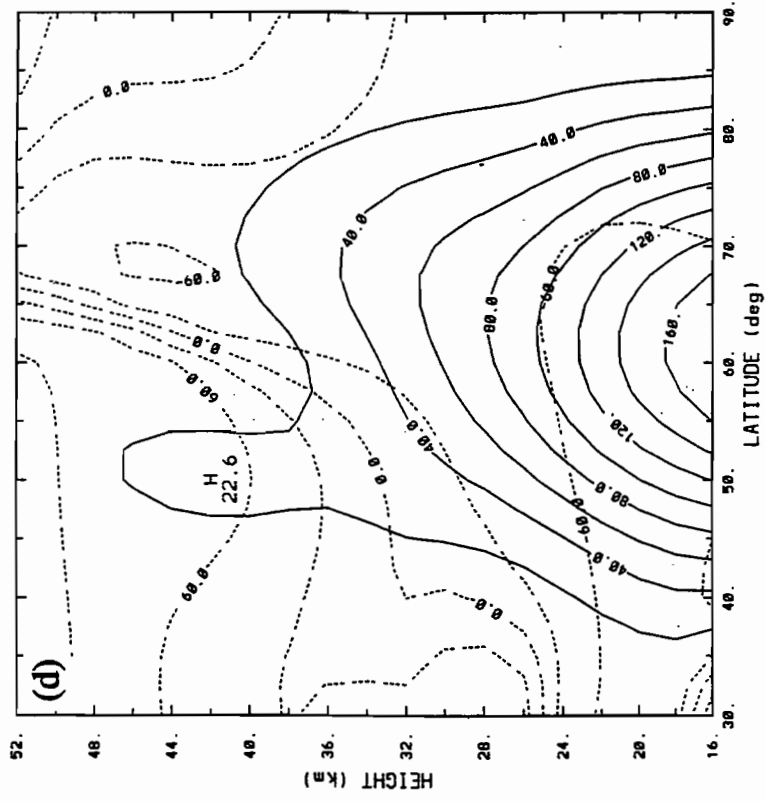


Fig. 4.11 Continued.

CHAPTER 5

DISCUSSION AND CONCLUSIONS

This work has extended previous modelling studies of stationary planetary waves in the winter stratosphere by the use of a nonlinear primitive-equations model, by the use of observed data from individual years to specify the zonal mean state and the forcing fields, and by computation of the monthly mean of the transient momentum flux and heat flux divergences, and the use of these fields as additional forcing terms in the model.

The observed January monthly mean circulation in the stratosphere varies greatly from one year to another. The zonal mean wind speed, the stationary wave amplitudes, and the transient momentum and heat flux divergences can all vary by 50% or more. This variability is reflected in the performance of the model, which is much more successful at reproducing the observed stationary wave structure for some years than for others.

A linear version of the model without forcing by the monthly mean of the transients is found to be able to reproduce many of the gross features of the observed stratospheric circulation. Zonal wavenumbers 2 and 3 are found to be trapped at lower levels, with wave 3 more strongly trapped than wave 2, in good agreement with observations. Only wave 1 is able to propagate in the stratosphere. The position of the height maximum near Alaska, a feature showing relatively little interannual variability in the real atmosphere, is correctly computed by this model. The position of the height

minima are less well reproduced, though there is some similarity between observations and model output.

This model's ability to reproduce the observed wave structure is deficient in several respects. The most notable of these is that the wave amplitudes computed by the model are much too weak. Zonal wavenumber 2 decays somewhat more rapidly with height in the model than in nature, but the main deficiency occurs with zonal wavenumber 1, which is much weaker in the linear model without transients than in nature. The performance of the model with respect to wave 2 is similar from year to year, but for wave 1 it varies greatly. For some years, the model reproduces the observed propagation of wave 1 into the stratosphere, though the model's wave amplitudes are too weak, while for other years the model computes a trapped wave which decays monotonically with height.

The linear model without transients is also able to reproduce the general features of the waves' phase structure, namely a westward tilt with height and a southwest-northeast tilt in the horizontal. There is somewhat more phase tilt in the model than in observations.

Inclusion of forcing by the monthly mean of transient momentum and flux divergences is found to produce a substantial improvement in the model's ability to reproduce the observed wave structure. In particular, the amplitude of wave 1 is increased substantially in two of the four years studied, and increased slightly for one year, bringing the model results into better agreement with observations, though the model amplitudes remain somewhat too weak. This suggests that the time-averaged

effects of transient fluxes are a significant forcing mechanism for stratospheric stationary waves, in addition to forcing by stationary waves from the troposphere. The phase structure of wave 1 and the amplitude and phase of wave 2 are less affected by the inclusion of forcing by transients than is the amplitude of phase 1.

Inclusion of nonlinear interactions among the stationary waves has a smaller effect on the model results than does inclusion of forcing by transients. The nonlinear model without transients yields somewhat larger wave 1 amplitudes than does the linear model without transients, but the improvement is modest. Nonlinear interactions among the stationary waves appear to be less important than those among transients for the forcing of wave 1. The nonlinear model without transients does yield a more realistic phase structure than the other versions of the model, by reducing the westward phase tilt with height.

For one of the years studied, 1984, all of the models perform poorly at reproducing the observed wave structure. The models' wave 2 for this year is not significantly worse than for other years, but none of the models correctly simulates the behaviour of wave 1 for 1984. All of the models compute a wave 1 which decays with height, while in nature this wave was found to have an amplitude maximum in the interior of the region studied. The 1984 circulation is anomalous in some respects. The mean zonal wind speed in the upper stratosphere is greater for this year than for the other years studied. This should produce stronger trapping of the stationary waves, and the maximum kinetic energy of zonal wave 1 is indeed found at a lower level in 1984 than in other years. However, the wave decays much too rapidly in the model. The forcing

due to transient flux divergences is smaller in 1984 than in the other years studied, so it is not surprising that the inclusion of forcing by transients does not produce a significant improvement in the model performance. A completely satisfactory explanation for the poor performance of the models in simulating wave 1 for this year has not been found.

Since the inclusion of either forcing by transients or nonlinear interactions among stationary waves tends to improve the model's ability to reproduce the observed circulation, it seems plausible to conjecture that including both of these mechanisms simultaneously would give an even more accurate simulation of the observed wave structure. Compared to the linear model without transients, the linear model with transients gives substantially greater wave amplitudes, though they remain somewhat too weak, while the nonlinear model without transients gives slightly greater wave amplitudes and a more accurate phase structure. It seems likely that a nonlinear model with transients should compute wave structures very similar in both amplitudes and phases to those observed in nature. Unfortunately, numerical difficulties in obtaining convergence to a solution of the coupled nonlinear equations of this model have prevented this experiment from being conducted successfully.

The difficulty in finding an exact solution using the nonlinear model with transients is not surprising. As we have seen above, the inclusion of forcing by transients significantly increases the amplitudes of the stationary waves computed by the linear model. The nonlinear interactions among these waves will therefore tend to be stronger, and the difference between the linear solution and that found at subsequent

iterations will be greater. Under these circumstances, the iterative technique, which works best for a weakly nonlinear system, is less likely to converge to an exact solution of the nonlinear equations. It may therefore be difficult to extend this line of research further, unless another solution technique is employed.

The model used in this work is an extension of those used in a series of studies, beginning with that of Matsuno (1970). These are grid point models in latitude and height, and spectral in longitude. At several points in this work, numerical difficulties were encountered at grid points near the North Pole. As described in Section 3.8, smoothing by averaging the values of fields at neighbouring grid points was employed to overcome these difficulties. In future work, it may be preferable to use a model which is spectral in both horizontal dimensions, in an effort to avoid numerical difficulties near the pole and to provide a more natural method of eliminating spurious small-scale structures through truncation of an expansion in spherical harmonics.

The present work has found that the behaviour of the stationary planetary waves in the stratosphere shows a strong interannual variability. It would be of interest to examine how this variability correlates with other phenomena known to show strong interannual variability, such as the quasi-biennial oscillation in the equatorial stratosphere, or the El Niño-Southern Oscillation. As discussed in Section 3.4, the present model includes strong Rayleigh friction at low latitudes to avoid numerical difficulties near the critical surface, so this model cannot be used to study possible tropical-extratropical interactions. A modification of the model to allow such studies would be of interest. There is, however, no known method of generalizing models of

the type used in this work to enable them to deal with critical layers, within which wave transience, dissipation, and nonlinearity may all be important. It may therefore be necessary to employ fully nonlinear time-dependent models to study these phenomena.

APPENDIX A

COEFFICIENTS OF MODEL EQUATIONS

In equations (3.10)-(3.12), the monthly means of the nonlinear interactions between the transients are given by:

$$(Tr)_u = - \left[\frac{u'}{\cos \theta} \frac{\partial u'}{\partial \lambda} + \frac{v'}{\cos \theta} \frac{\partial}{\partial \theta} (u' \cos \theta) + w \cdot \frac{\partial u'}{\partial z} \right], \quad (A.1)$$

$$(Tr)_v = - \left[\frac{u'}{\cos \theta} \frac{\partial v'}{\partial \lambda} + v' \frac{\partial v'}{\partial \theta} + w \cdot \frac{\partial v'}{\partial z} + (u')^2 \tan \theta \right], \quad (A.2)$$

$$(Tr)_T = - \left[\frac{u'}{\cos \theta} \frac{\partial \Phi'_z}{\partial \lambda} + v' \frac{\partial \Phi'_z}{\partial \theta} + w \cdot N^2 \right]. \quad (A.3)$$

In equations (3.15)-(3.17), the nonlinear interactions between the stationary waves are given by:

$$(St)_u = - \left[\frac{\hat{u}}{\cos \theta} \frac{\partial \hat{u}}{\partial \lambda} + \frac{\hat{v}}{\cos \theta} \frac{\partial}{\partial \theta} (\hat{u} \cos \theta) + \hat{w} \frac{\partial \hat{u}}{\partial z} \right], \quad (A.4)$$

$$(St)_v = - \left[\frac{\hat{u}}{\cos \theta} \frac{\partial \varphi}{\partial \lambda} + \hat{v} \frac{\partial \varphi}{\partial \theta} + \hat{w} \frac{\partial \varphi}{\partial z} + \tan \theta \hat{u}^2 \right], \quad (\text{A.5})$$

$$(St)_T = - \left[\frac{\hat{u}}{\cos \theta} \frac{\partial \hat{\Phi}_z}{\partial \lambda} + \hat{v} \frac{\partial \hat{\Phi}_z}{\partial \theta} + \hat{w} \hat{N}^2 \right], \quad (\text{A.6})$$

while the coefficients ω , β^* , ξ^* , and Z^* , which are functions of the zonal mean state, are given by:

$$\omega = \frac{[u]}{\cos \theta}, \quad (\text{A.7})$$

$$\beta^* = \frac{1}{\cos \theta} \frac{\partial}{\partial \theta} ([u] \cos \theta) - f^*, \quad (\text{A.8})$$

$$\xi^* = f^* + 2[u] \tan \theta - 2(a\Omega + \omega) \sin \theta, \quad (\text{A.9})$$

$$Z^* = \frac{\partial[\Phi]}{\partial\theta} = -\xi \cdot \frac{\partial[u]}{\partial z}. \quad (\text{A.10})$$

When the longitudinal dependence in the model equations is transformed from real to Fourier space, the nonlinear interactions of the stationary waves and those of the transients are given in (3.21)-(3.23) by:

$$P_k^S = -\frac{i}{2\pi} e^{-\frac{z-z_0}{2H}} \int_0^{2\pi} (St)_u e^{-ik\lambda} d\lambda, \quad (\text{A.11})$$

$$Q_k^S = \frac{1}{2\pi} e^{-\frac{z-z_0}{2H}} \int_0^{2\pi} (St)_v e^{-ik\lambda} d\lambda, \quad (\text{A.12})$$

$$R_k^S = -\frac{i}{2\pi} e^{-\frac{z-z_0}{2H}} \int_0^{2\pi} (St)_T e^{-ik\lambda} d\lambda, \quad (\text{A.13})$$

$$P_k^T = -\frac{i}{2\pi} e^{-\frac{z-z_0}{2H}} \int_0^{2\pi} (Tr)_u e^{-ik\lambda} d\lambda, \quad (\text{A.14})$$

$$Q_k^T = \frac{1}{2\pi} e^{-\frac{z-z_0}{2H}} \int_0^{2\pi} (Tr)_v e^{-ik\lambda} d\lambda, \quad (\text{A.15})$$

$$R_k^T = -\frac{i}{2\pi} e^{-\frac{z-z_0}{2H}} \int_0^{2\pi} (Tr)_T e^{-ik\lambda} d\lambda. \quad (\text{A.16})$$

In (3.25), ϵ and τ are functions of the zonal mean state, given by:

$$\epsilon = \Delta_k^2 + \beta^* \xi^*, \quad (\text{A.17})$$

$$\tau = \epsilon[N^2] + Z^{*2}. \quad (\text{A.18})$$

The coefficients and inhomogeneous terms of (3.26) are given by

$$A = -\tau \epsilon \Gamma_k, \quad (\text{A.19})$$

$$B = -\tau Z^* (\Gamma_k + \Delta_k), \quad (\text{A.20})$$

$$C = \tau \Delta_k [N^2], \quad (\text{A.21})$$

$$D = \tau \left\{ \frac{k}{\cos \theta} \left[\Gamma_k \Delta_k \frac{\partial [u]}{\partial z} + \xi^* Z^* \right] - \frac{1}{\cos \theta} \frac{\partial}{\partial \theta} (Z^* \Gamma_k \cos \theta) - \frac{\partial}{\partial z} (\epsilon \Gamma_k) \right\} + \Gamma_k \left\{ Z^* \frac{\partial \tau}{\partial \theta} + \epsilon \frac{\partial \tau}{\partial z} \right\}, \quad (\text{A.22})$$

$$E = \tau \left\{ \frac{k}{\cos \theta} \left[Z^* \frac{\partial [u]}{\partial z} - [N^2] (\beta^* + \xi^*) \right] + \frac{Z^*}{2H} (\Delta_k - \Gamma_k) + \frac{1}{\cos \theta} \frac{\partial}{\partial \theta} (\Delta_k [N^2] \cos \theta) - \frac{\partial}{\partial z} (Z^* \Delta_k) \right\} + \Delta_k \left\{ Z^* \frac{\partial \tau}{\partial z} - [N^2] \frac{\partial \tau}{\partial \theta} \right\}, \quad (\text{A.23})$$

$$F = \tau \left\{ \frac{k \Delta_k}{\cos \theta} \left[\frac{\Gamma_k}{2H} \frac{\partial [u]}{\partial z} - \frac{k [N^2]}{\cos \theta} \right] - \frac{1}{\cos \theta} \frac{\partial}{\partial \theta} \left[k \xi^* [N^2] + \frac{\Gamma_k Z^*}{2H} \cos \theta \right] + \frac{\partial}{\partial z} \left[\frac{k \xi^* Z^*}{\cos \theta} - \frac{\epsilon \Gamma_k}{2H} \right] \right\} + \frac{\partial \tau}{\partial \theta} \left[\frac{k \xi^* [N^2]}{\cos \theta} + \frac{\Gamma_k Z^*}{2H} \right] + \left[\frac{\partial \tau}{\partial z} + \frac{\tau}{2H} \right] \left[\frac{\epsilon \Gamma_k}{2H} - \frac{k \xi^* Z^*}{\cos \theta} \right], \quad (\text{A.24})$$

$$G^j = \tau \left\{ -\frac{k}{\cos \theta} X^j - \frac{1}{\cos \theta} \frac{\partial}{\partial \theta} (Y^j \cos \theta) - \frac{\partial V^j}{\partial z} + \frac{V^j}{2H} \right\} + \frac{\partial \tau}{\partial \theta} Y^j + \frac{\partial \tau}{\partial z} V^j. \quad (\text{A.25})$$

In (A.25), X^j , Y^j , and V^j are given by

$$X^j = \Delta_k \left[[N^2] P_k^j - \frac{\partial [u]}{\partial z} R_k^j \right] + \left[[N^2] \beta^* - Z^* \frac{\partial [u]}{\partial z} \right] Q_k^j, \quad (\text{A.26})$$

$$Y^j = [N^2](\xi^* P_k^j - \Delta_k Q_k^j) + Z^* R_k^j, \quad (\text{A.27})$$

$$V^j = Z^*(\Delta_k Q_k^j - \xi^* P_k^j) + \epsilon R_k^j. \quad (\text{A.28})$$

In (A.25)-(A.28), the superscript j may take the value S or T , for "stationary" and "transient," respectively, as used in (A.11)-(A.16).

By substituting (A.4) in (A.11), and using (3.20) to write the wind components in (A.4) as Fourier series, it can be shown that

$$P_k^S = -e^{\frac{z-z_0}{2H}} \sum_{\substack{m,n \\ m+n=k}} \left\{ \frac{k}{\cos \theta} \tilde{u}_m \tilde{u}_n + \frac{1}{\cos^2 \theta} \frac{\partial}{\partial \theta} (\tilde{u}_m \tilde{v}_n \cos^2 \theta) + \frac{\partial}{\partial z} (\tilde{u}_m \tilde{w}_n) \right\}. \quad (\text{A.29})$$

Similarly, we have

$$Q_k^S = e^{\frac{z-z_0}{2H}} \sum_{\substack{m,n \\ m+n=k}} \left\{ \frac{k}{\cos \theta} \tilde{u}_m \tilde{v}_n + \frac{1}{\cos \theta} \frac{\partial}{\partial \theta} (\tilde{v}_m \tilde{v}_n \cos \theta) + \frac{\partial}{\partial z} (\tilde{v}_m \tilde{w}_n) - \tan \theta \tilde{u}_m \tilde{u}_n \right\}, \quad (\text{A.30})$$

and

$$R_k^S = -e^{\frac{z-z_0}{2H}} \sum_{\substack{m,n \\ m+n=k}} \left\{ \frac{k}{\cos\theta} \bar{u}_m \bar{\Psi}_n + \frac{1}{\cos\theta} \frac{\partial}{\partial\theta} (\bar{v}_m \bar{\Psi}_n \cos\theta) \right. \\ \left. + \frac{\partial}{\partial z} (\bar{w}_m \bar{\Psi}_n) + \frac{\kappa}{H} (\bar{w}_m \bar{\Psi}_n) \right\}, \quad (\text{A.31})$$

where κ is the ratio of the gas constant and the heat capacity of dry air (R/c_p), and

$$\bar{\Psi}_n = \frac{\partial \bar{\Phi}_n}{\partial z} + \frac{\bar{\Phi}_n}{2H}. \quad (\text{A.32})$$

APPENDIX B

NUMERICAL SOLUTION OF MODEL EQUATIONS

Calculations are performed on a rectangular grid with a spacing of 1° in latitude and 1 km in height. This resolution is the same as that used by Jacqmin and Lindzen (1985). They found that with lower resolution, the model was very sensitive to small changes in the zonal mean state, but that this sensitivity decreased as the model resolution increased.

More precisely, the model has 90 grid points in latitude, with the southernmost grid point one-half grid space north of the equator, and the northernmost grid point one grid space south of the North Pole. This gives a grid spacing of $180/181$ degrees.

Let grid points be labelled (j, ℓ) , where j runs from 1 at the grid point nearest the equator to 90 at the grid point nearest the pole, and ℓ runs from 1 at the lower boundary to 65 at the upper boundary. We write Φ_j for the value of the solution $\tilde{\Phi}_k$ to the model equation (3.26) at the latitudinal grid point j , with Φ_j considered to be a continuous function of the vertical coordinate z , and $\Phi_{j\ell}$ for the value of $\tilde{\Phi}_k$ at grid point (j, ℓ) , with a similar notation for the coefficients A-G in (3.26). In order to simplify the notation, the wavenumber subscript k will be omitted in this appendix.

We wish to discretize the model equation (3.26). We replace the derivatives with respect to latitude with second-order centred finite differences, considering the coefficients A-G and the solution Φ to be continuous functions of z . Then at the latitude of grid point j we have

$$\begin{aligned}
A_j \frac{\partial^2 \Phi_j}{\partial z^2} + \frac{B_j}{2\Delta\theta} \left\{ \frac{\partial \Phi_{j+1}}{\partial z} - \frac{\partial \Phi_{j-1}}{\partial z} \right\} + \frac{C_j}{(\Delta\theta)^2} \{ \Phi_{j+1} - 2\Phi_j + \Phi_{j-1} \} \\
+ D_j \frac{\partial \Phi}{\partial z} + \frac{E_j}{2\Delta\theta} \{ \Phi_{j+1} - \Phi_{j-1} \} + F_j \Phi_j - G_j.
\end{aligned} \tag{B.1}$$

In order to evaluate (B.1) at grid point $j = 1$, we need the value of Φ at the "virtual" grid point $j = 0$. This grid point is one-half grid space south of the equator, so since the solution is assumed to be symmetric about the equator, we have $\Phi_0 = \Phi_1$. As discussed in Section 3.3, this choice of boundary condition near the equator does not strongly affect the results of this study, since strong Rayleigh damping is imposed at low latitudes, causing the wave amplitudes to be small at low latitudes.

In order to evaluate (B.1) at $j = 90$, we need the value of Φ at the "virtual" grid point $j = 91$. This is the North Pole, so $\Phi = 0$ there. Early versions of the model employing this boundary condition at the pole displayed numerical problems at high latitudes, so an alternative boundary condition was employed. Analytically, this is (3.27). Numerically, this takes the form $\Phi_{90} = 2^{-k}\Phi_{99}$. (B.1) is not solved at $j = 90$; this grid point is used to impose the boundary condition near the pole.

(B.1) can be expressed in matrix form as

$$\Lambda \frac{\partial^2 \vec{\Phi}}{\partial z^2} + M \frac{\partial \vec{\Phi}}{\partial z} + N \vec{\Phi} - \vec{R}, \tag{B.2}$$

where

$$\Lambda = \begin{pmatrix} A_1 & 0 & 0 & \dots & 0 \\ 0 & A_2 & 0 & \dots & 0 \\ 0 & 0 & A_3 & \dots & 0 \\ \dots & \dots & \dots & \dots & \dots \\ 0 & 0 & 0 & \dots & A_{89} \end{pmatrix},$$

and

$$M = \begin{pmatrix} D_1 - \frac{B_1}{2\Delta\theta} & \frac{B_1}{2\Delta\theta} & 0 & 0 & \dots & \dots & 0 & 0 \\ -\frac{B_2}{2\Delta\theta} & D_2 & \frac{B_2}{2\Delta\theta} & 0 & \dots & \dots & 0 & 0 \\ 0 & -\frac{B_3}{2\Delta\theta} & D_3 & \frac{B_3}{2\Delta\theta} & \dots & \dots & 0 & 0 \\ 0 & 0 & -\frac{B_4}{2\Delta\theta} & D_4 & \frac{B_4}{2\Delta\theta} & \dots & 0 & 0 \\ \dots & \dots & \dots & \dots & \dots & \dots & \dots & \dots \\ \dots & \dots & \dots & \dots & \dots & \dots & \dots & \dots \\ 0 & 0 & 0 & 0 & \dots & -\frac{B_{88}}{2\Delta\theta} & D_{88} & \frac{B_{88}}{2\Delta\theta} \\ 0 & 0 & 0 & 0 & \dots & \dots & -\frac{B_{89}}{2\Delta\theta} & D_{89} + 2^{-k} \frac{B_{89}}{2\Delta\theta} \end{pmatrix},$$

and

$$N - \begin{pmatrix} F_1 - \frac{C_1}{(\Delta\theta)^2} - \frac{E_1}{2\Delta\theta} & \frac{C_1}{(\Delta\theta)^2} + \frac{E_1}{2\Delta\theta} & 0 & \dots & 0 & 0 \\ \frac{C_2}{(\Delta\theta)^2} - \frac{E_2}{2\Delta\theta} & F_2 - \frac{2C_2}{(\Delta\theta)^2} & \frac{C_2}{(\Delta\theta)^2} + \frac{E_2}{2\Delta\theta} & \dots & 0 & 0 \\ 0 & \frac{C_3}{(\Delta\theta)^2} - \frac{E_3}{2\Delta\theta} & F_3 - \frac{2C_3}{(\Delta\theta)^2} & \dots & 0 & 0 \\ \cdot & \cdot & \cdot & \dots & \cdot & \cdot \\ \cdot & \cdot & \cdot & \dots & \cdot & \cdot \\ \cdot & \cdot & \cdot & \dots & \cdot & \cdot \\ 0 & 0 & 0 & \dots & F_{88} - \frac{2C_{88}}{(\Delta\theta)^2} & \frac{C_{88}}{(\Delta\theta)^2} + \frac{E_{88}}{2\Delta\theta} \\ 0 & 0 & 0 & \dots & \frac{C_{89}}{(\Delta\theta)^2} - \frac{E_{89}}{2\Delta\theta} & F_{89} + (2^{-k} - 2) \frac{C_{89}}{(\Delta\theta)^2} + 2^{-k} \frac{E_{89}}{2\Delta\theta} \end{pmatrix}$$

Here

$$\vec{\Phi} = (\Phi_1 \ \Phi_2 \ \Phi_3 \ \dots \ \Phi_{89})^T,$$

and

$$\vec{G} = (G_1 \ G_2 \ G_3 \ \dots \ G_{89})^T.$$

We now discretize (B.2) in the vertical, replacing derivatives with second-order finite differences, giving

$$\Lambda_l \frac{\bar{\Phi}_{l+1} - 2\bar{\Phi}_l + \bar{\Phi}_{l-1}}{(\Delta z)^2} + M_l \frac{\bar{\Phi}_{l+1} - \bar{\Phi}_{l-1}}{2\Delta z} + N_l \bar{\Phi}_l - \bar{G}_l, \quad (\text{B.3})$$

where Λ_l , M_l , N_l , $\bar{\Phi}_l$, \bar{G}_l represent the matrices and vectors as defined above, but evaluated at a given vertical level l , so, for example,

$$\bar{\Phi}_l = (\Phi_{1l} \quad \Phi_{2l} \quad \Phi_{3l} \quad \dots \quad \Phi_{(89)l})$$

and similarly for the other vectors and matrices. (B.3) can be rewritten as

$$AA_l \bar{\Phi}_{l-1} + BB_l \bar{\Phi}_l + CC_l \bar{\Phi}_{l+1} - \bar{G}_l, \quad (\text{B.4})$$

where

$$AA_l = \frac{\Lambda_l}{(\Delta z)^2} - \frac{M_l}{2\Delta z},$$

and

$$BB_l = N_l - \frac{2\Lambda_l}{(\Delta z)^2},$$

and

$$CC_l = \frac{\Lambda_l}{(\Delta z)^2} + \frac{M_l}{2\Delta z}.$$

(B.4) is an equation of the form which can easily be solved using the method of Lindzen and Kuo (1969). For each vertical level l , let

$$\vec{\Phi}_l = \alpha_l \vec{\Phi}_{l+1} + \vec{\beta}_l, \quad (\text{B.5})$$

where α_l is a matrix and $\vec{\beta}_l$ a vector to be determined. From (B.5) we have

$$\vec{\Phi}_{l-1} = \alpha_{l-1} \vec{\Phi}_l + \vec{\beta}_{l-1}. \quad (\text{B.6})$$

Substituting (B.6) in (B.4) gives

$$(AA_l \alpha_{l-1} + BB_l) \vec{\Phi}_l + CC_l \vec{\Phi}_{l+1} = \vec{G}_l - AA_l \vec{\beta}_{l-1},$$

or

$$\vec{\Phi}_l = -(AA_l \alpha_{l-1} + BB_l)^{-1} CC_l \vec{\Phi}_{l+1} + (AA_l \alpha_{l-1} + BB_l)^{-1} (\vec{G}_l - AA_l \vec{\beta}_{l-1}). \quad (\text{B.7})$$

Comparing (B.5) and (B.7) gives

$$\alpha_l = -(AA_l \alpha_{l-1} + BB_l)^{-1} CC_l, \quad (\text{B.8})$$

and

$$\bar{\beta}_l = -(AA_l \alpha_{l-1} + BB_l)^{-1} (\bar{G}_l - AA_l \bar{\beta}_{l-1}). \quad (\text{B.9})$$

At $l = 1$ (the lower boundary), the solution is specified, so $\bar{\beta}_1 = \bar{\Phi}_1$ and $\alpha_1 = 0$. Then we can use (B.8) and (B.9) to calculate α_l and $\bar{\beta}_l$ at all levels. The upper boundary condition is that the waves vanish, so $\bar{\Phi}_l = 0$ at the uppermost level (in this case, $l = 65$). Then (B.5) can be used to compute $\bar{\Phi}_l$ at all levels, completing the solution of the model equation.

REFERENCES

- Andrews, D.G., J.R. Holton, and C.B. Leovy, 1987: *Middle Atmosphere Dynamics*. Academic Press, 489 pp.
- Ashe, S., 1979: A nonlinear model of the time-average axially asymmetric flow induced by topography and diabatic heating. *J. Atmos. Sci.*, **36**, 109-126.
- Boville, B.A., 1987: The validity of the geostrophic approximation in the winter stratosphere and troposphere. *J. Atmos. Sci.*, **44**, 443-457.
- Charney, J.G., and P.G. Drazin, 1961: Propagation of planetary-scale disturbances from the lower into the upper atmosphere. *J. Geophys. Res.*, **66**, 83-109.
- Derome, J., 1984: On quasi-geostrophic, finite-amplitude disturbances forced by topography and diabatic heating. *Tellus*, **36A**, 313-319.
- Dickinson, R.E., 1973: A method of parameterization for infrared cooling between the altitudes of 30 and 70 kilometers. *J. Geophys. Res.*, **78**, 4451-4457.
- Egger, J., 1976: Nonlinear aspects of the theory of standing planetary waves. *Beitr. Phys. Atmos.*, **49**, 71-80.
- Elson, L.S., 1986: Ageostrophic motions in the stratosphere from satellite observations. *J. Atmos. Sci.*, **43**, 408-418.
- Holton, J.R., 1975: The dynamic meteorology of the stratosphere and mesosphere. *Meteorology Monograph No. 37*, American Meteorological Society, 216 pp.
- Holton, J.R. and C. Mass, 1976: Stratospheric vacillation cycles. *J. Atmos. Sci.*, **33**, 2218-2225.

- Jacqmin, D., and R.S. Lindzen, 1985: The causation and sensitivity of the northern winter planetary waves. *J. Atmos. Sci.*, **42**, 724-745.
- Lin, B.-D., 1982: The behavior of winter stationary planetary waves forced by topography and diabatic heating. *J. Atmos. Sci.*, **39**, 1206-1226.
- Lindzen, R.S., and H.-L. Kuo, 1969: A reliable method for the numerical integration of a large class of ordinary and partial differential equations. *Mon. Wea. Rev.*, **97**, 732-734.
- Longuet-Higgins, M.S., 1968: The eigenfunctions of Laplace's tidal equations over a sphere. *Phil. Trans. Roy. Soc. London*, **A262**, 511-607.
- Matsuno, T., 1970: Vertical propagation of stationary planetary waves in the winter northern hemisphere. *J. Atmos. Sci.*, **27**, 871-883.
- McLandress, C., and J. Derome, 1991: On the interactions among forced planetary waves in a stratospheric model. *J. Meteor. Soc. Japan*, **69**, 311-326.
- McLandress, C., and J. Derome, 1990: A study of stationary wave-wave interactions in a low order stratospheric model. *J. Meteor. Soc. Japan*, **68**, 539-548.
- Randel, W., 1987: The evaluation of winds from geopotential height data in the stratosphere. *J. Atmos. Sci.*, **44**, 3097-3120.
- Robinson, W.A., 1986: Interactions between stationary planetary waves in the stratosphere. *J. Atmos. Sci.*, **43**, 1006-1016.
- Schoeberl, M.R., and M.A. Geller, 1977: A calculation of the structure of stationary planetary waves in winter. *J. Atmos. Sci.*, **34**, 1235-1255.